MODELING, MONITORING, AND CONTROL OF PH-SHIFT REACTIVE CRYSTALLIZATION

SU QINGLIN

(B. Eng., M. Eng., Xiamen University, China)

A THESIS SUBMITTED

FOR THE DEGREE OF DOCTOR OF PHILOSOPHY

DEPARTMENT OF CHEMICAL AND BIOMOLECULAR ENGINEERING

NATIONAL UNIVERSITY OF SINGAPORE

2013

DECLARATION

I hereby declare that the thesis is my original work and it has been written by me in its entirety.

I have duly acknowledged all the sources of information which have been used in this thesis.

This thesis has also not been submitted for any degree in any university previously.

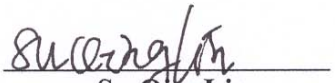

Su QingLin

10 August, 2013

Acknowledgements

I would like to express my heartfelt gratitude to my supervisor, Prof. Min-Sen Chiu, for his constant and patient guidance throughout my PhD study at National University of Singapore. Grateful acknowledgement is made to Prof. Richard D. Braatz at Massachusetts Institute of Technology for his sincere and constructive co-supervision of my research work. This thesis would not have been completed without their insightful elicitation and detailed comments on each step I made.

I sincerely thank the faculty in the Chemical and Biomolecular Engineering Department for their responsible teaching and professional nurturing to foster a sense of chemical engineering with special thanks to Prof. Lakshminarayanan Samavedham and Prof. Jian-Wen Jiang for their valuable inputs and advices during Oral Qualifying Examination. I warmly thank all my lab mates, Cheng Cheng, Yasuki Kansha, Martin Wijaya Hermanto, Xin Yang, Vamsi Krishna Kamaraju, Yan Li, Wen Huang for their excellent referential work, altruistic help, and moral support rendered to me.

Continuous and considerate assistance from laboratory staffs, Ms. Fam Hwee Koong Samantha, Mr. Boey Kok Hong, and Mr. Rajamohan s/o K Suppiah, to make a computing platform ready and available for my research, are really appreciated. I am also indebted to the National University of Singapore for the outstanding research facilities, friendly academic and administrative staffs, and the research scholarship provided for my research.

My sincere thanks also goes to my friends, Saw Eng Toon, Lim Khun Yeow Ashley, Cheng Xi Yu, Sha Meng, Naviyn Prabhu, Mohammad Sadegh Tavallali, and so on. Their ceaseless encouragement has been a great source of energy and they

often gave me much needed laughter. Their friendship has been a tremendous source of comfort.

I am very grateful to my family who have never limited my ambitions and have always had absolute confidence in me. Their moral understanding and encouragement have, and continues to, inspire me to go through the unknown and challenges in the life. Words cannot express how much I love them and how grateful I am to them.

Lastly, the work in this thesis would not have been possible without the people who have been showing their solicitude to me, I hope this thesis would console them a bit.

Contents

Summary

Crystallization is one of the most important unit operations for separation and purification in process manufacturing industries, by which solid crystals with high purity are precipitated from a solution. There are three common ways to induce the crystallization, viz., by cooling, antisolvent addition, and chemical reaction. With the recent research development prompted by the process analytical techniques (PAT) in batch cooling and antisolvent crystallization processes, the reactive crystallization process has also gained increasing interest due to its importance to process industries. This thesis investigated the modeling, monitoring, and control of a semi-batch pH-shift reactive crystallization process using the polymorphic L-glutamic acid as a model compound.

For better understanding of the effects of operating condition on crystalline product qualities, a first-principles mathematical model for the pH-shift reactive crystallization process was developed. The kinetic parameters were estimated by Bayesian inference from experimental data available in the literature, from which marginal probability distributions of the parameters can be obtained by Markov Chain Monte Carlo (MCMC) simulation. Validation results showed that the model predictions were in good agreement with the experimental observations. This model is the first result published to address the high supersaturation level, viz., kinetically controlled polymorphic crystallization, in the pH-shift reactive crystallization process using L-glutamic acid as a model compound.

Next, a moving-window multiway principal component analysis (MPCA) was put forward for online monitoring in the pH-shift reactive crystallization process. The moving-window idea of building multiple MPCA models at different time points was successfully introduced to tackle the transitional phase changes due to process

nonlinearity and time-varying characteristics observed in the reactive crystallization process. In comparisons with the conventional MPCA and multiway partial least squares (MPLS), the proposed method not only efficiently detects the abnormal batch, but also reflects the contributions of the control actions to revert the process to in-control state. This is a significant advantage for batch process operation when feedback control to reduce the false alarms works.

Direct design and control strategy, such as concentration control (C-control), has been popular in cooling and antisolvent crystallization for years. In this thesis, the JITL-based C-control strategy was developed by extending the conventional C-control strategy to incorporate a process model so that better performance can be achieved to cope with the highly nonlinear dynamics inherent in pH-shift reactive crystallization process. Additionally, it was found that tracking the polymorphic purity trajectory achieved much better performance than that of the solute concentration trajectory, indicating the deficiency of C-control strategy in dealing with the complicated polymorphic crystallization, whereas the polymorphic purity control gives improved performance because it is closely related to the progress of polymorphic crystallization and hence is more direct to the product quality.

Despite the success of model predictive control (MPC) in continuous process industries, the implementation of MPC or nonlinear model predictive control (NMPC) strategies in the batch/semi-batch crystallization process is rather limited, particularly, in the shrinking horizon mode for batch-end product quality control. Toward this end, the extended prediction self-adaptive control (EPSAC), which is one of the NMPC techniques that iteratively linearizes the nonlinear process model around the base input and output trajectories using convolution models, was reformulated as the JITL-EPSAC based on state-space models, which is the emerging trend in NMPC designs. Simulation studies showed the proposed EPSAC method outperformed its conventional counterpart in final product quality control for the pH-shift reactive crystallization process.

In an attempt to correct the bias left uncorrected during online batch-end product quality control in the presence of model-plant mismatch, a new integrated B2B-NMPC control strategy based on a MPLS model and the JITL-EPSAC technique was also proposed, exploring the repetitive nature of batch process to update the model kinetic parameters using information from previous batches. Comparing to the conventional B2B control strategy, the new integrated JITL-EPSAC scheme showed a much smoother and faster convergence to the set point of final product quality under multiple shifts of abnormal scenarios, showing its capability to maintain consistent production of on-spec product. This has never been demonstrated by direct design and control or NMPC control discussed in previous works.

List of Tables

List of Figures

Nomenclature

$\mathbf{A}, \mathbf{B}$	Coefficient matrices of state-space model
B_i, W_i	Between- and within- sequence variance of parameter *i*
a	Solute activity
B_i	Nucleation rate of the *i*-form crystals
C	Solute concentration
$C_{sat,i}$	Saturation concentration of the *i*-form crystals
D_{imp}	Impeller diameter
d_k	Unmeasured disturbances
$\delta(\cdot)$	Dirac delta function
$\mathbf{E}, \mathbf{F}$	Matrices of residuals
E_b	Activation energy for the nucleation rate
E_g	Activation energy for the growth rate
$\mathbf{e}$	Residual vector
ε	Vector of slack variables
F	Addition flowrate
f	System dynamics function
f_i	Total crystal size distribution of the *i*-form crystals

G_i	Growth rate of *i*-form crystals
γ	Activity coefficient
g	Measurements function
h	Linear and nonlinear constraints for the system
I_c	Ion strength
J	Optimization problem
K	Equilibrium constant for chemical reaction
K_{sp}	Solubility product
$k_{b\alpha}, k_{g\alpha}, k_{d\alpha}$	Nucleation, growth, and dissolution rates of α-form crystals
$k_{b\beta}, k_{g\beta}$	Nucleation and growth rates of β-form crystals
$k_{bi,0}$	Pre-exponential factor for the nucleation rate of *i*-form crystals
k_{vi}	Volumetric shape factor of the *i*-form crystals
L, L_0	Characteristic length of crystals and nuclei
$\mathrm{L}(\theta \mid \mathbf{y})$	Likelihood of θ
L_k	Characteristic length of crystals at the *k*th discretized point
ΔL	Discretization size of crystal length
λ	Eigenvalues
$M, M_{\max}$	Product property and its maximum value at the batch end
MW_{Glu}	Molecular weight of glutamic acid
M_s	Mean crystal size

m_i	The mass concentration of the *i*-form crystals
m_{Raman}	Mass concentration correction term for Raman measurement
μ	Chemical potential
$\mu_{i,n}$	The nth moment of the *i*-form crystals
N	Total samples in a batch
N_i	Number density of the *i* crystal form
N_p	Power number of the stirrer type
N_s	Stirring rate
N_{d_j}	Number of time samples of j^{th} variable in Bayesian inference
N_m	Number of measured variables in Bayesian inference
n	Markov chain length
n_p	Number of principal components
n_u	Number of inputs
n_x	Number of system states
n_y	Number of measured variables
P, P_d	Predicted and desired final product quality
P_α	Polymorphic purity of α -form crystals
P_y	Product yield
$\mathbf{P}_r$	Loading vector

$\Pr$	Probability function
$\Pr(\theta)$	Prior distribution of θ
$\Pr(\mathbf{y}\|\theta)$	Sampling distribution (or data distribution) for fixed parameters θ
Q	Statistical index
R	Universal constant
$\hat{R}_i$	Potential scale reduction factors
ρ_i	Density of the *i*-form crystals
S_i	Supersaturation of *i*-form crystals
σ_j	Standard deviation of the measurement noise in the j^{th} variable
T	Crystallizer temperature
T^2	Hotelling's statistical index
T_l	Local batch time
$\mathbf{t}_r$	Score vector for PCA or PLS
θ	A vector of unknown parameters of interest
$\theta_i^{c,s}$	Simulation draws of parameter *i* from step chain *c* at step *s*
$\theta_{\min}, \theta_{\max}$	Minimum and maximum values of θ
$u_{b,k+i}$	Predetermined future control scenario
u_k, u_k^j	Process inputs
δu_{k+i}	Optimizing future control actions
V	Crystallizer volume

$\mathbf{v}_k$	Noises on the measured variables
$\mathbf{W}_{\Delta u}, \mathbf{W}_{du}$	Weight matrices which penalizes excessive changes in the input variable which occur within-batch and inter-batch in the B2B or B2B-NMPC control strategy
$\mathbf{W}_p$	Weight matrix for the product quality in NMPC strategy
$\mathbf{W}_u$	Weight matrix for the change in input variables in NMPC strategy
$\mathbf{w}_k$	Noises on the system states
$w_{q,j}$	Weighting factor for j^{th} measurement.
$\mathbf{X}, \mathbf{Y}$	Database matrices for PCA or PLS model
$\underline{\mathbf{X}}$	Three dimensional array
$\boldsymbol{\xi}_k$	Noises on the unmeasured disturbances
$\boldsymbol{\Sigma}$	Covariance matrix
$\mathbf{x}_k$	System states at the *k*th sampling instance
$\mathbf{y}$	Collected data which is used to infer θ
$\mathbf{y}_{jk}, \hat{\mathbf{y}}_{jk}$	Measurement and predicted value of j^{th} variable at sampling instance *k*, respectively
$\mathbf{y}_k$	Measured variables
z	Ion charge

Chapter 1

Introduction

1.1 Motivation

Crystallization is one of the oldest unit operation for separation and purification in process manufacturing industry, including fine chemical, pharmaceutical, and food industries, where high purity is of the crucial requirement of the crystalline products. In addition to the molecular purity, control of polymorphic purity, crystal size distribution, crystal shape, and enantiomeric purity is of increasing interest recently. However, despite its long history and vast application in industries, crystallization process is still not very well understood as it involves many complex mechanisms (e.g., nucleation, crystal growth, fine dissolution, agglomeration, polymorph transfer, growth dispersion, etc.) (Towler et al., 2004; Hursthouse et al., 2009). Besides, crystallizations of small volume and high-value-added products are usually operated in batch or semi-batch mode. These make the consistent production of quality crystalline products very challenging.

The supersaturation, which is the difference between solute concentration and solute solubility, is usually treated as the driving force for crystallization process. The size, shape, and polymorphic purity of product crystals are dependent on the supersaturation profile achieved during crystallization process. Three common ways to generate supersaturation are by cooling, antisolvent addition, and chemical reaction. In cooling and antisolvent crystallizations, supersaturation results from reducing the solute solubility to be lower than the solute concentration by decreasing the solution temperature and increasing antisolvent mass fraction, respectively. While in reactive

crystallization, supersaturation results from increasing the solute concentration to be higher than the solute solubility by generating more solute through chemical reaction.

In reactive crystallization, the generation rate of supersaturation is usually very fast and the supersaturation level is high (Roelands et al., 2005; 2007; Qu et al., 2009). As a consequence, the formation of crystals results from rapidly occurring process, such as nucleation, crystal growth, agglomeration and attrition. In the case that the crystallizing solute is capable of forming different polymorphs, viz., a substance can have more than one crystal form and each form exhibits distinct solubility, the lower of the solubility, the more stable of the crystal form, the well known Ostwald's rule of stages predicts that the least thermodynamically stable form is produced first by spontaneous crystallization, which is subsequently transformed into a more stable one (Ostwald, 1897; Ng et al., 1996). However, this rule is not always valid since the high supersaturation level in reactive crystallization process leads to the reduced effects of this thermodynamic factor when the difference between their supersaturation levels due to the solubility difference becomes negligible. As a result, the kinetic factor becomes the controlling factor for the polymorph form formation. For example, the unexpected formation of the stable polymorph of L-glutamic acid was observed in a high supersaturation level during pH-shift precipitation (Roelands et al., 2005; Alatalo et al., 2008; Qu et al., 2009). Hence, this is very different from the thermodynamically controlled cooling or antisolvent crystallization whose supersaturation level is usually limited with an attempt to avoid the occurrence of the spontaneous nucleation.

Although semi-batch reactive crystallization is commonly employed in industrial practice for producing amphoteric compounds with pH-shift method (Black and Davey, 1988; Zhu and Garside, 1997), such as pharmaceutical intermediates and amino acids (Sheng et al., 2006), research studies of applying process system engineering tools to this process remain largely open in the literature. Recently, Borissova et al. (2005) presented the first mathematical model for the semi-batch pH-shift reactive crystallization, which used L-glutamic acid as a model compound. Alatalo et al. (2008) and Qu et al. (2009) applied the process analytical technologies (PAT) of attenuated total reflectance-Fourier transformed infrared (ATR-FTIR) and

Raman spectroscopy to in-line monitoring of the semi-batch pH-shift reactive crystallization process. In addition, Alatalo et al. (2010a; 2010b) and Hatakka et al. (2010) implemented the supersaturation and polymorphism control to the semi-batch pH-shift reactive crystallization of L-glutamic acid.

Encouraged by the importance of reactive crystallization in pharmaceutical and fine chemical industries, this study investigates the modeling, monitoring, and control of the reactive crystallization of L-glutamic acid, wherein the sodium glutamate reacts with sulfuric acid to form L-glutamic acid.

1.2 Contributions

The main contributions of this thesis in the area of modeling, monitoring, and control of semi-batch pH-shift reactive crystallization process can be summarized as follows:

(1) Process model based on first principles of chemical engineering can furtherance the understanding of crystallization process and facilitate the determination of optimal operating condition, as well as enhance the process control in manufacturing industry. In this study, a mathematical model for semi-batch pH-shift reactive crystallization of L-glutamic acid is developed that takes into account the effects of protonation and deprotonation in the species balance of glutamic acid, crystal size distribution, polymorphic crystallization, and non-ideal solution properties. The polymorphic crystallization mechanisms of α- and β- forms of glutamic acid are addressed by considering primary and secondary nucleation, size-dependent growth rate, and mixing effects on nucleation. The kinetic parameters are estimated by Bayesian inference from batch experimental data collected from literature. Probability distributions of the estimated parameters in addition to their point estimates are obtained by Markov Chain Monte Carlo (MCMC) simulation. Moreover, the developed model appears to be the first model developed for high supersaturation level compared to past studies on the modeling of reactive crystallization of L-glutamic acid (Borrisova et al., 2005).

(2) With the recent rapid development of *in situ* real-time measurement for crystallization process (Qu et al., 2009), such as ATR-FTIR, focused beam reflectance measurement (FBRM), particle vision measurement (PVM) and Raman spectroscopy, more and more process data are now becoming available for developing multivariate statistical process control (MSPC) tools to efficiently monitor, diagnose and control of crystallization process, which are critical for achieving process safety, consistency and quality improvement. Among the MSPC tools, the multi-way principal component analysis (MPCA) and multi-way partial least squares (MPLS) were introduced for batch process monitoring decades ago (Nomikos and MacGregor, 1994; 1995a; 1995b). To tackle the transitional phase changes due to process nonlinearity and time-varying characteristic in the semi-batch reactive crystallization (Golshan et al., 2010; Zhao et al., 2007; 2011), an integrated monitoring method based on moving window MPCA model together with batch-wise unfolding of batch data arrays using crystallizer volume as an indicator variable is developed in this work. Simulation results showed that, compared to the conventional MPCA or MPLS method, the proposed monitoring scheme is not only able to efficiently detect the abnormal batch, but also reflects the contributions of the control actions to revert the process to in-control state.

(3) Although concentration control (C-control) strategy has been shown to give effective and robust control performance for batch/semi-batch cooling and antisolvent crystallizations in recent years (Nagy et al., 2008a; Woo et al., 2009; Hermanto et al., 2009), no research work was reported concerning the application of C-control to the more challenging semi-batch pH-shift reactive crystallization. To this end, this study presents detailed analysis to show that it is not feasible to apply the conventional C-control to semi-batch pH-shift reactive crystallization. To circumvent this problem, a variant of C-control strategy by incorporating the Just-in-Time Learning (JITL) method to cope with strong process nonlinearity inherent in the pH-shift reactive crystallization is developed in this study. Besides, a new polymorphic purity

control is also proposed with an aim to control the polymorphic crystallization observed in the process.

(4) Model predictive control (MPC) or nonlinear MPC (NMPC) strategy is of increasing interest to both the academic and industrial sectors to address important control problems. However, its implementation to crystallization processes has been rather limited (Nagy and Braatz, 2003; Hermanto et al., 2009; Mesbah et al., 2011; Nagy and Braatz, 2012). To the best of our knowledge, there is no paper reported in the literature concerning the MPC or NMPC of semi-batch reactive crystallization. Among the NMPC design methods, the extended prediction self-adaptive control (EPSAC) algorithm iteratively linearizes the process around the base input and output trajectories using convolution models (De Keyser and Cauwenberghe, 1985; Ionescu and De Keyser, 2005; Rueda et al., 2005; De Keyser and Donald III, 2007; Tamas et al., 2007). However, the prediction of such models for operating points further away from the current sampling instant in the prediction horizon becomes less accurate due to process nonlinearity. This may even become worse when the EPSAC is applied in batch process control, where control objective is often to control the product quality at batch end (Hermanto et al., 2009; Su et al., 2012c). Therefore, a new EPSAC algorithm based on the JITL method is developed in this work. In the proposed JITL-based EPSAC design, the linearization is achieved by a set of local state-space models identified by the JITL method along the base trajectory. Simulation results of end-product quality control for the reactive crystallization process validate that the proposed EPSAC algorithm provides better control performance than its previous counterpart.

(5) In view of the fact that batch processes are operated in a repetitive mode, it is advantageous to implement the batch-to-batch (B2B) control to the reactive crystallization process, which uses information from previous batches to iteratively update the process model in order to obtain optimal batch operation. Moreover, the B2B control can be further enhanced by integrating the batch-to-batch control and NMPC (B2B-NMPC) strategies (Chin et al., 2000; Lee et

al., 2002; Paengjuntuek et al., 2008; Hermanto et al., 2011). In this study, a new integrated B2B-NMPC control strategy is developed based on the interaction between a first-principles model and a multi-way partial least square (MPLS) model (Nomikos and MacGregor, 1995b), where the MPLS model utilizes the initial conditions, measurement trajectories and end-point product qualities to estimate the kinetic parameters in the first-principles model. In doing so, while the NMPC performs online control to handle the constraints and disturbances, the B2B control refines the model iteratively by inferring from the previous batch operations. Simulation studies show that the proposed B2B-NMPC control strategy produces faster and smoother convergence while meeting all the constraints requirement, compared to the standard B2B control strategy.

1.3 Thesis organization

This thesis is organized as follows. In the next chapter, literature review on the fundamental of crystallization and the recent development of the modeling, monitoring, and control of crystallization process are presented. Chapter 3 presents the development of a first-principles model for semi-batch pH-shift reactive crystallization of L-glutamic acid, and Chapter 4 investigates the use of multivariate statistical monitoring for the reactive crystallization process. Five control strategies including the JITL-based C-control, polymorphic purity control, NMPC, B2B, and B2B-NMPC control strategies are discussed in Chapters 5 to 7. Finally, conclusions from the present work and suggestions for the future work are given in Chapter 8.

Chapter 2

Literature Review

This chapter presents a brief review on the fundamentals of crystallization process, including the definition, supersaturation, mechanism and kinetics, crystal size distribution, and polymorphism. Subsequently, recent developments on the modeling, monitoring, and control of batch/semi-batch crystallization processes are reviewed.

2.1 Crystallization fundamentals

Crystallization is usually defined as the process of precipitating solid solute from a solution, by which an ensemble of randomly organized molecules or ions dissolved in the solution come together to form an ordered three-dimensional molecular array which is called crystal (Toschev, 1973; Randolph and Larson, 1988; Davey and Garside, 2000). Due to the limited space and tight bonding nature of the atoms in this molecular array, or to be exact, the lattice structure of crystal, contaminants are not able to fit within this structure, which leads to the high purity of crystalline product. Hence, crystallization plays a vital role in the separation and purification process of manufacturing domains, such as fine chemical, pharmaceutical, and food industries, where purity is of the crucial requirement.

2.1.1 Crystal morphology and habit

Known as a supramolecular process, crystallization results in solid particulate crystals whose overall external shape and appearance are often described by terms of morphology and habit. Crystal morphology describes the appearance of faceted crystals due to the specific crystallographic faces showing, while crystal habit characterizes the crystal shape given by the relative length to width of the crystal

faces. Figure 2.1 gives an illustration of crystal morphology and habit (Toschev, 1973; Randolph and Larson, 1988).

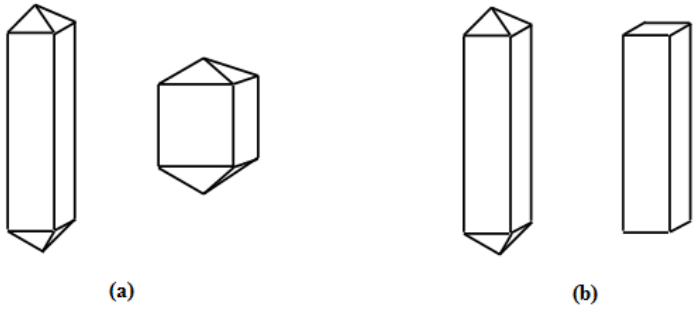

Figure 2.1: Schematic of crystal with different morphologies and habits. (a) Same morphology but different habit. (b) Same habit but different morphology.

Only certain morphologies are possible for any given crystal system (molecular lattice structure), but both morphology and habit depend on growth conditions and can vary with the level of supersaturation (Randolph and Larson, 1988; Gunawan et al., 2004; Ma et al., 2007). However, it is essential to note that due to the symmetric growth of crystal in most cases, such like a cube that the ratio among the length, width, and height remains the same as the cube is growing into a larger one, changes in morphology and habit are often neglected. Therefore, the characteristic length L, which is thought of as a length passing through the center of mass of the crystal and intersecting two opposing surfaces, and the volumetric shape factor k_v, which is a dimensionless constant ratio relating crystal volume v to the cube of length L, are both conveniently adopted to define the size and form of the crystal, respectively.

2.1.2 Supersaturation

Crystallization from solution occurs only if the solute concentration in a solvent exceeds its solubility. Such a solution is said to be supersaturated, where the difference between solute concentration and its solubility is usually termed as supersaturation and is treated as the driving force for crystallization processes (Randolph and Larson, 1988). Hence, the characterization of supersaturation is critically important for modeling of crystallization process. However, the definition of

supersaturation has not been received common agreement, as evidenced by various definitions reported in the open literatures.

From the thermodynamics perspective, the driving force for crystallization is the difference in chemical potential of the solute in solution and in crystal (Lundager Madsen, 1987; Randolph and Larson, 1988; Torrent-Burgués, 1994; Prausnitz et al., 1999; Mangin et al., 2009):

$$\Delta\mu = \mu - \mu^c = RT \ln\left(\frac{a}{a^*}\right) = RT \ln S \tag{2.1}$$

$$S = \frac{a}{a^*} = \frac{\gamma C}{\gamma^* C^*} \tag{2.2}$$

where μ and μ^c are the chemical potentials of the solute in solution and crystal, respectively; the superscript "*" means solution in its equilibrium state; a is the solute activity; γ is the activity coefficient, C is the solute concentration, and S is usually defined as the relative supersaturation. However, the absolute supersaturation, $S = C - C^*$, is also used in the literature (Ono et al., 2004; Borissova et al., 2005; Hu et al., 2005; Hojjati et al., 2007; Nagy, 2009).

Between the two definitions mentioned above, the relative supersaturation is more popularly used. For example, relative supersaturation was used in the studies of closed-loop implementation of a supersaturation control strategy (Grön et al., 2003), estimation of kinetic parameters for the polymorphic transformation of L-glutamic acid crystals (Hermanto et al., 2008), the crystallization of a salt of a weak organic acid and base (Jones et al., 2005), and a series of crystallization studies investigated by Mazzotti's group (Schöll et al., 2006a ; 2006b; 2007; Lindenberg et al., 2008; Lindenberg and Mazzotti, 2009; Cornel et al., 2009). Besides, Togkalidou et al. (2004) compared the identification results obtained from using relative and absolute supersaturation. Kee et al. (2009a) also compared the two supersaturations in the selective cooling crystallization of the α-form L-glutamic acid. It was found that the relative supersaturation provided more promising result. Similar comparative study can also be found by Alatalo et al. (2010a), where relative supersaturation achieved

better control performance. In view of this, the relative supersaturation is employed in our work.

2.1.3 Mechanism and kinetics

The crystallization processes consist of two frequently observed phenomena, nucleation and crystal growth, which directly contribute to the final crystalline product properties (Randolph and Larson, 1988). Nucleation is the step of creating a new solid phase from a supersaturated homogeneous phase, where the solute molecules dispersed in the solvent start to aggregate together to form stable clusters of nanometers under the current operating condition. These stable clusters are referred as the nuclei. It is at the stage of nucleation that atoms arranged in a defined and repeated manner that defines the internal crystal structure. The crystal growth is the subsequent growth of the nuclei, where the solute molecules moving from the bulk solution adsorb on the nuclei solid surface and are incorporated into the crystal lattice, resulting in the growth of nuclei to become crystals of visible size. As aforementioned, supersaturation is the driving force of crystallization, by which the rate of nucleation and crystal growth is driven, hence nucleation and crystal growth continue to occur simultaneously while the supersaturation exists.

The following discusses the nucleation and crystal growth with more details from the perspective of engineering purpose.

There are several mechanisms proposed for nucleation that are commonly lumped into one of the two categories (Randolph and Larson, 1988; Hermanto et al., 2008), viz., primary and secondary nucleation, as shown in Figure 2.2. Mechanism of formation of nuclei that is independent of the presence of other suspended crystals is classified as primary nucleation and is usually further partitioned as homogeneous nucleation and heterogeneous nucleation. Homogeneous nucleation occurs in the pure bulk solution and is associated with high levels of supersaturation, where the classical thermodynamic free energy minimization is used to derive the rate of homogeneous nucleation (Walton, 1969). In the heterogeneous nucleation, foreign surfaces and

particles promote nucleation as a result of an ordering process caused by interactions across the interface (Walton, 1969), which leads to a much lower supersaturation level that primary nucleation can occur. However, the supersaturation levels of heterogeneous nucleation are still too high for good crystal growth and production of crystals of desirable morphology (Clontz and McCabe, 1971).

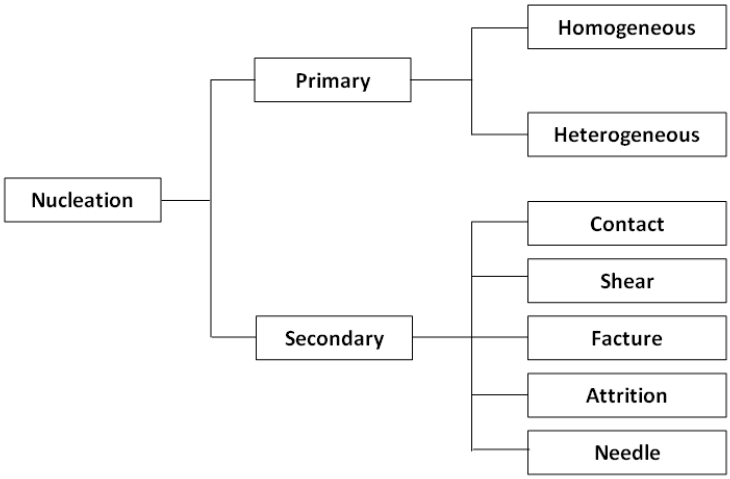

Figure 2.2: Nucleation mechanism.

Secondary nucleation describes the nucleation that takes place due to the presence of other solute crystals. Hence, the secondary nucleation always accompanies the primary nucleation and is the dominate mechanism in most industrial crystallizations (Randolph and Larson, 1962; Bostaris, 1976; Grootscholten et al., 1982). Secondary nucleation is more easily controlled than primary nucleation and occurs at supersaturation levels conductive to good crystal quality. There are a variety of proposed mechanisms whereby the crystals promote formation of new crystals (Clontz and McCabe, 1971; Johnson et al., 1972; Strickland-Constable, 1972; Botsaris, 1976; Randolph and Larson, 1988; Hermanto, 2008). The mechanism of secondary nucleation is usually simplified by assuming an empirical functional form. For example, the following expression is commonly used to describe secondary nucleation:

$$B = \frac{dN}{dt} = k_b \exp\left(-E_b / T\right) S^b \mu_k^j \tag{2.3}$$

where N is the number of nuclei formed per unit volume, t is the time, k_b, b, E_b, and j are empirical constants, μ_k is the kth moment of the crystal size distribution (CSD), R is the universal constants, and T is the temperature.

There are also many attempts that have been made to explain the mechanism and rate of crystal growth (White and Wright, 1971; Randolph and White, 1977; Girolami and Rousseau, 1985; Zumstein and Rousseau, 1987; Randolph and Larson, 1988; Janse and De Jong, 2005), which can be classified into three categories, namely, surface energy, diffusion, and adsorption-layer theories (Mullin, 1961). The surface energy theories are based on the postulation of Gibbs (1878) and Curie (1885) that the shape a growing crystal assumes is that which has a minimum surface energy. The diffusion theories originated by Noyes and Whitney (1897) and Nernst (1904) presume that matter is deposited continuously on crystal face at a rate proportional to the difference in concentration between the point of deposition and the bulk of the solution. It is also suggested that crystal growth is a discontinuous process, taking place by adsorption, layer by layer, on the crystal surfaces (Mullin, 1961). Moreover, growth rate is further complicated by a phenomenon known as growth rate dispersion. It describes the situation in which not all of the crystals grow at identical or constant rates though the crystallizer conditions remain constant.

For engineering purpose, the semiempirical power law has become the standard representation of the growth rate, which assumes the following form,

$$G = \frac{dL}{dt} = k_g \exp(-E_g / RT) L^{g_1} S^{g_2} \tag{2.4}$$

where k_g, g_1, g_2, and E_g, are empirical constants. Also notice that the growth rate is dependent on the crystal size L by power law. If $g_1 = 0$, G is size-independent and this assumption is usually referred to as McCabe's ΔL law. However, there are several examples of systems that violate this assumption. Size-dependent growth rate is usually attributed to either bulk diffusion effects or the Gibbs-Thomson effect. Garside et al. (1976) presents a theory of size-dependent surface integration kinetics.

2.1.4 Crystal size distribution

Crystallization is a typical particulate process, wherein the size of solid crystal may vary in a wide range and is generally characterized by the distribution of size or crystal size distribution (CSD). This is opposed to liquid or gaseous product, which is assumed to be continuous and homogeneous phase. The crystal size distribution can be the major determining factor for the end-use property of a particulate product, for example, filtration rate, dissolution rate, and bulk density (Randolph and Larson, 1988), and therefore affects the downstream processing, including filtration, drying, and milling (Borrisova et al., 2005). To this end, this section attempts to summarize the properties and equations of the crystal size distribution that are important to describe the crystallization process in a quantitative way.

The size distribution of final crystals in batch/semi-batch crystallization process is mainly resulted from the simultaneous nucleation and crystal growth while supersaturation exists. It is well understood that the earlier the nucleus is born in the solution, the longer time of growth it experiences and the larger size of final crystal. Besides, for a seeded crystallization process, where the crystallization is initiated by adding fine crystals, known as seeds, into the solution upon which crystal growth occurs, the size distribution of seeds also affects the final crystal size distribution. While in case that the nucleation could be efficiently suppressed in some seeded crystallization processes by lowering supersaturation level or adding additive (Kitamura, 2009; Kee et al., 2009a), the size distribution of final crystals is often much broader than the size distribution of seeds, which is often attributed either to the size-dependent growth rate or to the growth dispersion. In addition, factors like morphology change, polymorphic transformation, breakage, aggregation, and agglomeration also play vital roles in the final crystal size distribution in some circumstances (Randolph and Larson, 1988).

The most common way of tracking the CSD in batch crystallization processes is by the use of population balance equation, which describes the material balance that accounts for the distribution of different size crystals in the crystallizer, as shown

below, assuming perfect mixing, no morphology change, no agglomeration and breakage.

$$\frac{\partial N}{\partial t}+\frac{\partial}{L}\left(G\left(S,T,L\right)N\right)=B\left(S,T,N\right)\delta\left(L\right) \tag{2.5}$$

where δ is the Dirac delta function, nucleation rate B and crystal growth rate G can be calculated using Eqs. 2.3 and 2.4, respectively.

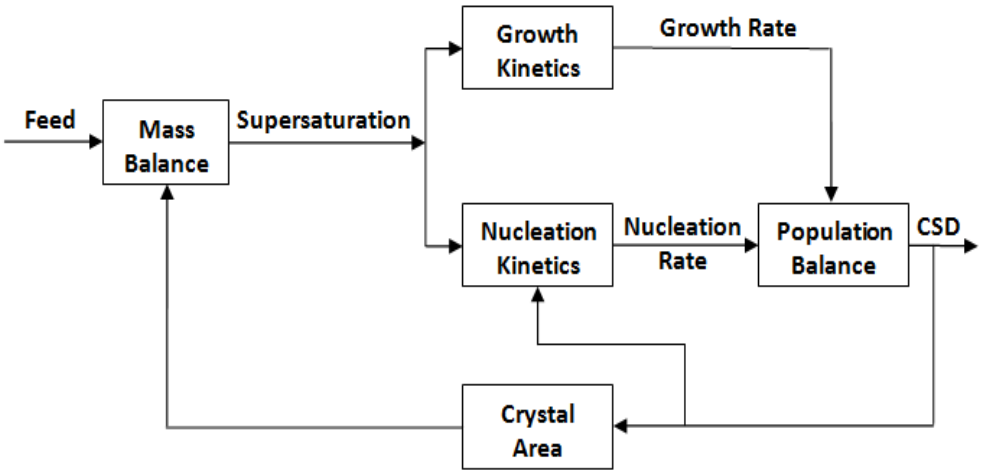

Figure 2.3: Information diagram showing interaction of crystallization factors.

The complex interaction of the crystal size distribution with the crystallization kinetics of nucleation and growth (Randolph and Larson, 1988) is illustrated in Figure 2.3, wherein the crystal surface area connects the mass balance and the population balance and also affects the nucleation in the form of the secondary nucleation.

2.1.5 Polymorphism

For some compounds, they can crystallize into more than one crystal form with different properties such as crystal morphology and habit, density, dissolution rate, bioavailability, melting point, hardness, and electrical properties. This is known as polymorphism that has attracted much research interest recently (Ono et al., 2004; Kee et al., 2009a; Hermanto et al., 2009; 2011), particularly in the pharmaceutical industry where safety and reliability are of paramount importance. For example, the unexpected appearance of a second polymorphic form of an active pharmaceutical ingredient used for the treatment of HIV resulted in substantially different dissolution and absorption characteristics, which highlights the importance of polymorphism in

the pharmaceutical industry (Blagden and Davey, 1999). It is noted that for our model compound, L-glutamic acid, the metastable α and stable β polymorphic forms are studied in their competitive crystallization behavior and transformation recently, which is reviewed in the rest of this subsection.

In Ono et al. (2004), the transformation of metastable α-form to the stable β-form of L-glutamic acid was observed to involve the dissolution of the α-form and the ensuing nucleation and growth of the β-form. Furthermore, the growth rate of the β-form was the rate-limiting step in the transformation. It was concluded by Roelands et al. (2005) that under high supersaturation level, both forms nucleate slowly but the β-form nucleates at the highest rate. Without mixing effect, the large number of β-form crystals depletes most of the supersaturation. With mixing, the fast-growing α-form crystals first reach the critical size for attrition. From that moment attrition generates a large number of secondary α-form nuclei that rapidly deplete the solution. This is in accordance with the experimental results observed in the studies by Alatalo et al. (2008) and Qu et al. (2009). Further study on the polymorphic precipitation mechanism was reported by Roelands et al. (2007) who observed different polymorphic behavior at low ($S \leq 13$) and high ($S \geq 17$) supersaturation.

2.2 Recent development on the modeling, monitoring, and control of crystallization processes

Process system engineering (PSE) is a broad category of engineering tools that include analysis, modeling, simulation, optimization, design, control, and operation of process system for the purpose of efficiently converting raw material to desired end product. The following is intended to summarize the recent development and application of PSE tools in terms of modeling, monitoring, and control of the batch/semi-batch crystallization processes.

2.2.1 Modeling of crystallization processes

As aforementioned in the previous section, modeling of the crystallization processes can be conveniently casted into three parts, single particle model (i.e., nucleation and

crystal growth), population balance model (e.g., crystal size distribution), mass balance equations (e.g., supersaturation), which comprise several nonlinear algebraic equations, partial differential equations (PDEs), and ordinary differential equations (ODEs), respectively. Among them, the PDE solver for population balance model has been received quite a lot of interests in the past few years (Costa et al., 2007).

For one-dimensional population balance model, viz., only the characteristic length is considered, conventional algorithms for hyperbolic partial differential equations are reported to be effective, for example, method of moments (for size-independent growth), method of characteristics, finite volume method (FVM) (Koren, 1993; Qamar et al., 2006; Mesbah et al., 2009), finite element method (FEM), weighted essentially non-oscillatory methods (Hermanto et al., 2009), as well as the combined quadrature method of moments and method of characteristics (Aamir et al., 2009). Recently, an entropic lattice Boltzmann method is proposed and shown to provide the same level of accuracy as the FVM methods with lower computational cost (Majumder et al., 2010).

For multi-dimensional population balance model, for example, the length and width of the crystal are considered individually, a pioneering work was reported by Gunawan et al. (2004) where high-resolution FVM method was developed to solve the multi-dimensional population balance models with orders-of-magnitude lower computational cost than other finite difference methods. Experimental investigation of the growth rate of the length and width of the needle-shaped β-form glutamic acid was reported in Ma et al. (2007), wherein the 2-dimensional population balance model was solved utilizing the method of classes, one of the discretization techniques that integrate population balance model over small interval of the particle size domain.

Generally, system identification and parameter estimation can be difficult for batch process due to the time-varying process dynamics, especially when the system is of large scale. Advantages of using Bayesian estimation over the weighted least squares for parameter estimation are well documented in the literature over the years, including in chemical reactions (Box and Draper, 1965), heat transfer in packed beds (Duran and White, 1995), microbial systems (Bois et al, 1997; Pouillot et al., 2003; Coleman and Block, 2006), microelectronics processes (Gunawan et al., 2003).

Recently, Hermanto et al. (2008) reported for the first time the application of this method in estimation of kinetics for the polymorphic transformation of L-glutamic acid crystals. The popularity of Bayesian inference is based on the fact that it is able to include prior knowledge in the statistical analysis and the resulting posterior distribution for the estimated parameters can be used to accurately quantify the accuracy of model prediction, which can be further incorporated into robust control strategies (Nagy and Braatz, 2003).

With the advances of chemometrics, for example, ATR-FTIR, Raman spectroscopy, and FBRM, people are gaining more and more insight into the crystallization processes. For example, Schöll et al. (2006a; 2006b) estimated the characteristic nucleation and growth rates of the two polymorphs in the solvent-mediated polymorphic transformation (SMPT) of L-glutamic acid. The growth mechanism of α-form in a temperature range of 25-45 ^{o}C and in a relative supersaturation range of 1-3 were studied by Schöll et al. (2007). Hermanto et al. (2008) presented a comprehensive model for the polymorphic transformation of L-glutamic acid crystals in a batch cooling crystallization, where first-order moments of both α and β polymorphs from FBRM were utilized to validate the model. By measuring the induction time at different supersaturations of the pH-shift crystallization of L-glutamic acid in stirred batch reactor using ATR-FTIR and FBRM, together with independently measured growth kinetics, the nucleation rates taking into account of temperature were developed by Lindenberg and Mazzotti, (2009). A mathematical model of the polymorphic transformation process was developed by Cornel et al. (2009), who suggested an attrition-based secondary nucleation mechanism for the β polymorph.

In the context of pH-shift reactive crystallization which is also commonly employed in industrial practice, modeling of this process remains largely open in the literature. To our knowledge, Borrisova et al. (2005) presented the first and only mathematical model for pH-shift reactive crystallization, which used L-glutamic acid as a model compound. Their model assumed ideal solution properties and a simple empirical power-law kinetic mechanism and did not include polymorphic crystallization phenomena and mixing effects on secondary nucleation. This motivates

this study to develop a more comprehensive model which includes the effect of non-ideal solution property, mixing effect and the marginal distributions of the kinetic parameters.

2.2.2 Multivariate statistical monitoring

On-line monitoring, diagnosis, and control of batch or semi-batch crystallization process are needed for various reasons such as safety, consistency, and quality improvement. With the recent development of *in situ* real-time measurement for crystallization processes, discussed previously, more and more process data are now becoming available for developing multivariate process system engineering tools to efficiently monitor, diagnose, and control of crystallization processes.

Different from the continuous operation, historical batch process data are composed of three dimensional array $\underline{X}$ ($I \times J \times K$), where I is the number of batches, J is the number of variables, and K is the number of sampling times in a given batch. To apply the multivariate statistical process control methods, for example, the multiway principal component analysis (MPCA) (Nomikos and MacGregor, 1994), $\underline{X}$ should be rearranged in a two-dimensional dataset X ($I \times JK$) as shown in Figure 2.4 by the widely applied batch-wise unfolding method, which captures the correlation information of the variables both within-time and time to time in terms of auto-correlated and cross-correlated relationships in process data. Furthermore, batch processes with multiple phases or transitional changes due to process nonlinearity are commonly encountered in process industries (Camacho et al., 2006; 2009). Process dynamics and correlations among variables also tend to change with these transitions across the batch, which is often the case in batch crystallization process due to the strong sensitivity of crystallization kinetics to supersaturation, temperature, and total crystal surface area in solution. Traditional approach where the MPCA model is constructed from data representing the whole batch process would not be sufficient to capture the varying process dynamics and correlation structure. Therefore, the use of multi-phase models offers several advantages (Zhao et al., 2007; Golshan et al., 2010). One approach is to build PCA models applicable to every sampling time point

based on a moving window along the batch-wise unfolded dataset as depicted in Figure 2.4. In this technique, a window with a fixed-size is selected at each sampling time in a way that the data of the current time is located at the front of the window, upon which a PCA model is built.

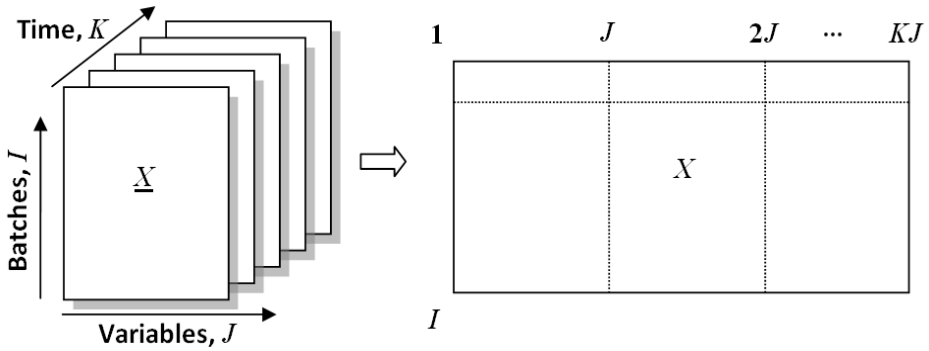

Figure 2.4: Batch-wise unfolding of batch process data.

In addition, the assumption that all batches have equal batch time does not usually hold, for example, longer batch time is typically needed due to the slower crystal growth rate compared with normal operating condition (Nagy et al., 2008a; Woo et al., 2009). To address this problem, different methods using rescaled batch time as a maturity index and tracking the batch operation with an indicator variable or using local batch time as the response vector were proposed in the literature (Zhao et al., 2011). Furthermore, data resampling and interpolation were also employed to calculate the corresponding measurements at regular interval of the maturity index. In this study, the crystallizer volume in place of batch time was proposed as an indicator variable which progressed monotonically in time and had the same starting and ending value for each batch.

2.2.3 Control of crystallization processes

The prevalence and high value of crystallization processes in pharmaceutical, fine chemical, and food industries have motivated the development of many control strategies (Rawlings et al., 1993; Braatz, 2002; Fevotte, 2002; Yu et al., 2004; Fujiwara et al., 2005). The solute concentration is a critical state variable to control during a crystallization, as the crystallization kinetics are usually written in terms of

the solute concentration, or equivalently, the supersaturation. A control strategy for batch and semibatch crystallizations that has become popular in recent years is to determine the optimal solute concentration or supersaturation trajectory against other system state throughout the run, and then design a feedback control system to maintain the optimal relationship between the states (Zhou et al., 2006; Hermanto et al., 2007; Nagy et al., 2008a; Woo et al., 2009). Detailed uncertainty and disturbance analyses carried out both experimentally and in simulation studies have shown that the approach ensures the consistent production of large crystal by suppressing excessive nucleation and the formation of undesired polymorphs (Kee et al., 2009a; 2009b). This so called concentration control (C-control) approach, in which trajectories of concentration vs. temperature or concentration vs. antisolvent mass fraction are tracked throughout the run, has been implemented in many cooling and antisolvent crystallizations (Zhou et al., 2006; Nagy et al., 2008a; Cote et al., 2009; Kee et al., 2009a; 2009b; Woo et al., 2009).

An advantage of the C-control is that it can be implemented without having to estimate the crystallization kinetics and cannot overshoot the desired concentration trajectory provided that the solubility curve is monotonic and the crystallization dynamic is slow compared to the control of cooling temperature or antisolvent addition within one sampling interval (Su et al., 2012a). However, the tracking is also conservative in that it will increase the overall batch time, which lowers the productivity of the equipment (Nagy et al., 2008a; Hermanto, 2008).

Furthermore, the implementation of C-control in both cooling and antisolvent crystallization relies only on the solute concentration trajectory, which is usually monotonically decreasing in these processes. However, its tracking performance may be too sluggish when applied to a reactive crystallization (Borrisova et al., 2005; Alatalo et al., 2008; Qu et al., 2009) where crystallization rate within one sampling interval can switch from very slow to very fast. Moreover, when competitive polymorphic crystallization occurs, for example, the polymorphs crystallize competitively under high supersaturation (Roelands et al., 2005; 2007), then the tracking of a concentration vs. temperature or concentration vs. antisolvent mass fraction trajectory may become inefficient as it only considers the total consumption

rate of solute by crystallization without providing information about their respective crystallization kinetics. One objective of this thesis is to extend the C-control to semibatch reactive crystallization to investigate these potential issues in more detail.

Driven by stringent specifications on product quality, tighter environmental regulation of effluent streams, and higher competition in the process industries, such as the pharmaceutical manufacturing, the development of nonlinear model predictive control (NMPC) techniques is of interest to both the academic and industrial sectors. The main benefit of NMPC lies in its capability to handle nonlinearities and time-varying characteristics inherent in process dynamics by performing real-time dynamic optimization with constraints and bounds imposed on both system states and manipulated variables (Manenti, 2011; Darby and Nikolaou, 2012). Toward this end, various NMPC design methods were developed using different techniques to deal with process nonlinearity, including successive linearization (Lee and Ricker, 1994), neural networks (Peng et al., 2007), robust control (Nagy and Braatz, 2003; Nagy and Allgöwer, 2007), multiple local models (Özkan et al., 2000; Cervantes et al., 2003; García-Nieto et al., 2008; Kuure-Kinsey and Bequette, 2010;), and hybrid models (Hermanto et al., 2011).

Among various NMPC design methods, the extended prediction self-adaptive control (EPSAC) algorithm (De Keyser and Cauwenberghe, 1985) adopted a unique approach to predict process variables through iterative optimization around the pre-specified base input trajectory and corresponding base output trajectory. In this manner, the outputs in the prediction horizon are obtained as the sum of a base term and an optimization term. The former is computed based on a nominal process model using the current values of input variables obtained from the predefined base input trajectory, while the latter obtained from a finite step response or impulse response model, from which a quadratic programming (QP) problem is formulated and can be solved iteratively (Hermanto et al., 2009). Though successful applications of EPSAC have been reported in the literature (De Keyser and Cauwenberghe, 1985; Gálvez-Carrillo et al., 2009; Niño et al., 2009), which includes the control of a polymorphic crystallization (Hermanto et al., 2009; 2011), one potential drawback of the previous EPSAC algorithms is the incorporation of finite step response or impulse models in

the formulation of the control algorithm. Since parameters of these two convolution models are obtained by introducing a step change to the current input value specified by the base input trajectory, those model parameters obtained far away from the current sampling instant become less accurate due to process nonlinearity, leading to inevitable modeling error that degrades the achievable control performance. This shortcoming may become even worse when the EPSAC is applied to batch process control, where the objective is often to control the product quality at batch end. As a large number of step response parameters are needed at the beginning of the batch run to predict the future process outputs for the remaining batch time, this eventually leads to inaccurate predicted outputs and poor control performance as a result. Hence, another aim of this thesis is to formulate the EPSAC algorithm using state-space models due to its inherent flexibility to represent stable, integrating, and unstable processes (Garcia et al., 1989; Morari and Lee, 1999; Qin and Badgwell, 2003; Froisy, 2006; Manenti, 2011; Darby and Nikolaou, 2012), and to validate its applicability in the pH-shift reactive crystallization process.

Owing to the repetitive nature of batch process operation, it would be possible to improve the operation of the next batch using the information of the current and previous batches, which has initiated the learning type control, for example, iterative learning control (ILC), repetitive control (RC), batch-to-batch, or run-to-run control (Bonvin, 1998; Bonvin et al., 2006; Ahn et al., 2007; Wang et al., 2009). Though batch-to-batch control strategy has been widely studied in most chemical processes such as polymerization process (Clarke-Pringle and MacGregor, 1998; Doyle III et al., 2003; Xiong and Zhang, 2003; Zhang, 2008), rapid thermal processing (Lee and Lee, 2007), and so on, the application to crystallization processes, however, has been very limited until recently, when the NMPC and B2B techniques were integrated using a hybrid model to compensate the uncertainties in crystallization kinetics (Hermanto et al., 2011). Thus, it is also of interest to investigate the application of batch-to-batch control and integrated batch-to-batch and NMPC control to the pH-shift reactive crystallization process.

Chapter 3

Modeling of the pH-shift Reactive Crystallization of L-glutamic Acid

In this chapter, a comprehensive kinetic model of the pH-shift reactive crystallization of L-glutamic acid was developed based on the *in situ* monitored experimental data available in the literature, from which the crystallization kinetic parameters were estimated by the state-of-the-art Bayesian estimation method.

3.1 Introduction

The pH-shift reactive crystallization is one of the most commonly used reactive crystallizations for separation and purification of amino acids and other amphoteric chemicals (Black and Davey, 1988; Zhu and Garside, 1997), wherein acid or base solution is continuously added into the crystallizer that is initially filled with saturated solution to induce chemical reactions transforming a high soluble solute into a less soluble one, which is then precipitated from the solution. Despite the rising research interest in the pH-shift reactive crystallization (Borissova et al., 2005; Alatalo et al., 2008; 2010a; 2010b; Qu et al., 2009), mathematical modeling of this process remains largely open in the literature.

The weighted least squares (Bard, 1974; Bates and Watts, 1988; Mendes and Kell, 1998) has been applied to the kinetic parameters estimation for various crystallization systems (Ono et al., 2004; Schöll et al., 2006b; Caillet et al., 2007; Fevotte et al., 2007; Kee et al., 2011). When the weighted least squares method is used for parameter estimation, the linearized statistics or the likelihood ratio approach is often

used to quantify the parameter uncertainties (Beck and Arnold, 1977; Hermanto, 2008). In the linearized statistics approach, the model is linearized around the optimal parameter estimates and the parameter uncertainty is represented by a χ^2 distribution. As a consequence, this method gives inaccurate uncertainty estimate for highly nonlinear processes (Beck and Arnold, 1977). In the likelihood ratio approach, model nonlinearity is taken into account while approximating the distribution which is analogue to the well-known *F* statistic (Beck and Arnold, 1977). Nevertheless, this method also falls short to address the physical constraints on the model parameters.

Unlike the weighted least squares method, the Bayesian inference (Gelman et al., 2004) avoids the presumed probability distribution function for estimated parameters. Besides, it is able to include prior knowledge in the statistical analysis, such as constraints on estimated parameters, resulting in models with higher predictive capability, particularly for highly nonlinear processes.

The Bayesian philosophy differs from the frequentist in the use of the term "probability" (Gelman et al., 2004). Frequentist, upon which the weighted least squares is based (Beck and Arnold, 1977), restricts the application of the term probability to summaries of hypothetical replicate data sets, while Bayesian uses probability to describe the unknown quantities (Hermanto, 2008). This essential difference, in turn, results in the difference between their descriptions of estimation result. The frequentist interval estimate is called a confidence interval, it is an interval determined by the replicate observations. In other words, this confidence is only a description of the mechanisms providing the interval rather than of the interval itself. For example, it assumes the unknown parameter as a fixed quantity, which is either in the interval or not in the interval. Therefore, there is no probability involved with the parameter itself. In contrast, parameters are random variables and are described by their own probability distribution in Bayesian method (Bretthorst, 1990; Coleman and Block, 2006), from which intervals are drawn and termed as credible intervals that can be directly regarded as having a high probability of containing the unknown

quantity. Hence, Bayesian inference facilitates a common sense interpretation of statistical conclusion.

This chapter is organized as follows. The next section describes the development of a mathematical model for semi-batch pH-shift reactive crystallization process using L-glutamic acid as a model compound. This is followed by the brief introduction of Bayesian inference for model parameter estimation. The results of model parameters estimation obtained using experimental data from literature are discussed, followed by the conclusions in the last section.

3.2 Mathematical model

3.2.1 Species balance model

For the model compound of L-glutamic acid (GA), the dissolution of monosodium glutamate (MSG) in pure water due to protonation and deprotonation mechanism can be represented by (Borrisova et al., 2005):

$$\mathrm{Glu}^{1+} \rightleftharpoons \mathrm{Glu}_{(\mathrm{aq})} + \mathrm{H}^{+} \qquad K_{a1} = 6.20\times10^{-3} \tag{3.1}$$

$$\mathrm{Glu}_{(\mathrm{aq})} \rightleftharpoons \mathrm{Glu}^{1-} + \mathrm{H}^{+} \qquad K_{a2} = 4.57\times10^{-5} \tag{3.2}$$

$$\mathrm{Glu}^{1-} \rightleftharpoons \mathrm{Glu}^{2-} + \mathrm{H}^{+} \qquad K_{a3} = 2.14\times10^{-10} \tag{3.3}$$

$$\mathrm{Glu}_{(\mathrm{aq})} \overset{K_{sp}}{\rightleftharpoons} \mathrm{Glu}_{(\mathrm{solid})} \tag{3.4}$$

where Glu^{1+} is the protonated form with an overall charge of +1; Glu^{1-} is the deprotonated form with an overall charge of −1, viz., MSG; Glu^{2-} is the fully deprotonated form with an overall charge of −2; $\mathrm{Glu}_{(\mathrm{aq})}$ and $\mathrm{Glu}_{(\mathrm{solid})}$ are the GA zwitterion with an overall charge of zero in aqueous solution and solid, respectively; K_{ai} (i = 1, 2, 3) are the respective equilibrium constants; and K_{sp} is the solubility product for GA (Alatalo et al., 2010a; 2010b). The four solute-related species can

coexist in the solution, which change their respective concentrations or fractions in solution with varying pH, as shown in Figure 3.1.

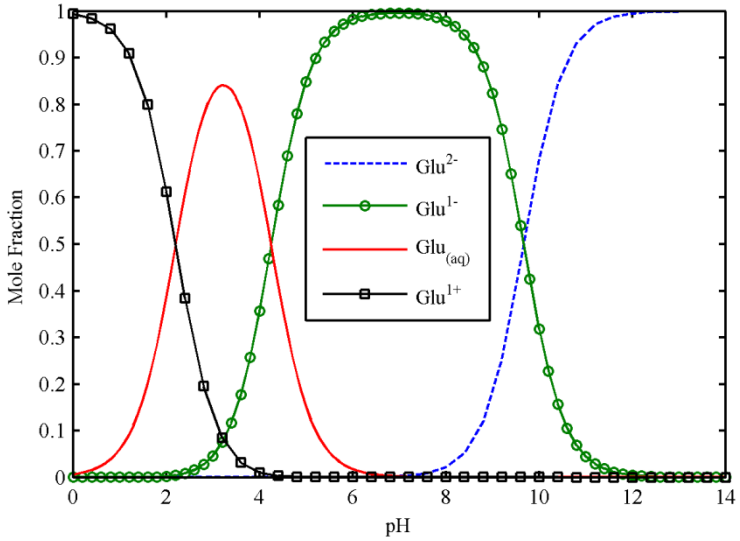

Figure 3.1: Mole fractions of different ionic species of L-glutamic acid in the solution as a function of pH.

In the experimental system of Alatalo et al. (2008), the crystallizer was initially filled with MSG solution and then sulfuric acid was continuously pumped into the crystallizer, which produced glutamic acid according to the overall reaction:

$$\text{Na-Glu} + \frac{1}{2}\text{H}_2\text{SO}_4 \rightleftharpoons \text{Glu(aq)} + \frac{1}{2}\text{Na}_2\text{SO}_4 \qquad (3.5)$$

With continuous addition of the sulfuric acid, decreasing the pH of the solution favors the conversion of sodium glutamate into glutamic acid. However, due to the protonation/deprotonation as indicated in reactions (3.1) to (3.3), glutamic acid will be further protonated. For any particular value of the pH within the range of operation, there are always at least two species in the solution as shown in Figure 3.1.

It is usually assumed that the species balance for glutamic acid in solution will reach dynamic equilibrium instantaneously when sulfuric acid is added into the crystallizer (Borrisova et al., 2005). For the various species in solution, only the zwitterion glutamic acid precipitates because of its lowest intrinsic solubility. Either or both of two polymorphic forms of glutamic acid, namely, metastable α-form and stable β-form, can nucleate or grow competitively in solution depending on the

solution concentration. As the β-form is more stable, a solution-mediated polymorphic transformation (SMPT) from metastable α-form to the stable β-form takes place, when $C_\beta^* < C < C_\alpha^*$, as shown below (Cisternas et al., 2006; Alatalo et al., 2008):

$$\alpha\text{-Glu}_{(solid)} \xrightarrow{\text{Dissolution}} \text{Glu}_{(aq)} \tag{3.6}$$

$$\text{Glu}_{(aq)} \xrightarrow{\text{Crystallization}} \beta\text{-Glu}_{(solid)} \tag{3.7}$$

with the intrinsic solubility of two polymorphs given as follows:

$$C_\alpha^* = 7.4\times10^{-2} \ \text{mol/L} \tag{3.8}$$

$$C_\beta^* = 5.6\times10^{-2} \ \text{mol/L} \tag{3.9}$$

The dissociations of sulfuric acid and the autoprotolysis of water are also considered:

$$H_2SO_{4(aq)} \rightarrow HSO_4^- + H^+ \tag{3.10}$$

$$HSO_4^- \rightleftharpoons SO_4^{2-} + H^+ \qquad K_{as} = 0.0105 \tag{3.11}$$

$$H_2O \rightleftharpoons H^+ + OH^- \qquad K_w = 1\times10^{-14} \ (25\ ^\circ\text{C}) \tag{3.12}$$

The solution during crystallization conditions has sufficient water that H_2SO_4 rapidly dissociates with subsequent formation of HSO_4^-. Furthermore, the activity-based equilibrium constant $K_a = K_c K_\gamma$, where K_c is the concentration-based equilibrium constant and K_γ is computed by activity coefficients, is employed to deal with the non-ideal solution properties, which is less restrictive compared to Borrisova et al. (2005) where ideal solution was assumed. The activity coefficient of electrically neutral glutamic acid, $\text{Glu}_{(aq)}$, is assumed to be one. The activity coefficients, γ_i, for other ions are calculated based on the modified Bates-Guggenheim equation with parameter values A = 1.175 and B = 0.15 (Alatalo et al., 2008):

$$\ln\gamma_i = -Az_i^2 \frac{\sqrt{I_c}}{1+1.5\sqrt{I_c}} + BI_c \tag{3.13}$$

where I_c and z denote the ion strength and ion charge, respectively.

3.2.2 Population balance model

The crystal size distribution is an important concern in industrial manufacturing, due to its effect on product performance and on downstream processing, such as washing, filtering, drying, and milling (Borissova et al., 2005). During crystallization the size distribution can be affected by many factors, such as nucleation, the size distribution of crystal seeds, growth dispersion, breakage, attrition, agglomeration, polymorphism, and changes in morphology.

For a perfectly mixed batch crystallizer, in which it is assumed that (a) crystal nuclei are of negligible size, (b) crystal breakage and agglomeration are negligible, and (c) crystal shape are uniform, the crystal size distribution can be expressed as the distribution of the number of crystals over the size range, as characterized by the population balance equation:

$$\frac{\partial\left(N_i V\right)}{\partial t}+\frac{\partial\left(G_i N_i V\right)}{\partial L}=0, \quad i=\alpha,\beta \tag{3.14}$$

where L is the characteristic length of the i polymorphic form of glutamic acid, m; N_i is the number density of the i polymorphic form, #/m^4; V is the solution volume, m^3; G_i is the growth rate of the i polymorphic form, m/s. Because the solution volume of a semi-batch crystallizer is time-varying, it is convenient to redefine the number density on the basis of the total operating volume of the system such that (Borissova et al., 2005; Nagy et al., 2008b):

$$f_i = N_i V \tag{3.15}$$

$$\frac{\partial f_i}{\partial t}+\frac{\partial\left(G_i f_i\right)}{\partial L}=0 \tag{3.16}$$

where f_i is the number density over the total solution volume, #/m; and the boundary conditions are:

$$f_i(L,0)=\begin{cases}0 & \text{unseeded}\\ f_{seed,i}(L) & \text{seeded}\end{cases} \tag{3.17}$$

$$f_i(0,t)=f_{i,in} \tag{3.18}$$

where $f_{seed,i}(L)$ is the size distribution of crystal seeds for the *i* polymorphic form; $f_{i,in}$ is the population density of nuclei for the *i* polymorphic form at size zero, which can be obtained as follows:

$$f_{i,in}=\frac{B_i V}{G_i} \tag{3.19}$$

where B_i is the nucleation rate of the *i* polymorphic form, #/(m^3·s).

Based on the crystal size distribution, the average length, total number, surface area, volume, and mass of the crystals can be computed from the *n*th moments of the size distribution,

$$\mu_{i,n}=\int_0^\infty L^n f_i dL \qquad n=0,1,2,3,\cdots \tag{3.20}$$

where $\mu_{i,0}$ is the total number of crystals for the *i* polymorphic form in the crystallizer, $\mu_{i,1}$ is the total length, $\mu_{i,1}/\mu_{i,0}$ is the number-averaged length, $\mu_{i,2}$ is proportional to the total surface area, and $\mu_{i,3}$ is proportional to the total volume of the crystals.

The total concentration of the various glutamic ions $C_{T,Glu}$, links the species balance and population balance models together:

$$C_{T,Glu}=C_{Glu^{2-}}+C_{Glu^{1-}}+C_{Glu_{(aq)}}+C_{Glu^{1+}} \tag{3.21}$$

$$C_{T,Glu}=\frac{C^0_{T,Glu}V_0}{V}-\frac{\rho_\alpha k_{v\alpha}\left(\mu_{\alpha,3}-\mu^0_{\alpha,3}\right)+\rho_\beta k_{v\beta}\left(\mu_{\beta,3}-\mu^0_{\beta,3}\right)}{MW_{Glu}V} \tag{3.22}$$

where $C_{T,Glu}^{0}$ is the initial total concentration of various glutamic species, V_0 is the initial solution volume, ρ_i is the density of glutamic acid of the *i* polymorphic form, k_{vi} is the volumetric shape factor of the *i* polymorphic form, $\mu_{i,3}^{0}$ is the initial total volume of the *i* polymorphic form, and MW_{Glu} is the molecular weight of glutamic acid.

3.2.3 Crystallization mechanism and kinetics

The crystallization mechanism includes nucleation and crystal growth, which are both driven by supersaturation. In this context, for a highly saturated solution during a pH-shift reactive crystallization, it is appropriate to use the relative supersaturation definition (Prausnitz et al., 1999; Togkalidou et al., 2004; Kee et al., 2009a)

$$S_i = \frac{C}{C_i^*} \qquad i = \alpha, \beta. \tag{3.23}$$

This study considers both primary and secondary nucleation of α- and β-forms and the effect of mixing intensity, *I*, is also taken into account in the nucleation. Furthermore, the effect of *α*-form crystals on the secondary nucleation of *β*-form crystals was also considered, to take into account that *β*-form crystals can nucleate from the surface of *α*-form crystals. The growth and nucleation expressions are assumed to have similar dependencies on supersaturation as reported in past studies (Schöll et al., 2006a; 2007; Lindenberg et al., 2008), with a length-dependent term included in the crystal growth kinetic expression. The expressions for the crystallization kinetics are:

α-form crystallization kinetics when $S_\alpha > 1$:

$$B_\alpha = k_{b,\alpha 1} \left(\ln S_\alpha\right)^{b_{\alpha,1}} \exp\left(-\frac{E_{b,\alpha 2}}{\left(\ln S_\alpha\right)^2}\right) I^{b_{\alpha,2}} + k_{b,\alpha 2} m_\alpha^{b_{\alpha,3}} \left(\ln S_\alpha\right)^{b_{\alpha,4}} I^{b_{\alpha,5}} \tag{3.24}$$

$$k_{b,\alpha 1} = k_{b,\alpha 0} \exp\left(-\frac{E_{b,\alpha 1}}{RT}\right) \tag{3.25}$$

$$G_\alpha = k_{g,\alpha 1}\left(\ln S_\alpha\right)^{g_{\alpha,1}} \exp\left(-\frac{E_{g,\alpha 2}}{\ln S_\alpha}\right)\exp\left(-\frac{L}{L_{\alpha,0}}\right) \tag{3.26}$$

$$k_{g,\alpha 1} = k_{g,\alpha 0}\exp\left(-\frac{E_{g,\alpha 1}}{RT}\right) \tag{3.27}$$

β-form crystallization kinetics when $S_\beta > 1$:

$$\begin{aligned} B_\beta = {} & k_{b,\beta 1}\left(\ln S_\beta\right)^{b_{\beta,1}} \exp\left(-\frac{E_{b,\beta 2}}{\left(\ln S_\beta\right)^2}\right) I^{b_{\beta,2}} \\ & + \left(k_{b,\beta 2} m_\alpha^{b_{\beta,3}} + k_{b,\beta 3} m_\beta^{b_{\beta,4}}\right)\left(\ln S_\beta\right)^{b_{\beta,5}} I^{b_{\beta,6}} \end{aligned} \tag{3.28}$$

$$k_{b,\beta 1} = k_{b,\beta 0}\exp\left(-\frac{E_{b,\beta 1}}{RT}\right) \tag{3.29}$$

$$G_\beta = k_{g,\beta 1}\left(\ln S_\beta\right)^{g_{\beta,1}} \exp\left(-\frac{E_{g,\beta 2}}{\ln S_\beta}\right)\exp\left(-\frac{L}{L_{\beta,0}}\right) \tag{3.30}$$

$$k_{g,\beta 1} = k_{g,\beta 0}\exp(-\frac{E_{g,\beta 1}}{RT}) \tag{3.31}$$

where m_i is the mass concentration of the *i* polymorphic form of glutamic acid in the solution, kg/m^3; $L_{i,0}$ is the critical characteristic length of the *i* polymorphic form, m; *R* is the universal gas constant, 8.314 J/mol·K; and *T* is the temperature, K.

The mixing intensity is calculated by (Cornel et al., 2009)

$$I = \frac{N_p D_{imp}^5 N_s^3}{V} \tag{3.32}$$

where N_p is the power number for the stirrer type, D_{imp} is the impeller diameter, m, and N_s is the stirring rate, s^{-1}.

Finally, when the solute concentration is below the solubility of the α-form glutamic acid, the polymorphic transformation from the α- to β-form may occur through SMPT. Thus, it is necessary to consider the dissolution of the α-form in the kinetic scheme, which is given as (Hermanto et al., 2008; Cornel et al., 2009)

$$G_\alpha = k_{d,\alpha}\left(S_\alpha - 1\right) \quad S_\alpha \le 1 \tag{3.33}$$

where $k_{d,\alpha}$ is the dissolution rate constant. The dissolution of β-form is avoided after the crystallization occurs, and so is not considered in this study.

3.2.4 Numerical solution

The mathematical model combining all the above equations consists of partial differential equations (PDEs), ordinary differential equations (ODEs), and nonlinear algebraic equations that need to be solved simultaneously. In order to obtain the crystal size distribution of both polymorphs, numerical techniques that reduce the PDEs into ODEs by discretization of the length axis are common choices. The high-resolution finite-volume method with second-order accuracy and flux-limiting functions (Mesbah et al., 2009) was used here. The characteristic crystal length L was first discretized as shown in Figure 3.2, which is the same as in the standard finite volume method. The equations obtained after discretization are (Koren, 1993; Qamar et al., 2006; Mesbah et al., 2009)

$$if \quad GL_i^+ \ge 0$$

$$if \ i = 0: \ \left(Gf\right)_{1/2} = G_{in} f_{in,0}$$

$$if \ i = 1: \ \left(Gf\right)_{3/2} = G_{3/2}\left(\frac{f_1 + f_2}{2}\right)$$

$$if \ i = N: \ \left(Gf\right)_{N+1/2} = G_{N+1/2}\left(f_N + \frac{f_N - f_{N-1}}{2}\right)$$

$$else: \ \left(Gf\right)_{L_i^+} = G_{L_i^+}\left[f_i + \tfrac{1}{2}\varphi\left(\gamma_i^+\right)\left(f_i - f_{i-1}\right)\right],$$

$$\gamma_i^+ = \frac{f_{i+1} - f_i + \varepsilon}{f_i - f_{i-1} + \varepsilon}, \quad \varepsilon = 1\times 10^{-10}$$

$$\frac{df_i}{dt} + \frac{(Gf)_{L_i^+} - (Gf)_{L_i^-}}{L_i^+ - L_i^-} = 0$$

else:

$$if\ \ i = 0:\ \ (Gf)_{1/2} = G_{1/2}\left[f_1 + \frac{f_1 - f_2}{2}\right]$$

$$if\ \ i = N-1:\ \ (Gf)_{N-1/2} = G_{N-1/2}\frac{f_N + f_{N-1}}{2}$$

$$if\ \ i = N:\ \ (Gf)_{N+1/2} = G_{in} f_{in,N}$$

$$else: (Gf)_{L_i^+} = G_{L_i^+}\left[f_{i+1} + \tfrac{1}{2}\varphi\left(\gamma_i^+\right)\left(f_{i+1} - f_{i+2}\right)\right]$$

$$\gamma_i^+ = \frac{f_i - f_{i+1} + \varepsilon}{f_{i+1} - f_{i+2} + \varepsilon}, \quad \varepsilon = 1\times 10^{-10}$$

$$\frac{df_i}{dt} + \frac{(Gf)_{L_i^-} - (Gf)_{L_i^+}}{L_i^- - L_i^+} = 0$$

end

where $\varphi\left(\gamma_i^+\right) = \max\left\{0,\ \min\left\{2\gamma_i^+,\ \min\left\{\tfrac{1}{3} + \tfrac{2}{3}\gamma_i^+,\ 2\right\}\right\}\right\}$.

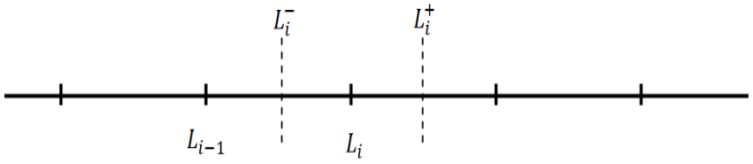

Figure 3.2: Cell-centered finite volume grid.

Using the Matlab ODE solver *ode45*, these ODEs were solved simultaneously with the conservation equations:

$$\frac{dV}{dt} = F \tag{3.34}$$

$$\frac{dC_{T,Glu}}{dt} = -\frac{C_{T,Glu}}{V}\frac{dV}{dt} \tag{3.35}$$

$$\frac{dC_{Na^+}}{dt} = -\frac{C_{Na^+}}{V}\frac{dV}{dt} \tag{3.36}$$

$$\frac{dC_{T,S}}{dt} = -\frac{C_{T,S}}{V}\frac{dV}{dt} + \frac{C_{0,S}F}{V} \tag{3.37}$$

$$C_{T,S} = C_{HSO_4^-} + C_{SO_4^{2-}} \tag{3.38}$$

where F is the sulfuric acid addition flowrate, m^3/s; C_{Na^+} is the concentration of sodium ion, mol/m^3; $C_{T,S}$ is the total concentration of sulfuric related ions, mol/m^3; and $C_{0,S}$ is the concentration of sulfuric acid added into the system, mol/m^3.

3.3 Bayesian inference

The parameters in the first-principles model in the last section were determined by Bayesian estimation. For ease of reference, a brief summary of Bayesian inference is provided in this section. Readers can refer to the literature (Bretthorst, 1990; Carlin and Louis, 2000; Gelman et al., 2004; Hermanto et al., 2008) for detailed discussions on this topic.

The main idea of Bayesian inference lies in Bayes' rule:

$$\Pr(\boldsymbol{\theta}|\mathbf{y}) = \frac{\Pr(\mathbf{y}|\boldsymbol{\theta})\Pr(\boldsymbol{\theta})}{\Pr(\mathbf{y})} \tag{3.39}$$

where $\boldsymbol{\theta}$ is a vector of unknown parameters and $\mathbf{y}$ is a vector of the observations, such as measurements of state variables at different time points, to be used to infer $\boldsymbol{\theta}$. $\Pr(\boldsymbol{\theta})$ is the prior distribution of $\boldsymbol{\theta}$, $\Pr(\mathbf{y}|\boldsymbol{\theta})$ is referred as the *sampling distribution* for fixed parameters $\boldsymbol{\theta}$ and is also referred to as the *likelihood function* $L(\boldsymbol{\theta}|\mathbf{y})$ when the data $\mathbf{y}$ are known and the parameters $\boldsymbol{\theta}$ are unknown. $\Pr(\boldsymbol{\theta}|\mathbf{y})$ is referred as the

Bayesian posterior distribution of $\boldsymbol{\theta}$ and $\Pr(\mathbf{y})$ acts as a normalizing constant to ensure that the Bayesian posterior integrates to unity, which is often neglected as it does not affect the shape of the posterior distribution of $\boldsymbol{\theta}$.

The critical point about Bayesian inference, as shown in Eq. (3.39), is that it provides a principle way of combining new evidence with prior beliefs, through the application of Baye's rule. Contrast this with frequentist inference, which relies only on the evidence as a whole, with no reference to prior beliefs. Baye's rule can be applied iteratively. That is, after observing some evidence, the resulting posterior probability can then be treated as a prior probability, and a new posterior probability computed from new evidence. This allows for Bayesian principles to be applied to various kinds of evidence whether viewed at all once or over time. This procedure is term Bayesian updating (Gelman et al., 2004).

When the model structure is assumed correct and the measurement noise is distributed normally with zero mean and unknown variance, then the likelihood function can be characterized as follows (Hermanto et al., 2008):

$$\begin{aligned} L(\boldsymbol{\theta}\,|\,\mathbf{y}) &= L(\boldsymbol{\theta}_{sys},\boldsymbol{\sigma}\,|\,\mathbf{y}) \\ &= \prod_{j=1}^{N_m}\prod_{k=1}^{N_{d,j}} \Pr\left(y_{jk}\,|\,\boldsymbol{\theta}_{sys},\boldsymbol{\sigma}\right) \\ &= \prod_{j=1}^{N_m}\prod_{k=1}^{N_{d,j}} \frac{1}{\sqrt{2\pi}\sigma_j}\exp\left(-\frac{\left(y_{jk}-\hat{y}_{jk}\left(\boldsymbol{\theta}_{sys}\right)\right)^2}{2\sigma_j^2}\right) \\ &= \frac{1}{\prod_{j=1}^{N_m}\left(\sqrt{2\pi}\sigma_j\right)^{N_{d,j}}}\exp\left(-\sum_{j=1}^{N_m}\sum_{k=1}^{N_{d,j}}\frac{\left(y_{jk}-\hat{y}_{jk}\left(\boldsymbol{\theta}_{sys}\right)\right)^2}{2\sigma_j^2}\right) \end{aligned} \tag{3.40}$$

where $\boldsymbol{\theta}=\left[\boldsymbol{\theta}_{sys},\boldsymbol{\sigma}\right]^T$ is the vector of parameters of interest, which consists of the system/model ($\boldsymbol{\theta}_{sys}$) and noise ($\boldsymbol{\sigma}$) parameters, y_{jk} and $\hat{y}_{jk}$ are the measurement and

predicted value of the *j*th variable at sampling instance *k*, respectively, N_m is the number of measured variables, $N_{d,j}$ is the number of time samples of the *j*th variable, and σ_j is the standard deviation of the measurement noise in the *j*th variable. This likelihood function assumes that the measurement noises are independent.

An informative prior distribution $\Pr(\boldsymbol{\theta})$ that specifies the minimum and maximum possible values of $\boldsymbol{\theta}$ is used in this study:

$$\Pr(\boldsymbol{\theta}) \propto \begin{cases} \mathbf{1} & if\ \boldsymbol{\theta}_{\min} \le \boldsymbol{\theta} \le \boldsymbol{\theta}_{\max} \\ 0 & otherwise \end{cases} \tag{3.41}$$

which means that all values of $\boldsymbol{\theta}$ between $\boldsymbol{\theta}_{min}$ and $\boldsymbol{\theta}_{max}$ have equal probability.

The product of the likelihood $L(\boldsymbol{\theta}|\mathbf{y})$ and prior distribution $\Pr(\boldsymbol{\theta})$ specifies the Bayesian posterior, which is the joint probability distribution for all parameters after data have been observed, and from which all parameter estimates of interest (e.g. means, modes, and credible intervals) are calculated. However, the conventional approach to calculate the above estimates often involves complicated integrals of the Bayesian posterior density which are analytical intractable. To overcome this drawback, Markov Chain Monte Carlo (MCMC) integration (Tierney, 1994; Liu, 2001; Gelman et al., 2004) was applied to compute these integrals in an efficient manner. MCMC does not require approximation of the posterior distribution by a Gaussian distribution (Chen et al., 2004; Coleman and Block, 2006; Lang et al., 2007). Therefore, in this study, the MCMC integration (Gelman et al., 2004) was applied to compute the mean, mode, and credible intervals (aka Bayesian confidence intervals) associated with each of the parameters in an efficient manner.

The Markov chain is a sequence of random variables $\boldsymbol{\theta}^0$, $\boldsymbol{\theta}^1$, ... , drawn from approximate distributions and then corrected to better approximate the Bayesian posterior distribution, for which, for any *s*, the distribution of $\boldsymbol{\theta}^{s+1}$ given all previous $\boldsymbol{\theta}^s$ depends only on the most recent value, $\boldsymbol{\theta}^s$. During application, several parallel chains can be drawn. Parameters from each chain *c*, $\boldsymbol{\theta}^{c,s}$, *s* = 1, 2, 3, ... , are produced by starting at some point $\boldsymbol{\theta}^{c,0}$ and then, for each step *s*, drawing $\boldsymbol{\theta}^{c,s+1}$ from a jumping

distribution $T_s\left(\boldsymbol{\theta}^{c,s+1} \mid \boldsymbol{\theta}^{c,s}\right)$ that depends on the previous draw, $\boldsymbol{\theta}^{c,s}$. The jumping probability distributions must be constructed so that the Markov chain converges to the target posterior distribution. Here, the combination of differential evolution (DE) with MCMC was adopted to construct the Markov chains (Ter Braak, 2006). For monitoring the convergence of the chains, potential scale reduction factors $\left(\hat{R}_i\right)$ were adopted to monitor the convergence of the Markov chains (Gelman et al., 2004), which are calculated from

$$\hat{R}_i = \sqrt{\frac{\hat{var}^+\left(\boldsymbol{\theta} \mid \mathbf{y}\right)_i}{W_i}} \tag{3.42}$$

$$\hat{var}^+\left(\boldsymbol{\theta} \mid \mathbf{y}\right)_i = \frac{n-1}{n} W_i + \frac{1}{n} B_i \tag{3.43}$$

$$B_i = \frac{n}{m-1} \sum_{c=1}^{m} \left(\bar{\theta}_i^c - \bar{\theta}_i\right)^2 \tag{3.44}$$

$$W_i = \frac{1}{m} \sum_{c=1}^{m} \left(d_i^c\right)^2 \tag{3.45}$$

$$\bar{\theta}_i^c = \frac{1}{n} \sum_{s=1}^{n} \theta_i^{c,s} \tag{3.46}$$

$$\bar{\theta}_i = \frac{1}{m} \sum_{c=1}^{m} \bar{\theta}_i^c \tag{3.47}$$

$$\left(d_i^c\right)^2 = \frac{1}{n-1} \sum_{s=1}^{n} \left(\theta_i^{c,s} - \bar{\theta}_i^c\right)^2 \tag{3.48}$$

where $\theta_i^{c,s}$ is the simulation draws of parameter i from step chain c at step s, B_i and W_i are the between- and within- sequence variances of parameter i, respectively, m is the number of parallel chains, with each chain of length n. When $\hat{R}_i$ is near 1 for all

θ_i, then the simulation is stopped and the probability distribution of each parameter can be observed by plotting the Markov chains in histograms, and the mean, mode, and credible intervals can be calculated accordingly.

3.4 Results and discussion

3.4.1 Experimental data

The model parameters in the mathematical model of the previous sections were fit to some of the experimental data of Qu et al. (2009), with the remaining data used for model validation. Other physical parameters for glutamic acid crystallization could be found in literature (Hermanto et al., 2009). For ease of reference, the experimental procedure conducted in Qu et al. (2009) is briefly summarized here.

The precipitation experiments were performed in a 1-liter jacketed crystallizer equipped with a thermostat and an overhead stirrer. The experiments were carried out in semi-batch mode starting from 650 mL of initial solution of MSG in the crystallizer. During the precipitation, 320 mL of sulfuric acid solution with the same molarity as MSG was pumped into the crystallizer at a fixed flow rate of 8 mL/min. All experiments were carried out at 25^{o}C, and were monitored *in situ* using a pH meter, attenuated total reflection Fourier transform infrared (ATR-FTIR) spectroscopy, and a Raman immersion probe. The ATR-FTIR and Raman probes were used to measure the glutamic acid concentration and polymorphic mass fraction of the α form, respectively, throughout the batch. The size distribution of product crystals was determined at the end of each batch. As large fluctuations in the reported Raman measurement was observed for the first half of the batch, the Raman measurement could be influenced by the size or the amount of crystals present in the solution. As a result, the fluctuated data were not used for parameter estimation. To achieve good fitting for the polymorphic purity experimental data, a mass

concentration correction term, m_{Raman}, kg/m^3, was used to calculate the α-form polymorphic mass fraction, $F_{m,\alpha}$:

$$F_{m,\alpha} = \frac{m_\alpha}{m_\alpha + m_\beta + m_{Raman}} \tag{3.49}$$

There were eight sets of experimental data as summarized in Table 3.1, where six experiments (E1 to E3 and E6 to E8) were used to estimate the model parameters by Bayesian inference and the data from the remaining two experiments (E4 and E5) were used for validation.

3.4.2 Parameter estimation

There are twenty-nine model parameters to be estimated, which include twenty-six kinetic parameters, two power numbers for the impellers, and the aforementioned Raman correction term. Besides, four additional measurement noise parameters for pH, ATR-FTIR, Raman measurement, and crystal size distribution were also estimated (see Table 3.2). Since all the experiments were conducted at constant temperature, the estimated kinetic parameters in crystallization mechanism (3.25), (3.27), (3.29) and (3.31) were $k_{b,\alpha 1}$, $k_{g,\alpha 1}$, $k_{b,\beta 1}$ and $k_{g,\beta 1}$ instead. Table 3.2 shows the mean, mode, and 95% credible intervals of the estimated parameters obtained by Bayesian inference. For the sake of limited space, only the marginal probability distributions of the estimated parameters for the α-form nucleation kinetics are shown in Figure 3.3. These distributions can be incorporated into model predictive control and other control algorithms that have been designed to be robust to stochastic parameter uncertainties (Nagy and Braatz, 2003).

The initial parameters for the Markov chains were first obtained by minimizing the weighted difference between the experimental measurements y_{jk} and model predictions $\hat{y}_{jk}$.

$$J = \min_{\boldsymbol{\theta}_{sys}} \sum_{j=1}^{N_m} \sum_{k=1}^{N_{d,j}} \frac{w_{q,j}}{N_{d,j}} \left(y_{jk} - \hat{y}_{jk}\left(\boldsymbol{\theta}_{sys}\right) \right)^2 \tag{3.50}$$

where $w_{q,j}$ is a weighting factor that is the inverse of an estimate of the error variance σ_j^2. Initially, σ_j was set to the standard deviation of the actual measurement. A set of parameters were then estimated by solving the optimization problem (3.50). The standard deviations for the errors in the *j*th measured variable were then re-estimated and used as σ_j to iteratively solve the parameter estimation optimization of (3.50) until no significant difference between the given and estimated standard deviations was detected (Kee et al., 2011).

Figures 3.4 to 3.7 compare model predictions, using the mode estimates of the parameters in Table 3.2, with the experimental data used in fitting the model parameters. For the glutamic acid concentration measurement given in Experiment E3 in Figure 3.4, the solute concentration reflects the combined effects of the solute generation, dilution, and lumped depletion due to the nucleation and growth of the α and β polymorphs. The steep decrease of the solute concentration after 1000 s is in correspondence to the sharp increase of the α-form polymorph mass fraction in Figure 3.6(E3) and the increase in pH for a short period of time displayed in Figure 3.7(E3). In addition, dome-shaped concentration profiles as seen in Figure 3.4 and similar CSD results as observed in Experiments E1 and E2 of Figure 3.5 were observed in the other experiments. The change in the stirring rate from 250 to 500 rpm resulted in stronger secondary nucleation in Experiment E2 than E1, as indicated in nucleation kinetics (3.24) and (3.28), which made the crystal size distribution shift to the smaller size range, as shown in Figure 3.5. Similar results were also obtained for other experiments that had high stirring rate.

As in Figure 3.5, the predicted CSDs are bimodal whereas the experimental CSD are unimodal. the small peek of the predicted crystal size distribution at less than 100 μm for E2 in Figure 3.5 is too small to be observable within the accuracy of a CSD measurement. For E1, the first peek of the predicted crystal size distribution occurs at

about 100 μm. The particle size distributions were experimentally determined by Qu et al. (2009) after the crystals were filtered and dried (Hatakka et al., 2010), and the images in Fig. 4 of their work show a population of much smaller crystals adhered to the surface of larger crystals, but such a smaller population of crystals does not appear in the experimental CSD data in their Fig. 10 that were used in this study and partly shown in Figure 3.5. Smaller crystals often have a tendency to stick to the surface of larger crystals, which would cause any small crystals associated with the first peak in the CSD to show up in the measured CSD by Qu et al. (2009) as parts of larger crystals.[1] Such a systematic experimental bias in the CSD measurements would explain both why our mathematical model predicts a higher amount of small crystals and a smaller amount of the largest crystals than reported in the CSDs in the original experimental work (Qu et al., 2009). Potential biases in measured crystal size distributions are well established in the literature (Rawlings et al., 1993; Loizeau et al., 1994; Abbas et al., 2002).

3.4.3 Model validation

With the mode estimates of the parameters in Table 3.2, validation of the developed model using the datasets from Experiments E4 and E5 are provided in Figures 3.8 and 3.9. The data from Experiments E4 and E5 were not used in the above parameter estimation, and the experimental conditions are different from Experiments E3 and E6 in the stirring rate and impeller type used, respectively. The α-form mass fraction in Experiments E4 and E5 have a high degree of fluctuation in the first half of the batch which is why equation (3.49) used to alleviate this data limitation. The rather precise pH measurements in both experiments are very well predicted by the model (see Figure 3.9). The good agreement of the validation results shown in Figures 3.8 and 3.9 provides some confidence that the first-principles model of pH-shift reactive crystallization can be used in process control studies, as long as the control systems are designed to be reasonably robust to model uncertainties.

[1] It is challenging to quantify a population of small crystals stuck to the surfaces of a much larger population of large crystals.

Table 3.1: Summary of experimental data.

No.	Reagent concentration	Mixing intensity	Impeller type	Measurement data
E1	0.75 M	250 rpm	Six flat blade disc turbine	pH value ■ Glutamic acid concentration □ Polymorphic mass fraction ■ Crystal size distribution ■
E2	0.75 M	500 rpm	Six flat blade disc turbine	pH value □ Glutamic acid concentration □ Polymorphic mass fraction ■ Crystal size distribution ■
E3	1.00 M	250 rpm	Six pitched blade turbine	pH value ■ Glutamic acid concentration ■ Polymorphic mass fraction ■ Crystal size distribution □
E4	1.00 M	500 rpm	Six pitched blade turbine	pH value ■ Glutamic acid concentration □ Polymorphic mass fraction ■ Crystal size distribution □
E5	1.25 M	250 rpm	Six flat blade disc turbine	pH value ■ Glutamic acid concentration □ Polymorphic mass fraction ■ Crystal size distribution □
E6	1.25 M	500 rpm	Six pitched blade turbine	pH value ■ Glutamic acid concentration □ Polymorphic mass fraction ■ Crystal size distribution □
E7	1.50 M	250 rpm	Six flat blade disc turbine	pH value ■ Glutamic acid concentration □ Polymorphic mass fraction ■ Crystal size distribution □
E8	1.50 M	500 rpm	Six pitched blade turbine	pH value ■ Glutamic acid concentration □ Polymorphic mass fraction ■ Crystal size distribution □

* Due to the fact that feeding up would cause imperfect mixing, which was inconsistent with the assumption of perfect mixing in the model, this paper only considers data sets that employed feeding down.

* ■: Data available, □ : Data unavailable.

Table 3.2: Estimated model parameters.

Kinetics	Parameter	Mean	Mode	95% Credible Interval
α nucleation	$k_{b,\alpha1}$	9.83×10^{10}	9.99×10^{10}	$(7.20, 12.31) \times 10^{10}$
	$b_{\alpha,1}$	5.21×10^{-1}	5.01×10^{-1}	$(3.78, 6.75) \times 10^{-1}$
	$E_{b,\alpha2}$	1.04×10^{1}	1.04×10^{1}	$(0.90, 1.22) \times 10^{1}$
	$b_{\alpha,2}$	9.59×10^{-1}	9.73×10^{-1}	$(7.78, 11.40) \times 10^{-1}$
	$k_{b,\alpha2}$	6.99×10^{7}	6.74×10^{7}	$(5.28, 9.03) \times 10^{7}$
	$b_{\alpha,3}$	9.81×10^{-1}	9.18×10^{-1}	$(7.37, 12.40) \times 10^{-1}$
	$b_{\alpha,4}$	4.93×10^{-1}	4.96×10^{-1}	$(3.43, 6.25) \times 10^{-1}$
	$b_{\alpha,5}$	9.64×10^{-1}	9.96×10^{-1}	$(6.90, 11.72) \times 10^{-1}$
α growth	$k_{g,\alpha1}$	9.68×10^{-7}	9.84×10^{-7}	$(7.43, 11.58) \times 10^{-7}$
	$g_{\alpha,1}$	4.93×10^{-1}	5.16×10^{-1}	$(3.46, 6.16) \times 10^{-1}$
	$E_{g,\alpha2}$	8.27×10^{-1}	8.88×10^{-1}	$(5.43, 10.18) \times 10^{-1}$
	$L_{\alpha,0}$	10.14×10^{-4}	9.91×10^{-4}	$(7.32, 12.95) \times 10^{-4}$
β nucleation	$k_{b,\beta1}$	5.03×10^{14}	4.86×10^{14}	$(3.80, 6.30) \times 10^{14}$
	$b_{\beta,1}$	5.30×10^{0}	4.75×10^{0}	$(4.05, 6.91) \times 10^{0}$
	$E_{b,\beta2}$	3.09×10^{1}	3.10×10^{1}	$(2.68, 3.63) \times 10^{1}$
	$b_{\beta,2}$	1.01×10^{0}	1.02×10^{0}	$(0.81, 1.20) \times 10^{0}$
	$k_{b,\beta2}$	7.39×10^{7}	7.15×10^{7}	$(5.62, 9.53) \times 10^{7}$
	$b_{\beta,3}$	9.75×10^{-1}	9.32×10^{-1}	$(7.61, 11.79) \times 10^{-1}$
	$k_{b,\beta3}$	7.63×10^{7}	7.46×10^{7}	$(6.09, 9.90) \times 10^{7}$
	$b_{\beta,4}$	9.52×10^{-1}	9.20×10^{-1}	$(7.29, 11.68) \times 10^{-1}$
	$b_{\beta,5}$	9.81×10^{-1}	9.71×10^{-1}	$(7.22, 12.25) \times 10^{-1}$
	$b_{\beta,6}$	10.02×10^{-1}	9.60×10^{-1}	$(7.16, 13.13) \times 10^{-1}$
β growth	$k_{g,\beta1}$	1.14×10^{-7}	1.07×10^{-7}	$(0.93, 1.40) \times 10^{-7}$
	$g_{\beta,1}$	2.69×10^{0}	2.58×10^{0}	$(1.97, 3.53) \times 10^{0}$
	$E_{g,\beta2}$	8.70×10^{-1}	8.81×10^{-1}	$(6.67, 10.61) \times 10^{-1}$
	$L_{\beta,0}$	2.71×10^{-4}	2.77×10^{-4}	$(1.74, 3.49) \times 10^{-4}$
Power Number	${N_P}^{*}$	6.28×10^{-1}	6.04×10^{-1}	$(5.11, 7.84) \times 10^{-1}$
	${N_P}^{\#}$	5.68×10^{-1}	5.84×10^{-1}	$(4.00, 6.89) \times 10^{-1}$
Raman Corrections	m_{Raman}	5.08×10^{-1}	5.12×10^{-1}	$(3.63, 6.55) \times 10^{-1}$
Measurement noise	σ_{pH}	2.02×10^{-1}	1.99×10^{-1}	$(1.61, 2.46) \times 10^{-1}$
	$\sigma_{ATR-FTIR}$	1.78×10^{-2}	1.78×10^{-2}	$(1.39, 2.27) \times 10^{-2}$
	σ_{Raman}	1.04×10^{-1}	1.05×10^{-1}	$(0.84, 1.29) \times 10^{-1}$
	σ_{CSD}	1.46×10^{-3}	1.41×10^{-3}	$(1.11, 1.96) \times 10^{-3}$

* : six pitched blade turbine; # : six flat blade disc turbine

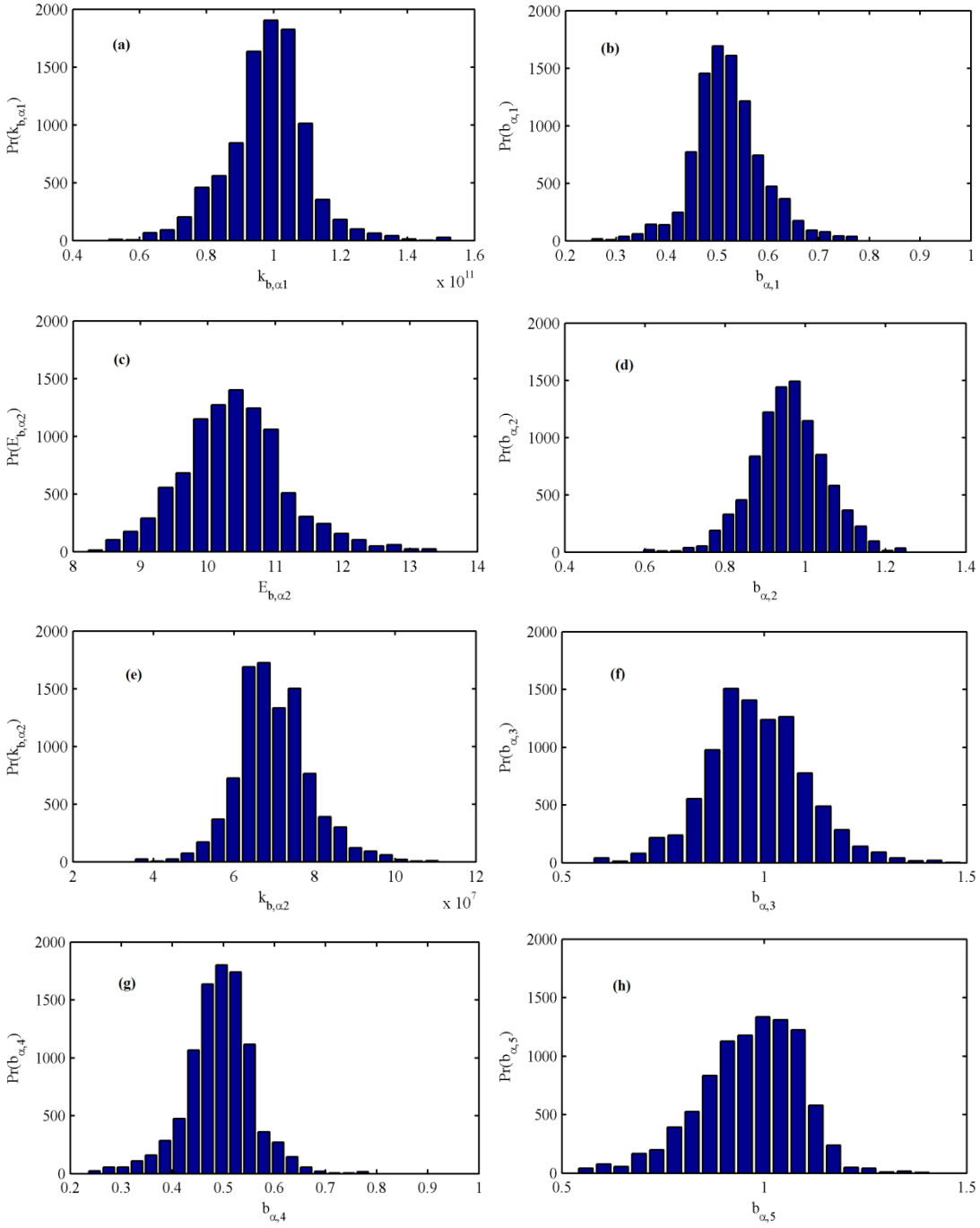

Figure 3.3: The marginal distributions of parameters obtained for α-form nucleation kinetics.

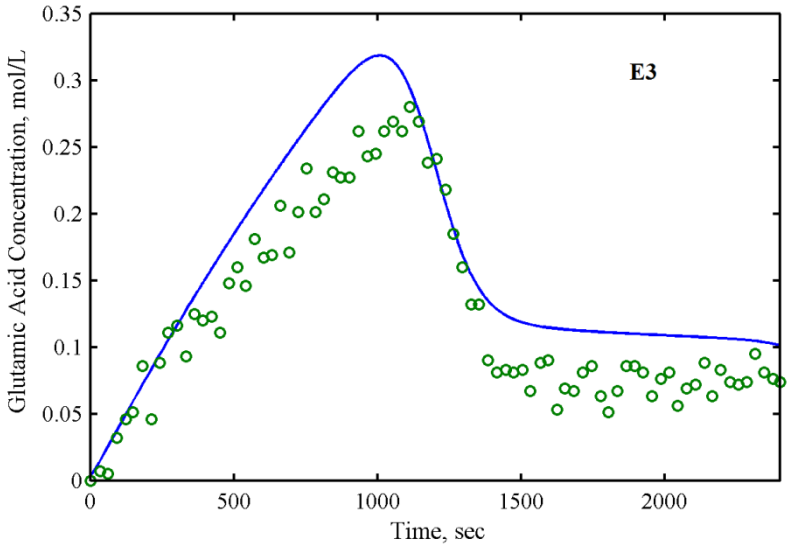

Figure 3.4: Comparison between the model predictions and experimental measurements for the glutamic acid concentration in Experiment E3 (solid line: model predictions; circles: experimental data).

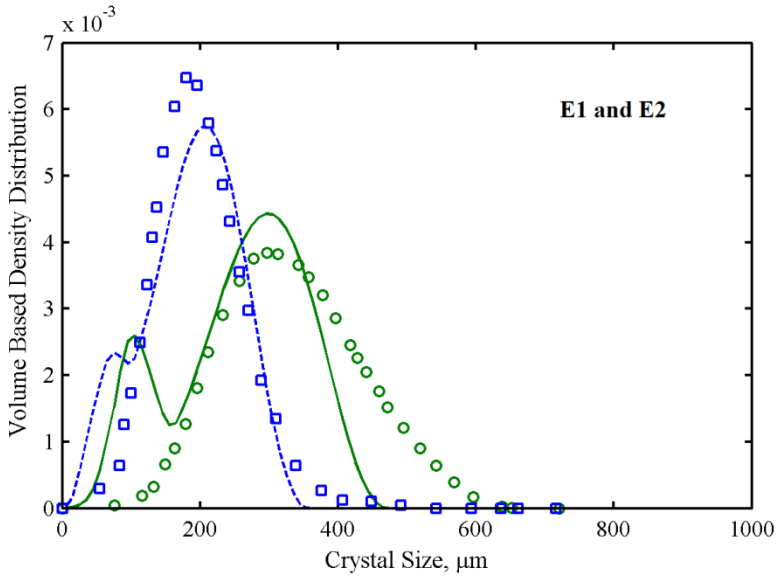

Figure 3.5: Comparison between the model predictions and experimental measurements for the crystal size distribution (lines: model predictions; markers: experimental data; solid line and circle: E1; dash line and square: E2).

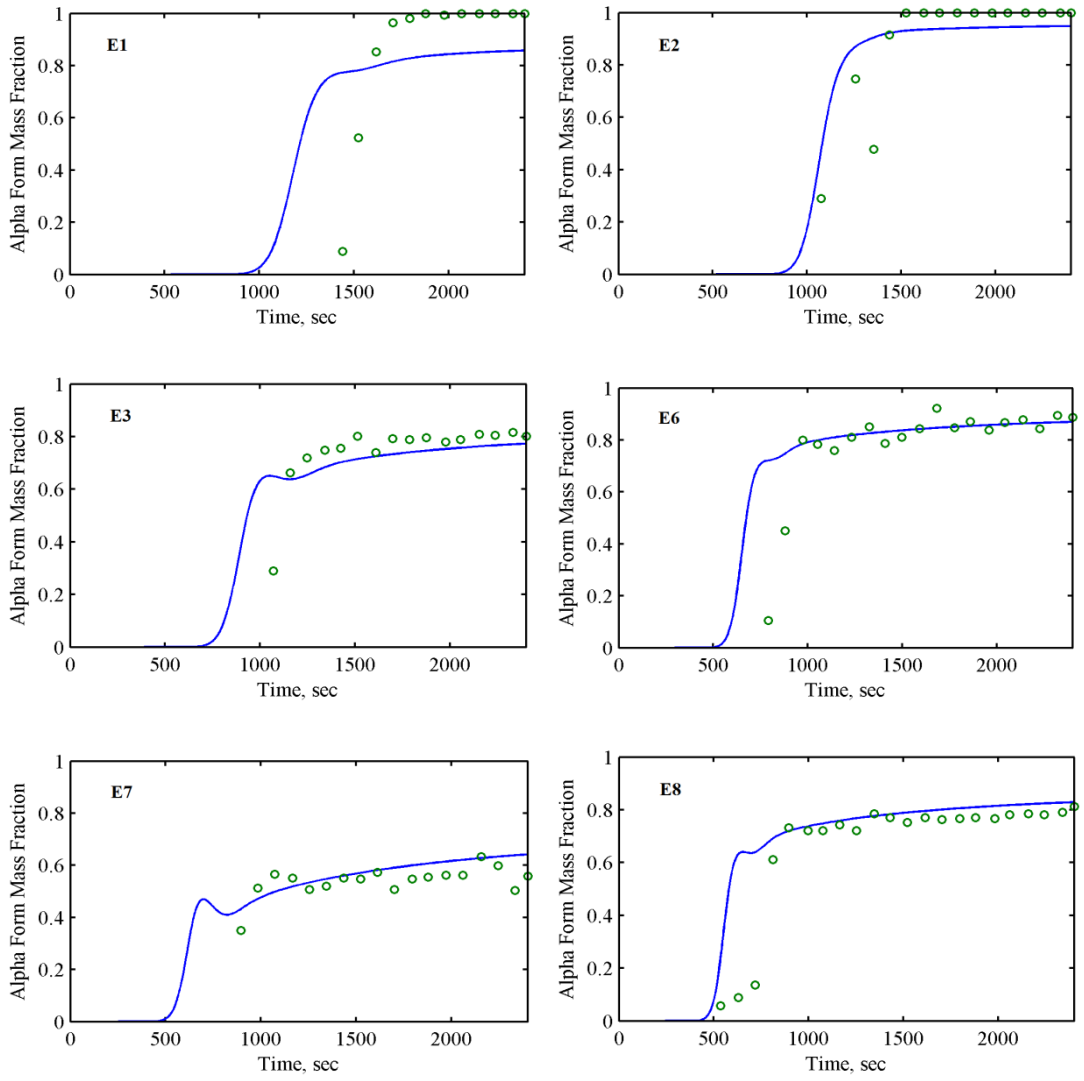

Figure 3.6: Comparisons between model predictions and experimental measurements for the α-form polymorphic mass fraction (solid lines: model predictions; circles: experimental data).

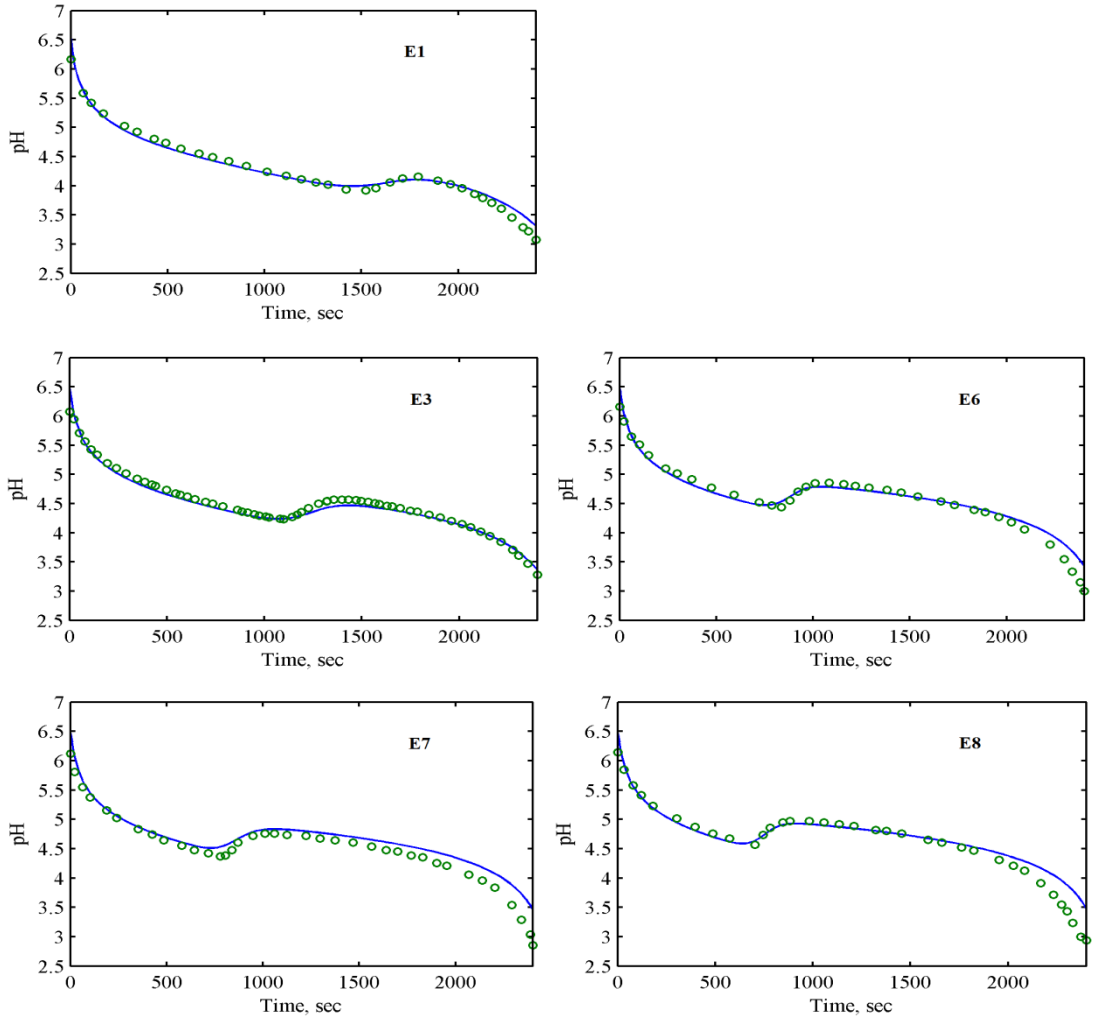

Figure 3.7: Comparisons between model predictions and experimental measurement for the solution pH (solid lines: model predictions; circles: experimental data).

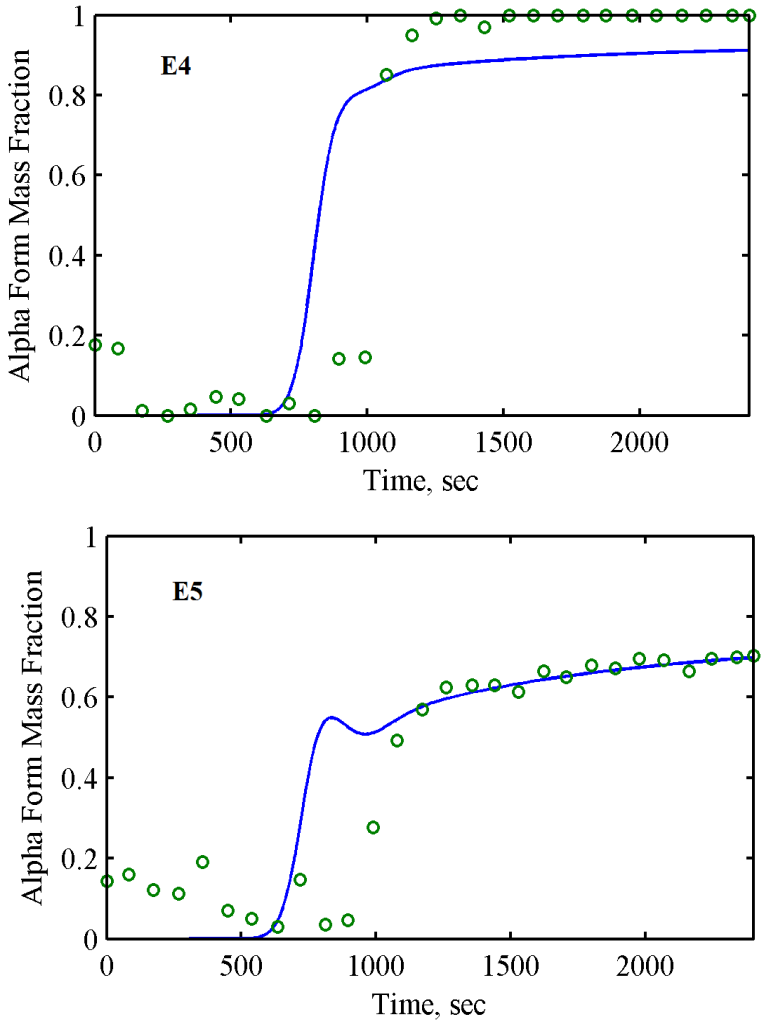

Figure 3.8: Validation results for the α-form polymorphic mass fraction (solid lines: model predictions; circles: experimental data).

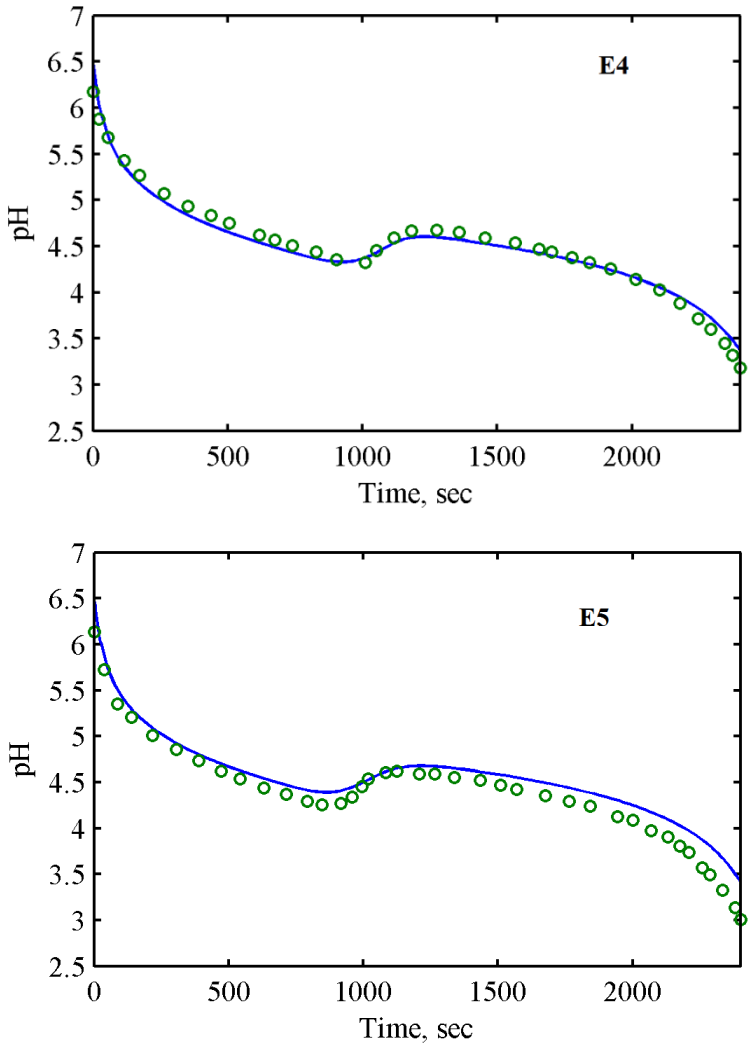

Figure 3.9: Validation results for the solution pH (solid lines: model predictions; circles: experimental data).

3.5 Conclusions

A mathematical model is developed for the semi-batch pH-shift reactive crystallization of L-glutamic acid, taking into account the species balance of the glutamic-related ions, non-ideal solution properties, polymorphic crystallization kinetics, mixing effects, and population balances of the solute crystals. For the population balance model, a finite volume method is employed to reduce the PDEs into a set of ODEs that are then solved together with the nonlinear algebraic equations for the species balances. Experimental data from literature are used to estimate the model parameters using Bayesian inference. The agreement between the experimental data and the predicted outputs of the resulting mathematical model is sufficiently good to justify the use of the model in process control studies.

Chapter 4

Statistical monitoring of the pH-shift Reactive Crystallization of L-glutamic Acid

In this chapter, an integrated monitoring method based on moving window MPCA with batch-wise unfolding of process data array using crystallizer volume as an indicator variable is presented for the semi-batch pH-shift reactive crystallization process of L-glutamic acid under study in this thesis.

4.1 Introduction

For low-volume, high-value added products, such as fine chemicals, pharmaceuticals, and biomolecules, crystallization processes are commonly operated in batch or semi-batch mode to achieve agile and flexible operation. With the recent development of *in situ* real-time measurements for crystallization processes (Alatalo et al., 2008; Qu et al., 2009), such as attenuated total reflection Fourier transform infrared spectroscopy (ATR-FTIR), focused beam reflectance measurement (FBRM), particle vision measurement (PVM), and Raman spectroscopy, more and more process data are now becoming readily available for developing multivariate process system engineering tools to efficiently monitor, diagnose, and control of crystallization processes, which are critically important for various reasons such as safety, consistency, and quality improvement. However, few investigations regarding the monitoring of crystallization processes are available in the literature, especially for the more complex reactive crystallization.

Both cooling and antisolvent crystallization processes are normally monitored using the ATR-FTIR for solute concentration (Kee et al., 2009a) or augmented with the Raman spectroscopy for polymorphic crystallization (Hermanto et al., 2008; Qu et al., 2009) because they are often operated within the metastable zone with limited supersaturation level and are therefore thermodynamically controlled, meaning that as long as the solute concentration or supersaturation is well monitored and controlled around the prescribed level, the final product qualities could be guaranteed. This explains why the concentration control (C-control) as well documented to be robust for these crystallization processes (Zhou et al., 2006; Nagy et al., 2008a; Woo et al., 2009; Kee et al., 2009a).

However, unlike batch cooling or antisolvent crystallization processes, the semi-batch pH-shift reactive crystallization process (Borissova et al., 2005; Alatalo et al., 2008; Qu et al., 2009) is often operated with relatively high supersaturation level and is kinetically controlled, and it even become more complicated in case of the competitive polymorphic crystallization, which is observed in the semi-batch pH-shift reactive crystallization of L-glutamic acid where metastable α-form and stable β-form nucleate and grow simultaneously and competitively. In this case, the solute concentration is a combined result of the polymorphic crystallization as well as the effects of reaction and dilution by sulfuric acid addition. Owing to the complexity and nonlinearity in process dynamics resulting from the high supersaturation level, multivariate monitoring technique is proposed for the pH-shift reactive crystallization process in this chapter.

Research approaches to batch process monitoring have seen the use of state estimation approaches (Jazwinski, 1970), knowledge-based approaches (Ramesh et al., 1989), and multivariate statistical approaches (Nomikos and MacGregor, 1995a). The first method takes advantage of a mechanistic model to describe the process and the monitoring procedure is based on the state estimation method. The second approach uses expert systems and artificial intelligence methods to process the data, hence it relies on the knowledge of the operators and engineers about the process. The last method is based on the philosophy of statistical process control (SPC), which has

found its wide applications due to its simplicity and efficiency, among which the multiway principal component analysis (MPCA) and multiway partial least squares (MPLS) were introduced for batch process modeling and monitoring decades ago (Nomikos and MacGregor, 1994; 1995a; 1995b). Generally, a vast amount of historical database on the measurement profiles is needed with completed batch runs that produce on-spec products. Subsequent to data acquisition, multivariate statistical analysis methods can thus be used to empirically model the successful historical operation batches. The variation within this data serves as reference distribution, against which the performance of independent new batches can then be compared (Zhao et al., 2011). Applications and extensions of these methods have been reported extensively. For example, to address the uneven batch time problem, handling methods were reported, such as using rescaled batch time as a maturity index, tracking the batch progress with an indicator variable, or using local batch time as the response vector (Zhao et al., 2011). To deal with the multiple phases or transitional changes due to process nonlinearity and time-varying characteristics, ideas of building multiple MPCA models at different operation regions were also suggested (Zhao et al., 2007; 2011; Doan and Srinivasan, 2008; Golshan et al., 2010; Sun et al., 2011).

Motivated by the aforementioned discussion, an integrated monitoring method based on moving window MPCA model together with batch-wise unfolding of batch data array using crystallizer volume as an indicator variable is proposed in this work.

4.2 Methodologies

4.2.1 Principal component analysis

Principal component analysis (PCA) is a well-known multivariate statistical method that decomposes a set of observations of possibly correlated variables into a set of values of linearly uncorrelated variables using an orthogonal transformation. Subsequently, the dominant correlations are extracted and contained in these uncorrelated variables which are also termed as principal components. These principal components are guaranteed to be independent only if the data set is jointly normally

distributed. In this regard, original process data are usually preprocessed by mean-centering and variance-scaling of each variable (Geladi and Kowalski, 1986).

PCA decomposes a data matrix $\mathbf{X}$ ($I \times J$) consisting of J measurement variables for I observations into a series of np principal components,

$$\mathbf{X} = \sum_{r=1}^{r=np} \mathbf{t}_r \mathbf{p}_r^T + \mathbf{E} \tag{4.1}$$

where $\mathbf{p_r}$ is a loading vector of $J \times 1$, $\mathbf{t_r}$ a score vector of $I \times 1$, and $\mathbf{E}$ the residual. This factoring procedure of (4.1) can be done either by eigenvalue decomposition of the covariance matrix of $\mathbf{\Sigma} = \mathbf{X}\mathbf{X}^T / (I-1)$ (Cheng and Chiu, 2005; Fujiwara et al., 2009) or by singular value decomposition (SVD) of the data matrix $\mathbf{X}$. Usually, the principal components are ordered such that the first one describes the largest variation in the data $\mathbf{X}$, the second one the second largest variation, etc.. Besides, each succeeding component is orthogonal to the proceeding components. Hence, only a few of them are needed to explain most of the significant variation in the observations. In such a way, PCA provides a simpler and more parsimonious description of the data covariance structure than the original data (Nomikos and MacGregor, 1994), which shows its applicability to efficiently monitor the multivariate continuous process where a large number of variable measurements can be lumped together and viewed in a reduced space, and variations in the process variance can be indicated by just few statistical indices.

For example, if the first np principal components are selected for process monitoring, the prediction of PCA model is calculated as follows when a new measurement data $\mathbf{x}_{new}$ ($J \times 1$) arrives (Geladi and Kowalski, 1986; Cheng and Chiu, 2005; Golshan et al., 2010).

$$\hat{\mathbf{x}}_{new} = \mathbf{P}_{np}\mathbf{t} \tag{4.2}$$

where $\mathbf{P}_{np} = \left[\mathbf{p}_1, \mathbf{p}_2, \cdots, \mathbf{p}_{np}\right]$, and $\mathbf{t} = P_{np}^T \mathbf{x}_{new}$ is the score vector of $np \times 1$ corresponding to $\mathbf{x}_{new}$. The resulting residual is defined as:

$$\mathbf{e} = \mathbf{x}_{new} - \hat{\mathbf{x}}_{new} = \left(\mathbf{I} - \mathbf{P}_{np}\mathbf{P}_{np}^T\right)\mathbf{x}_{new} \tag{4.3}$$

Then the two commonly used statistical variables of Hotelling's T^2 and sum of squares of the residuals Q can be calculated by **t** and **e**, respectively, to be compared against their respective control limits (Jackson and Mudholkar, 1979; Cheng and Chiu, 2005; Fujiwara et al., 2009).

$$T^2 = \mathbf{t}^T \mathbf{\Lambda}_{np}^{-1} \mathbf{t} \tag{4.4}$$

$$Q = \mathbf{e}^T \mathbf{e} \tag{4.5}$$

where $\mathbf{\Lambda}_{np}$ is a diagonal matrix constructed by the first np eigenvalues of $\mathbf{\Sigma}$. For a normally operated process, these two statistics will remain within their control limits.

4.2.2 Multiway principal component analysis

Complexities in batch process, such as finite duration, presence of significant nonlinearity, absence of steady-state operation, as well as the fact that the measured variables are autocorrelated in time and extremely highly correlated with one another at any given time, lead to the direct use of the PCA method impossible in batch process monitoring. To accommodate these difficulties in batch process, a multivariate statistical method of multiway principal component analysis (MPCA) is introduced by Nomikos and MacGregor (1994), summarizing both the variables and their time histories, which is then statistically and algorithmically consistent with PCA and has the same goals and benefits (Wold et al., 1987).

In batch process, large number of multivariate observations taken throughout the normal batch history are composed of a three-dimensional array $\underline{\mathbf{X}}$ ($I \times J \times K$), where I is the number of batches, J is the number of variables, and K is the number of sampling intervals in a given batch. The objective of MPCA is to unfold this three-

way array $\underline{\mathbf{X}}$ into a two-dimensional matrix so that the ordinary PCA can be applied (Nomikos and MacGregor, 1994). For example, $\underline{\mathbf{X}}$ can be rearranged into a two-dimensional dataset $\mathbf{X}$ ($I \times JK$) by the widely acknowledged batch-wise unfolding method (Camacho et al., 2009), viz., putting each of its slices ($I \times J$) side by side along the time index K, which allows to analyze the variability among the batches in $\underline{\mathbf{X}}$ with the information in the data with respect both to variables and their time variation are summarized. Besides, by subtracting the mean from each column in $\mathbf{X}$, viz., mean-centering, MPCA removes the average trajectory from each of the variables and explains the variation of the variables about their average trajectories. Hence, the central idea of MPCA for batch process monitoring is to use the results of this analysis as the reference distribution to characterize the normal operation of the process and to evaluate the behavior of new batches by comparing against this reference distribution.

However, a problem arises during the on-line application of the MPCA as the new observation vector $\mathbf{x}_{new}$ ($KJ \times 1$), representing the entire trajectories history, is not complete until the end of the batch. For example, if the process is at the kth time interval, $\mathbf{x}_{new}$ has only its first kJ rows complete, and it is missing all the future observations. Several approaches have been studied to overcome this deficiency (Golshan et al., 2010). The objective of all these approaches is to fill in the future values in the $\mathbf{x}_{new}$ vector in such a way that the predicted $\mathbf{t}$ scores at each time will be as close as possible to those that would be predicted, if one had the full $\mathbf{x}_{new}$ matrix. It was assumed by (Nomikos and MacGregor, 1994; 1995a) that the future deviations in $\mathbf{x}_{new}$ from the mean trajectory will remain constant at their current values for the duration of the batch or that the future observations are in perfect accordance with their mean trajectories as calculated from the reference database $\mathbf{X}$ (Nomikos and MacGregor, 1995b). Nelson et al. (1996) presented an analysis of several methods including the Single Component Projection (SCP) method, the Projection to the Model Plane (PMP) method, and the Conditional Mean Replacement (CMR) method. Arteaga and Ferrer (2002) also discussed the method of Trimmed Score Regression

(TSR). The PMP method projects the new vector of observations with missing data onto the plane defined by the model of principal components and the resulted missing part of the data vector would be consistent with the model (Golshan et al., 2010). Caution must be used at the beginning of a new batch in which this method may give quite large and unexplainable **t** scores because there is so little information to work with (Nomikos and MacGregor, 1995b).

For a new observation $\mathbf{x}_{new}$, the PMP divides it into two parts (Golshan et al., 2010):

$$\mathbf{x}_{new}^{T} = \left[\mathbf{x}_{new}^{*T}, \mathbf{x}_{new}^{\#T} \right] \tag{4.6}$$

where $\mathbf{x}_{new}^{*}$ corresponds to the past data and $\mathbf{x}_{new}^{\#}$ to the missing future data. The loading matrix can also be divided into two parts in the same way as $\mathbf{x}_{new}$.

$$\mathbf{P}^{T} = [\mathbf{P}^{*T}, \mathbf{P}^{\#T}] \tag{4.7}$$

Thus, the MPCA model of the form of Eq. (4.1) can also be partitioned as:

$$\mathbf{x}_{new} = \begin{bmatrix} \mathbf{x}_{new}^{*} \\ \mathbf{x}_{new}^{\#} \end{bmatrix} = \begin{bmatrix} \mathbf{P}^{*}\mathbf{t} \\ \mathbf{P}^{\#}\mathbf{t} \end{bmatrix} \tag{4.8}$$

Then the known part of the data can be used for score estimation, as shown below.

$$\hat{\mathbf{t}} = \left(\mathbf{P}_{np}^{*T} \mathbf{P}_{np}^{*} \right)^{-1} \mathbf{P}_{np}^{*T} \mathbf{x}_{new}^{*} \tag{4.9}$$

where only the first *np* principal components are considered in the MPCA model. Thus, in this way, the conventional monitoring scheme of PCA of Eqs. (4.2-4.4) can be followed for batch process monitoring. However, it is also noted that, instead of the *Q* statistic of Eq. (4.5) in PCA, it is more convenient in MPCA to use the squared prediction error (SPE) and its corresponding control limits only with the latest on-line measurements at time interval *k* (Nomikos and MacGregor, 1995a; 1995b):

$$SPE_k = \sum_{c=(k-1)J+1}^{kJ} \mathbf{e}(c)^2 \tag{4.10}$$

4.2.3 Multiway partial least squares

Batch-end product qualities are important controlling factors for its end-user performances, which are measured only upon the completion of the batch. Usually, a range of quality measurements are made on a sample of the product in a quality control laboratory. Though recent development in the process analytical technologies (PAT) has made the real-time measurement of product quality possible (Braatz, 2002; Yu et al., 2004; Nagy and Braatz, 2012), this does not change the fact that there is a time lag between the measurement and the batch-end product qualities. Hence, most batch or semi-batch processes are operated, in some sense, in an open loop manner with respect to the batch-end product quality variables (Nomikos and MacGregor, 1995b), unless they are predicted and controlled on-line (Hermanto et al., 2009; 2011). As a result, batch processes usually suffer a lack of reproducibility from batch to batch variations due to disturbances. And these variations may be difficult for an operator to discern, but could have an adverse effect on the final product quality. In light of this, the mulitway partial least squares (MPLS) was proposed by Nomikos and MacGregor (1995b) to take into account the final product qualities in batch process monitoring.

As aforementioned, the MPCA grounded on the statistical process control (SPC) schemes only makes use of process measurement trajectories taken during the batch, i.e., the unfolded data matrix **X**. While measurements on batch-end product quality variables, e.g., **Y** ($I \times M$), where M is the number of quality variables, are only to help classify whether a batch is normal or not. However, in MPLS, both the process data (**X**) and product quality data (**Y**) can be used in an interactive fashion while the same multivariate SPC monitoring ideas that are developed using MPCA can be directly extended (Nomikos and MacGregor, 1995b). Analogous to MPCA, the relation between MPLS and PLS is that MPLS is equivalent to performing ordinary PLS on an unfolded two dimensional measurement data **X** and a product quality data **Y**.

For example, MPLS decompose the **X** and **Y** matrices into a summation of *np* scores vectors ($\mathbf{t}_r$) and loading vectors ($\mathbf{p}_r$), plus some residual matrices **E** and **F**:

$$\mathbf{X} = \sum_{r=1}^{r=np} \mathbf{t}_r \mathbf{p}_r^T + \mathbf{E}, \quad \mathbf{Y} = \sum_{r=1}^{r=np} \mathbf{t}_r \mathbf{q}_r^T + \mathbf{F} \tag{4.11}$$

This decomposition summarizes and compresses the data with respect to both **x** and **y** variables and time into low dimensional spaces that describe the operation of the process which is most closely related to final product quality (Nomikos and MacGregor, 1995b). Thus, MPLS not only extracts and monitors the information from the process measurement trajectories that is more relevant to the final quality variables compared to MPCA, as by Eqs. (4.2-4.4, and 4.10), but also provides on-line predictions of the final product qualities, as by the predictability of the PLS model of Eq. (4.11).

For the missing data problem in on-line monitoring, instead of Eq. (4.9), MPLS adopts the following equation for PMP method:

$$\hat{\mathbf{t}} = \left(\mathbf{W}_{np}^{\#T} \mathbf{P}_{np}^{\#} \right)^{-1} \mathbf{W}_{np}^{\#T} \mathbf{x}_{new} \tag{4.12}$$

where **W** (*KJ* × *np*) is the weight matrix in PLS algorithm (Geladi and Kowalski, 1986).

4.3 Moving-window MPCA monitoring

Batch processes with multiple phases or transitional changes due to process nonlinearity and time-varying characteristics are commonly encountered in industries (Camacho et al., 2006; 2009). Process dynamics and correlations among variables also tend to change with these transitions across the batch. Traditional SPC approaches, such as MPCA and MPLS, in which the PCA or PLS model is constructed from measurement trajectory data representing the whole batch process would not be accurate to capture the varying process dynamics and correlation structure. And this is getting worse during on-line application when there is a need for

missing data imputation. Therefore, the use of multi-phase models offers several advantages (Doan and Srinivasan, 2008; Golshan et al., 2010; Zhao et al., 2011; Sun et al., 2011). One approach is to build MPCA models applicable to every time point based on a moving window along the batch-wise unfolded dataset as depicted in Figure 4.1. In this technique, a moving window with a fixed-size of *Ws* is selected at each sampling time in a way that the data of the current time *k* is located at the front of the window, upon which a MPCA model is built based on $\mathbf{X}_k \left(I \times JW_s\right)$.

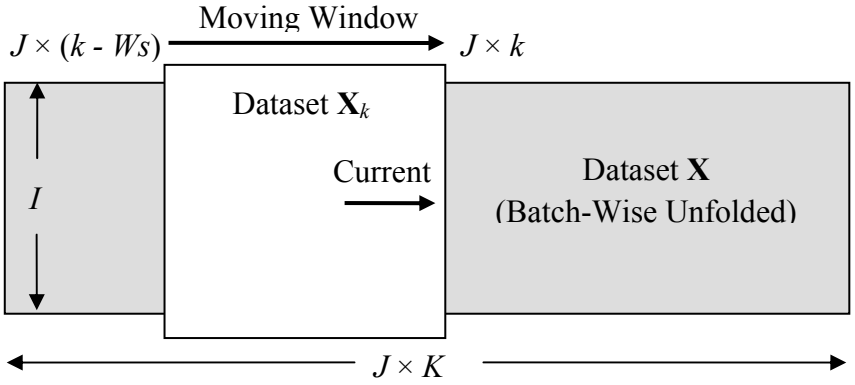

Figure 4.1: Schematic of moving-window MPCA approach along the batch-wise unfolded dataset.

During implementation, when new observation $\mathbf{x}_{k,new}$ $\left(JWs \times 1\right)$ at sampling time *k* is available, two statistical indices T^2 and Q can be calculated with corresponding MPCA model at time *k*, as shown below.

$$T_k^2 = \mathbf{t}_k{}^T \mathbf{\Lambda}_{np}^{-1} \mathbf{t}_k \tag{4.13}$$

$$Q_k = \sum_{c=(k-Ws)J+1}^{kJ} \mathbf{e}\left(c\right)^2 \tag{4.14}$$

where $\mathbf{t}_k$ is the corresponding score vector for the new observation $\mathbf{x}_{k,new}$ calucated based on the respective MPCA model. Additionally, since the current measurement is at the front of the moving window, there is no missing data in the $\mathbf{x}_{k,new}$.

Statistical confidence limits for Hotelling's T^2 are calculated using the F-distribution for MPCA model at sampling time k as follows (Cheng and Chiu, 2005):

$$T_{\alpha,k}^2 = \frac{np\left(I-1\right)}{I-np} F_{np,I-1,\alpha} \tag{4.15}$$

where α is the confidence limit, expressed as a fraction; $F_{np,I-1,\alpha}$ is the F-distribution with degrees of freedom np and $I-1$ at significance level α. Similarly, confidence limits for the square prediction error Q at each sampling time can be calculated on the basis of the chi-squared distribution (Jackson and Mudholkar, 1979; Cheng and Chiu, 2005):

$$Q_{\alpha,k} = \theta_1 \left[1 - \frac{\theta_2 h_0 \left(1-h_0\right)}{\theta_1^2} + z_\alpha \frac{\sqrt{2\theta_2 h_0^2}}{\theta_1} \right]^{\frac{1}{h_0}} \tag{4.16}$$

$$h_0 = 1 - \frac{2\theta_1\theta_3}{3\theta_2^2} \tag{4.17}$$

$$\theta_i = \sum_{j=np+1}^{J} \lambda_j^i, \; i = 1,2,3. \tag{4.18}$$

$$\mathbf{\Sigma}_k = \frac{\mathbf{X}_k^T \mathbf{X}_k}{I-1} \tag{4.19}$$

where λ_i are the eigenvalues of the matrix $\mathbf{\Sigma}_k$ and are arranged in descending order, $Q_{\alpha,k}$ is the confidence limit at sampling time k at the α level and z_a is the Normal variable at significance level α which has the same sign as h_0.

4.4 Case study

4.4.1 Nominal process

A first-principles mathematical model developed in Chapter 3 from the reported experiments was used to simulate the semi-batch pH-shift reactive crystallization of L-glutamic acid. The nominal operating procedure is summarized. The crystallizer is initially half-filled with 0.65 L monosodium glutamate (MSG, 1.0 mol/L), then the

sulfuric acid (SA, 1.0 mol/L) is continuously added to generate the glutamic acid and to induce the crystallization without seeding. The addition flowrate of SA is constrained between 0 and 16 mL/min with a maximum crystallizer volume of 0.97 L. The default batch time and sampling interval are 40 min and 1 min, respectively. A nominal flowrate profile for SA is selected for producing on-spec product in terms of polymorphic purity, mean crystal size, and product yield, which are randomly chosen from a Pareto front of a multi-objectives optimization (Su et al., 2012a). Details of the multi-objective optimization will be further discussed in Chapter 5.

4.4.2 Off-line training

Measurement trajectories of pH value, crystallizer volume, solute concentrations by ATR-FTIR, mean crystal size by FBRM or PVM, and polymorphic purity of metastable α polymorph by Raman spectroscopy, as well as two batch-end product qualities, are collected for off-line training database of **X** and **Y**, respectively. Two batch-end product quality variables are defined as below:

$$Quality\ 1 = \left(P_{\alpha,tf} - 0.8255\right) - \left(0.01 * M_{s,tf} - 0.2506\right)^2 + \left(P_{y,tf} - 0.8088\right) \quad (4.20)$$

$$Quality\ 2 = \sqrt{\frac{m_{0,tf} m_{2,tf}}{m_{1,tf}} - 1} \quad (4.21)$$

where P_α is the polymorphic purity of α-form; M_s is the volume based mean crystal size, μm; and P_y is the product yield of crystals, the subscript *tf* means the batch end; m_i is the *i*th moment of crystal size distribution. Quality 2 is the coefficient of variation of the crystal size distribution. Fifty normal batches were generated to construct the database, wherein nominal addition profile of sulfuric acid was implemented with a Normal noise of N (0, 1.0) at each time interval and varying initial concentrations of monosodium glutamate and sulfuric acid with noise of N (0, 0.02) for each batch to serve as the common operational disturbances in batch process. Additional database of 10 bathes was also generated for the validation purpose. Variations of the batch-end product qualities in the reference and validation database can be found in Figure 4.2.

Very often the assumption that all batches have equal batch time does not hold in crystallization process, for example, the sluggish crystal growth rate may result in longer batch time to finish the batch (Zhou et al., 2006; Nagy et al., 2008a). To efficiently monitor the progress of crystallization as well as the control actions when abnormal batches occur (Su et al., 2012a; 2012c), for the studied semi-batch crystallization process, the crystallizer volume in place of batch time was employed as an indicator variable which progresses monotonically in time and has the same starting and ending value for each batch, i.e., from 0.65 to 0.97 L. Accordingly, data resampling and interpolation were also employed to calculate the corresponding measurements at regular intervals of the crystallizer volume (Zhao et al., 2011). Besides, data preprocessing of mean centering and variance scaling was also employed to the data matrices of **X** and **Y**.

The combined effects of reaction, dilution and kinetically controlled crystallization of the studied process result in the highly nonlinear behavior of system dynamics and the time-varying characteristics, as well as the transitional changes of correlation among measured variables, as shown in Figure 4.3 for the measurement data **X**. There are no distinct phases but transitional changes from upper left to the lower right. Hence, monitoring scheme based on the proposed moving window MPCA together with batch-wise unfolding of batch data arrays using crystallizer volume as an indicator variable was considered for the case study, and was compared with the conventional MPCA and MPLS methods using the same reference database.

First, proper training of the reference database for MPCA, MPLS and moving-window MPCA was made individually to best explain the variations in the database by choosing the number of principal components used, which was 3 for both MPCA and MPLS, and 1 for moving-window MPCA. The fewer principal components for moving-window MPCA is because of the smaller dataset $\mathbf{X}_k$ within the moving window. The size of the moving window was also fine-tuned to be 4 for the proposed method. And note that at the start of the batch, the size of the moving window is increased from 1 until it reaches the desired window size.

Figure 4.4 shows the monitoring result of 10 normal batches in the validation database for MPCA, MPLS and moving-window MPCA. It is observed that the SPE statistics of MPCA and MPLS, though few overshoots of the control limits are found, can be well constrained within their control limits of 99%; while the Q statistic of moving-window MPCA is much better that most of the data are within the limit of 95%. Additionally, the Q statistic and its control limits are also much smoother than that of SPE. Owing to the missing data imputation in MPCA and MPLS, the T^2 statistics suffer large errors at the beginning of the batch since there is no enough information to infer the score vectors. Whereas, this is not the case in the moving-window MPCA as no missing data problem is arisen and the T^2 statistics are always within the control limit of 99%.

The predicted measurements by MPLS are also provided in Figure 4.2, in that it is observed that MPLS can make good predictions of the batch-end product qualities.

4.4.3 On-line application

For on-line application purpose, monitoring statistics are conveniently plotted against the batch time instead of the regular crystallizer volume intervals. This favors the monitoring when the total batch time is extended due to process uncertainties. Three case studies are considered in this work to compare the on-line monitoring performances of MPCA, MPLS and moving-window MPCA.

The first case study situated the batch process subject to the initial concentration disturbance of sulfuric acid, which was increased from the nominal 1.00 to 1.10 mol/L. Figure 4.5 shows the resulted monitoring performances by MPCA, MPLS and moving-window MPCA. All the monitoring methods were able to detect the abnormality at about 5 minutes after the start of the batch first by SPE or Q statistics. Then the T^2 statistics continued the violation of the control limits throughout the rest of the batch. However, it should be pointed out that the initial violations of the T^2 statistics of MPCA and MPLS observed in Figure 4.5 may be either due to the missing data imputation or the abnormal initial operating conditions. Therefore, there

may be difficult to tell whether a violation is a false alarm at the beginning of the batch for MPCA and MPLS.

The second case study considered an abnormal scenario in the crystallization kinetics where the α-form crystal growth rate was decreased by 20% while the nominal optimal addition flowrate profile was followed. The monitoring performances of MPCA, MPLS and moving-window MPCA are given in Figure 4.6. The detection of the abnormality was made at about 20 minutes after the start of the batch by both two statistics in any of the three monitoring methods, demonstrating the capability of the multiway schemes in the batch process monitoring (Nomikos and MacGregor, 1994; 1995b).

The third case study was to implement the polymorphic purity control, which will be discussed in Chapter 5, to handle the growth rate uncertainty considered in the second case study. The control scheme was found to be able to bring the batch process back to the normal by tracking the predefined nominal optimal trajectories and accordingly slowing down the sulfuric acid addition and extending the batch time. The monitoring results are shown in Figure 4.7, where the moving-window MPCA correctly reflects the efficiency of the control scheme, whereas the MPCA and MPLS are less promising with several false alarms at the later phase of the batch time in the Q statistic. Advantage of the moving-window MPCA to correctly reflect the control actions is largely due to the fact that it concentrates only on individual phase of the batch operation, meaning that control actions against the kinetic uncertainties in previous phases are not accumulated to the later phase, which segments and alleviates the overall violation of the corrected batch operation against the reference distribution. To some extent, this is necessary and reasonable as it is obvious from the perspective of process dynamics that the current system dynamics are mostly affected by previous system states that are within a limited time range (Camacho et al., 2009). While the MPCA and MPLS focus on the measurement trajectories taken throughout the whole batch considering the equal contributions of the operation from each time point.

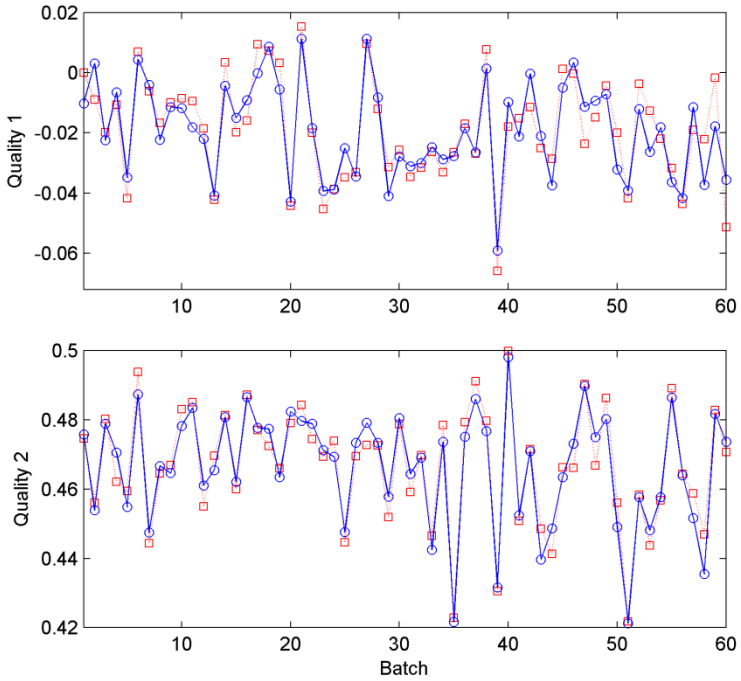

Figure 4.2: Predictions of the batch-end product qualities by MPLS (□: process data; ○: predicted data; the first 50 batches are in the training database, the last 10 batches are unseen data).

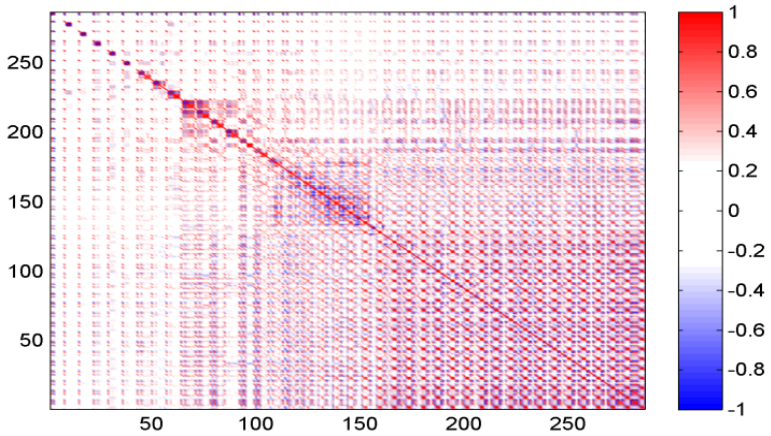

Figure 4.3: Correlation of measured variables after batch-wise unfolding and data preprocessing.

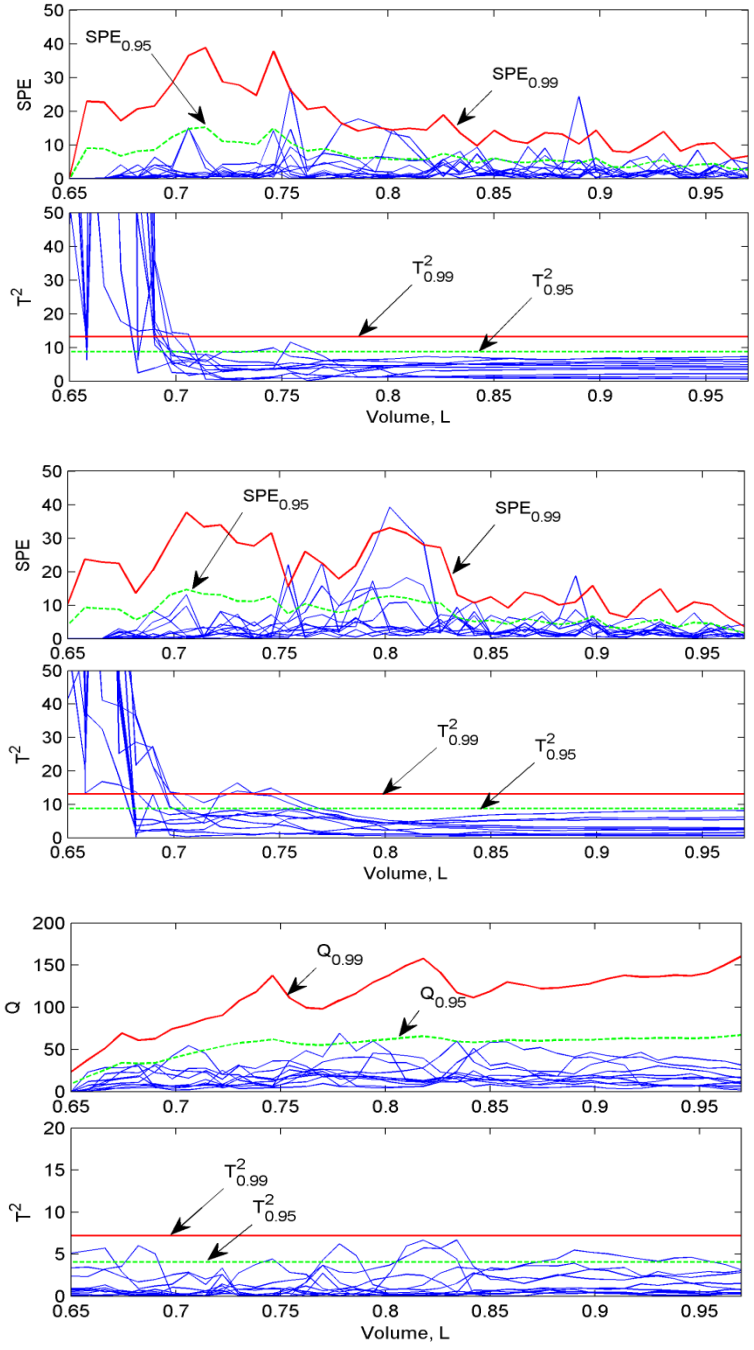

Figure 4.4: Monitoring with MPCA (top), MPLS (middle) and moving-window MPCA (bottom) for 10 unseen normal process.

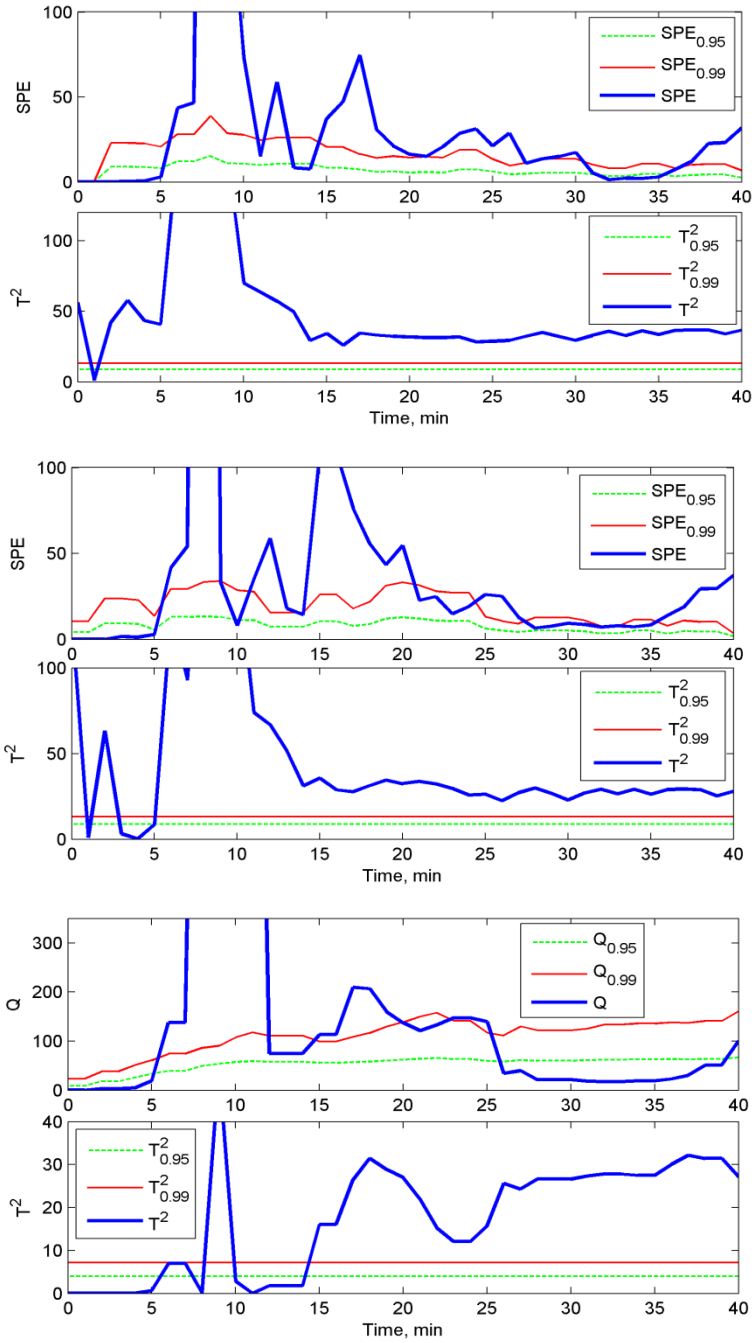

Figure 4.5: Monitoring with MPCA (top), MPLS (middle) and moving-window MPCA (bottom) for Case 1: initial concentration disturbance.

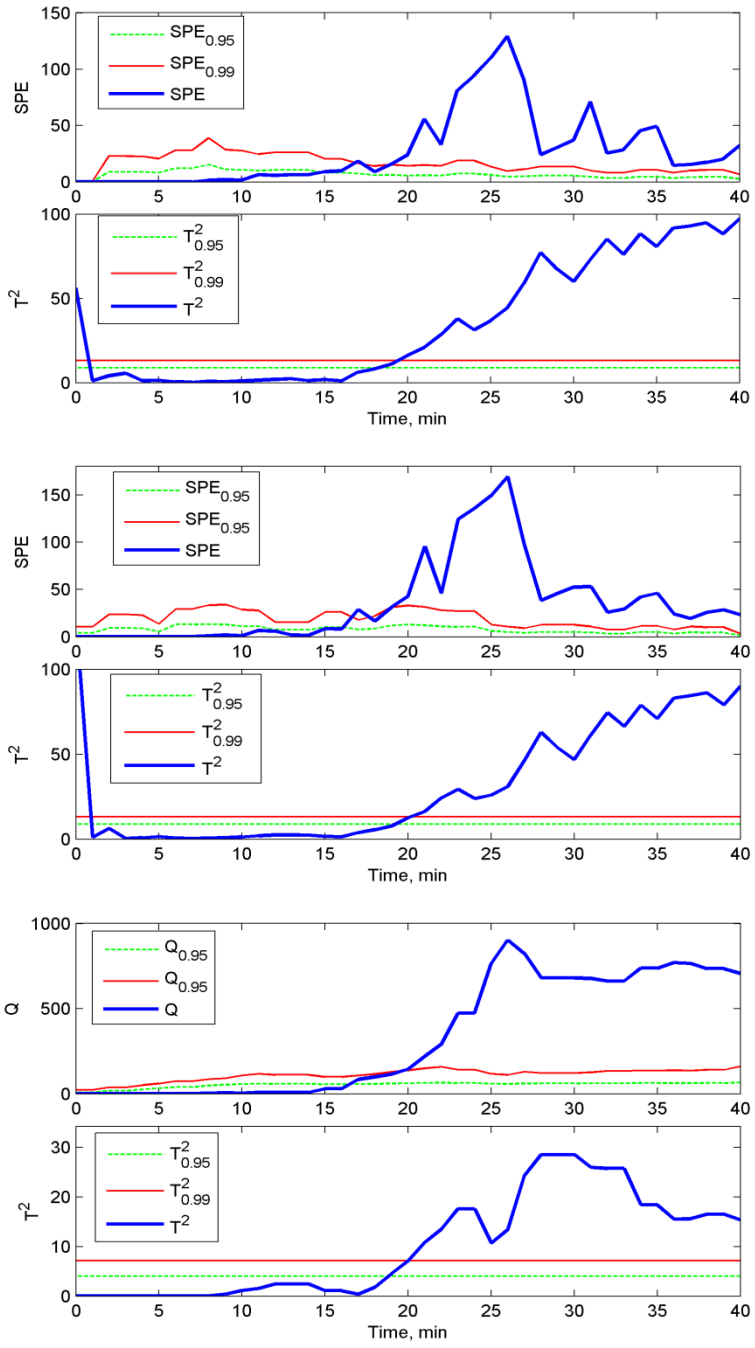

Figure 4.6: Monitoring with MPCA (top), MPLS (middle) and moving-window MPCA (bottom) for Case 2: kinetic uncertainty without control.

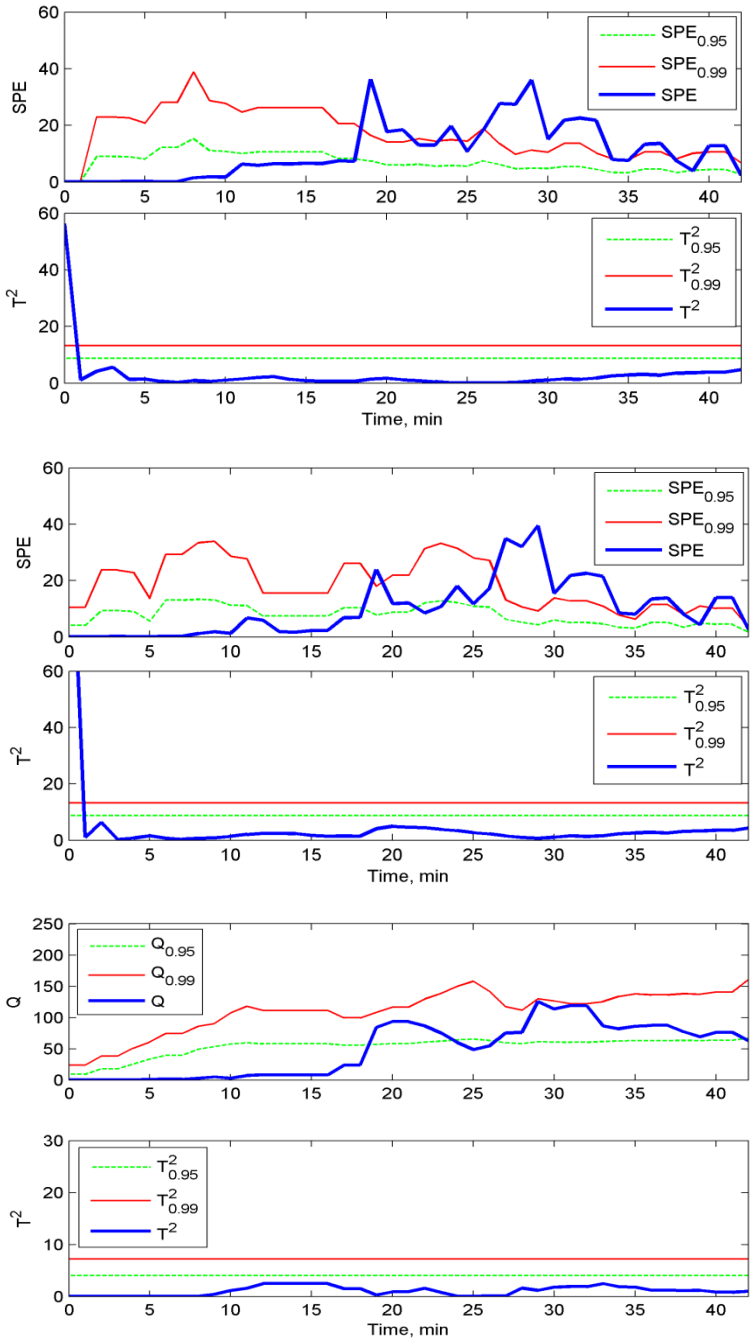

Figure 4.7: Monitoring with MPCA (top), MPLS (middle) and moving-window MPCA (bottom) for Case 3 : kinetic uncertainty with control.

4.5 Conclusions

By constructing the MPCA models at each operating time point, the moving-window MPCA is able to handle the process nonlinearity and time-varying characteristics in the batch processes. Advantages of the proposed method compared to the conventional MPCA and MPLS were demonstrated in the application to a semi-batch pH-shift reactive crystallization of L-glutamic acid, where the moving-window MPCA can not only efficiently detect the abnormal batch, but also reflect the contributions of the control actions to revert the process to in-control state. This is significant in batch process operation and monitoring to reduce the false alarms.

CHAPTER 4. STATISTICAL MONITORING OF THE PH-SHIFT REACTIVE CRYSTALLIZATION OF L-GLUTAMIC ACID

Chapter 5

Direct Design & Control of the pH-shift Reactive Crystallization of L-glutamic Acid

The direct design and control strategy is well documented to be robust against the crystallization kinetic uncertainties in cooling and antisolvent crystallization processes. This chapter investigates the feasibility to extend this control strategy to the semi-batch pH-shift reactive crystallization process of L-glutamic acid studied in this thesis as well as to develop new control strategies for this process.

5.1 Introduction

The prevalence and high value added of batch and semi-batch crystallization processes in pharmaceutical, fine chemical, and food industries have motivated the development of many control strategies (Rawlings et al., 1993; Braatz, 2002; Fevotte, 2002; Yu et al., 2004; Fujiwara et al., 2005). The direct design and control strategy which avoids the development of first-principles model has been received many applications in research and in industry for cooling and antisolvent crystallization (Ward et al., 2011; Tabora, 2012).

The solute concentration is a critical state variable for controlling crystallization processes, as the crystallization kinetics are usually written in terms of the supersaturation, which is the difference between the solute concentration and a saturated concentration. To this end, a direct design and control strategy for batch and semi-batch crystallizations that has become popular in recent years is to determine an optimal solute concentration or supersaturation trajectory against other manipulated

system state throughout the run, and then design a feedback control system to maintain the optimal relationship between the states (Zhou et al., 2006; Nagy et al., 2008a). Similar studies can also be found in tracking of necessary conditions of optimality (Srinivasan et al., 2008). Detailed uncertainty and disturbance analysis carried out both experimentally and in simulations have shown that the approach ensures the consistent production of large crystals by maintaining the supersaturation level within the metastable zone and suppressing excessive nucleation and the formation of undesired polymorphs (Kee et al., 2009a; 2009b; Yu et al., 2011). This so-called concentration control (C-control) approach, in which the trajectories of concentration vs. temperature or concentration vs. antisolvent mass fraction are tracked throughout the batch, has been implemented in many cooling and antisolvent crystallizations (Zhou et al., 2006; Nagy et al., 2008a; Kee et al., 2009a; 2009b; Cote et al., 2009; Yu et al., 2011; Tabora, 2012).

However, application of C-control to the more challenging semi-batch pH-shift reactive crystallization processes that are also common in industrial practice receives little attention. This motivates this work to investigate whether conventional C-control strategy can be successfully applied to a semi-batch pH-shift reactive crystallization using L-glutamic acid as a model compound. However, since our analysis shows that the straightforward extension of C-control is not feasible due to highly nonlinearity of the corresponding desired concentration trajectory, which has a dome-shaped profile resulting from the combined effects of reaction, crystallization, and dilution, an enhanced C-control strategy by incorporating the Just-in-Time Learning (JITL) method (Cheng and Chiu, 2004; Su et al., 2012a; 2012b), which has good predictive performance to provide useful information for C-control design to track the dome-shaped concentration trajectory closely for improved control performance, is developed in this study.

On the other hand, unlike the cooling and antisolvent crystallizations that are thermodynamically controlled with a limited supersaturation level, for a kinetically controlled and polymorphic crystallization process with relatively high supersaturation, the polymorphic purity is an important system state indicating the

competitive mechanism of polymorphic crystallization, which can be measured on-line by Raman spectroscopy (Alatalo et al., 2008; Qu et al., 2009). Thus, other than controlling the solute concentration, direct design and control based on the polymorphic purity, i.e., polymorphic purity control, is also suggested for the studied reactive crystallization process with an aim to directly control the product property of interest.

This chapter is organized as follows. The next section reviews the conventional C-control strategy applied to batch cooling crystallization. Section 5.3 gives detailed account of the proposed JITL-based C-control strategy. The direct design and control strategy based on polymorphic purity is introduced in Section 5.4, followed by the simulation studies comparing the proposed methods with the optimal flowrate control in Section 5.5. Finally, concluding remarks are made.

5.2 Conventional C-control strategy

Two methods for implementing conventional C-control have been employed for batch cooling crystallization with main difference in the choice of set point for a lower-level PID control loop, i.e., concentration set point (Nagy et al., 2008a) or temperature set point (Zhou et al., 2006), as outlined in Figure 5.1. It was argued that the controller tuning is much more difficult for the former, particularly for complicated crystallization systems (Alatalo et al., 2010b), so this study considers only the latter approach.

For illustration purpose, the implementation of conventional C-control for batch cooling crystallization (Zhou et al., 2006) is schematically shown in Figure 5.2, where the solid curve represents the desired concentration vs. temperature trajectory.

Suppose the process is operated at point A with current solute concentration $C(k)$ and temperature $T(k)$, C-control determines new set point $T^{set}(k)$ for the temperature controller by drawing a horizontal line from point A to intersect the target trajectory at point B as shown in Figure 5.2, from which $T^{set}(k)$ is specified to be the abscissa of point B. The physical significance of horizontal line aforementioned is that C-control

assumes negligible crystallization effect on the solute concentration when the solution is cooled down from the current temperature $T(k)$ to new set point $T^{set}(k)$. In practice, although the lower-level PID temperature controller can track new set points by the next sampling instant, i.e., $T(k+1) = T^{set}(k)$, the process cannot reach to point B as solute concentration at the next sample, $C(k+1)$, should be smaller than $C(k)$ due to crystallization effect, which is shown by the vertical line connecting point B to point E in Figure 5.2. Hence, by repeating the procedure of A→B→E, the desired trajectory can be tracked fairly closely by implementing C-control provided that the deviation between B and E is small, which is the case when the crystallization kinetics are slow within one sampling instant. This control strategy can be similarly applied to antisolvent crystallization by replacing the concentration vs. temperature trajectory by the concentration vs. antisolvent mass fraction trajectory (Zhou et al., 2006) and taking into account the dilution effect (Woo et al., 2009).

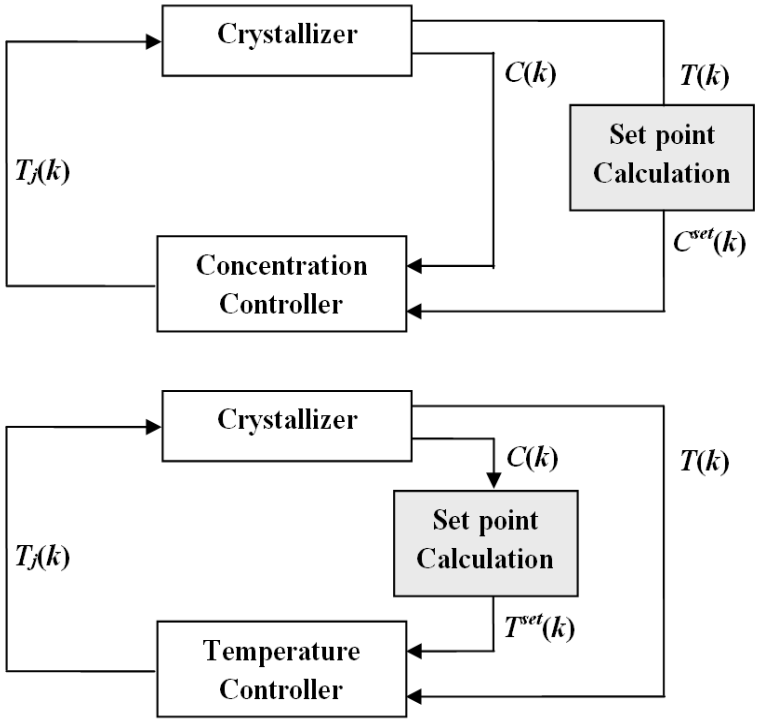

Figure 5.1: Implementation of conventional C-control using a concentration (top) or temperature (bottom) feedback controller.

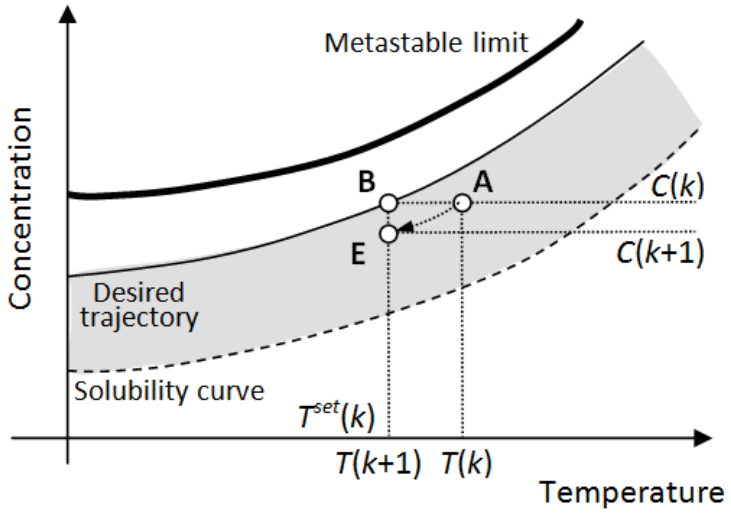

Figure 5.2: Conventional C-control for a batch cooling crystallization.

Although conventional C-control has received successful applications for both batch/semi-batch cooling and antisolvent crystallizations, it cannot be applied to control a more complicated semi-batch pH-shift reactive crystallization whose desired concentration vs. volume trajectory to be tracked by the C-control is dome-shaped (see Figure 5.3) resulting from the combined effects of reaction, crystallization, and dilution (Borissova et al., 2005; Alatalo et al., 2008; Qu et al., 2009). Consequently, the implementation of conventional C-control is not feasible because when the process is operated at the left-hand side of the dome-shape trajectory, for example point A in Figure 5.3(a) with current solute concentration $C(k)$ and corresponding solution volume $V(k)$, the implementation of conventional C-control is to draw a horizontal line from point A to intersect with the dome-shape curve at point B and the set point $V^{set}(k)$ is specified to be the corresponding abscissa of point B. However, as can be seen from Figure 5.3(a), $V^{set}(k)$ is smaller than $V(k)$, which is not possible to be implemented as solution volume increases monotonically since the start-up of process operation. On the other end, when the process operation lies at the right-hand side of the trajectory, for example at the point E, corresponding to current solute concentration $C(m)$ and solution volume $V(m)$, it is possible to implement the conventional C-control in a similar fashion as what is practiced for cooling and antisolvent crystallization.

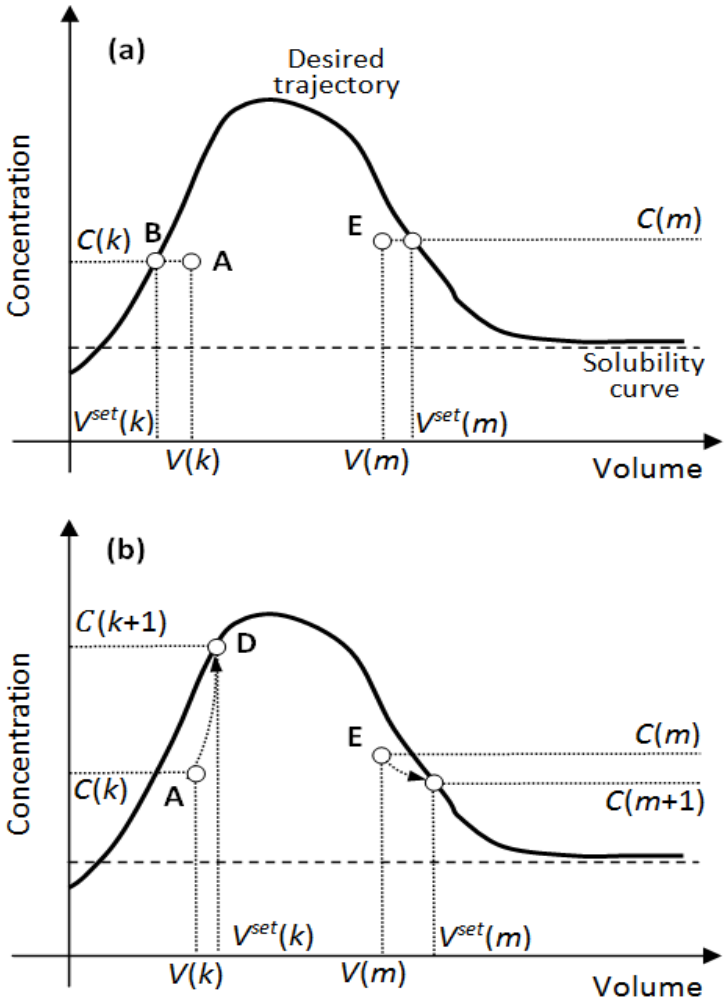

Figure 5.3: Applications of (a) conventional C-control and (b) proposed C-control for a semi-batch pH-shift reactive crystallization.

Therefore, to cope with challenging process characteristics inherent in semi-batch pH-shift reactive crystallization that impede the implementation of conventional C-control strategy, a variant of conventional C-control is developed in the next section to achieve improved performance.

5.3 JITL-based C-control strategy

Before we discuss the proposed C-control strategy, it is worthwhile pointing out that the conventional C-control strategy is in fact a model-based controller design method, which motivates the development of proposed C-control strategy. Suppose the desired

concentration vs. temperature trajectory for cooling crystallization in Figure 5.2 is given by

$$C(k) = f\left[T(k)\right] \tag{5.1}$$

where f denotes the nonlinear function describing the desired trajectory between process output C and process input T. Furthermore, given the nonlinear function g representing input and output relationship for cooling crystallization system, the following equation holds.

$$C\left(k+1\right) = C\left(k\right) + \int_{T(k)}^{T(k+1)} g\left(T\right) dT \tag{5.2}$$

The implementation of C-control is to solve the following optimization problem subject to constraints, if any, to track the desired trajectory of Eq.(5.1).

$$\begin{aligned} T^{set}\left(k\right) &= \arg\min \left\| f\left[T\left(k+1\right)\right] - C\left(k+1\right) \right\| \\ &= \arg\min \left\| f\left[T\left(k+1\right)\right] - C\left(k\right) - \int_{T(k)}^{T(k+1)} g\left(T\right) dT \right\| \\ &= \arg\min \left\| f\left[T^{set}\left(k\right)\right] - C\left(k\right) - \int_{T(k)}^{T^{set}(k)} g\left(T\right) dT \right\| \end{aligned} \tag{5.3}$$

where a lower level PID temperature controller is assumed to reach new set point within one sampling instant, i.e., $T(k+1) = T^{set}(k)$.

As discussed previously, conventional C-control strategy illustrated in Figure 5.2 neglects the crystallization effect when temperature decreases from $T(k)$ to $T^{set}(k)$, meaning that $g(T) = 0$ or equivalently, $C\left(k+1\right) = C\left(k\right)$ based on Eq. (5.2). Therefore, the optimal solution for Eq. (5.3) can be obtained by solving Eqs. (5.1) and (5.2) simultaneously, which is equivalent to the conditions inferred by the intersect B in Figure 5.2. In the case of semi-batch antisolvent crystallization, the C-control problem can be analogously formulated by replacing temperature T in Eqs. (5.1) to (5.3) by W which is the mass fraction of antisolvent. Therein, the corresponding

$g(W)$ only considers the dilution of solute concentration resulting from the addition of antisolvent (Woo et al., 2009).

Motivated by the on-going analysis, by replacing the temperature T in Eqs. (5.1) to (5.3) by volume V, a model-based C-control approach by incorporating a process model capable of predicting the solute concentration in complicated pH-shift reactive crystallization is developed in the ensuing discussion. Suppose the process is operated at point A in Figure 5.3(b) with current volume $V(k)$ and solute concentration $C(k)$, the proposed C-control determines new set point $V^{set}(k)$ for the volume controller by predicting the dotted line A→D to intersect the desired trajectory at point D and the set point $V^{set}(k)$ is specified to be the corresponding abscissa of point D, i.e., $V^{set}(k) = V(k+1)$. Therefore one key step to determine the intersect is to predict future concentration at point D, $C(k+1)$, by the process model using current and past process data $V(k)$ and $C(k)$ as well as a pre-specified $V^{set}(k)$. The intersect D is then obtained when the point $[V(k+1), C(k+1)]$ discussed above is located at desired trajectory.

In this paper, a data-based Just-in-Time Learning (JITL) modelling method (Cheng and Chiu, 2004; Fujiwara et al., 2009; Ge and Song, 2010; Su et al., 2012b) is incorporated for the proposed C-control strategy. There are three main steps in the JITL methods to predict future process output corresponding to a query data: (a) relevant data samples in the reference database are searched to match the query data by some nearest neighbourhood criterion; (b) a local model is built based on the relevant data; (c) model output is calculated based on the chosen local model and the query data. The local model is then discarded right after the prediction is obtained. When the next query data comes, a new local model will be built according to the above procedure. In the proposed C-control design, future solute concentration $C(k+1)$ is predicted by the JITL method using the following ARX model:

$$C(k+1) = \alpha_1^k C(k) + \beta_1^k V(k) + \beta_2^k V(k+1) \tag{5.4}$$

The implementation of proposed JITL-based C-control is summarized as following:

(1) At sampling instant k, both $C(k)$ and $V(k)$ are measured;

(2) For a chosen value of $V^{set}(k)$, which by assumption is the solution volume at the $k+1$ sampling instant, i.e., $V(k+1) = V^{set}(k)$;

(3) The predicted concentration at the $k+1$ sampling instant, $C(k+1)$, is obtained by the JITL method using query data $q = [C(k), V(k), V(k+1)]$; while the solute concentration $\tilde{C}(k+1)$ in the target trajectory corresponding to $V(k+1)$ is readily obtained, for example, by interpolation;

(4) By comparing $C(k+1)$ and $\tilde{C}(k+1)$, the bisection method is used to update $V^{set}(k)$ subject to constraints due to the minimum and maximum flowrates;

(5) Repeat Steps 2 to 4 until $V^{set}(k)$ converges and this corresponding $V^{set}(k)$ is set as the set point for the lower-level PID controller.

5.4 Polymorphic purity control strategy

It is worthwhile pointing out that the simplicity and robustness of the conventional C-control strategy in batch cooling crystallization mainly rely on the monotonic decreasing relationship between solute concentration and temperature. Thus, a simple intersection in the desired trajectory, as shown in Figure 5.2, is possible to find a feasible temperature setpoint. Similar observation is also found for batch antisolvent crystallization. Although solute concentration is used in the proposed JITL-based C-control strategy for a challenging semi-batch reactive crystallization, however, with the recent development of *in situ* real-time measurements for crystallization processes that may also show monotonic decreasing or increasing and are more product quality related, alternative system state variable can also be considered in the direct design and control. For example, the polymorphic purity by Raman spectroscopy (Alatalo et al., 2008; Qu et al., 2009), which is an important system state, particularly, for the polymorphic crystallization encountered in the studied process, showing a monotonic increasing throughout the batch. Besides, batch time is also an important system state that behaves monotonic increasing throughout the batch. If the batch time is plotted

against the desired optimal crystallizer volume trajectory as shown in Figure 5.4, then tracking this time vs. crystallizer volume trajectory, actually, is the optimal flowrate control, wherein the nominal optimal flowrate profile is followed.

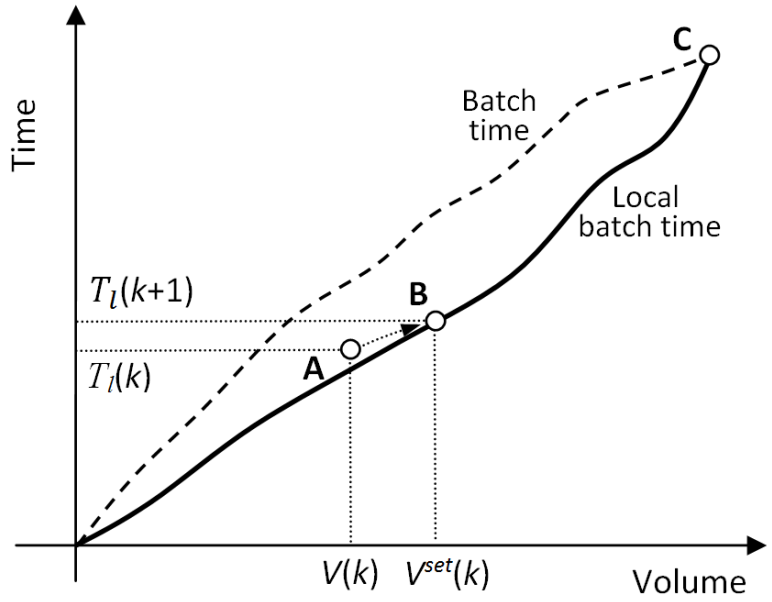

Figure 5.4: Batch time and local batch time.

Therefore, by combining the batch time and one of those monotonically increasing product property variables would also lead to a desired optimal trajectory that can be tracked on line by simple intersection. For example, the local batch time, T_l, defined in such a way that the batch time is scaled by those interested product property variables, M, shown as follows.

$$T_l = t \times \left[\frac{M}{M_{max}} \right]^w \tag{5.5}$$

where t is the batch time, M_{max} is the nominal maximum value of this variable at the batch end, w is a tuning parameter balancing priorities between batch time and state tracking. Therefore, the local bath time is devised to reflect the progress of the interested state variable inside the crystallizer and take control actions accordingly. Similar to Eqs. (5.1) to (5.3), the implementation of local batch time tracking can be represented as follows

$$T_l = f(V) \tag{5.6}$$

$$T_l(k+1) = t(k+1) \times \left[\frac{M(k)}{M_{max}} \right]^w \tag{5.7}$$

$$V^{set}(k) = \arg\min \left\| f\left[V^{set}(k) \right] - T_l(k+1) \right\| \tag{5.8}$$

where the process model (5.7) neglects the crystallization effect by assuming $M(k+1) = M(k)$. As the crystal property M is only directly affected by crystallization effect, the volume set point for next sampling time, $V^{set}(k)$, is obtained by solving Eqs. (5.6) and (5.7) simultaneously as schematically shown in Fig. 5.4. In the next section, the α-form polymorphic purity is incorporated to characterize the local batch time which is referred as the polymorphic purity control in this thesis.

5.5 Results and discussion

5.5.1 Nominal optimal trajectories

The first-principles mathematical model developed in Chapter 3 from the published data (Alatalo et al., 2008; Qu et al., 2009) was used to simulate the semi-batch pH-shift reactive crystallization of L-glutamic acid. The nominal experimental procedure can be found in Chapter 4. For ease of reference, this procedure is also briefly summarized here. The 0.97 L crystallizer is initially filled with 0.65 L of monosodium glutamate (MSG) of 1.0 mol/L and the default batch time is 40 min. The manipulated variable is the addition flowrate of sulfuric acid (SA) of 1.0 mol/L, which is constrained between 0 and 16 ml/min while adjusted every minute to achieve the maximum polymorphic purity of α-form, volume-based mean crystal size, and product yield of the final crystalline product at the batch end. The Pareto-optimality front for this multi-objective optimization is shown in Figure 5.5, which is solved using the Non-dominated Sorting Genetic Algorithm-II (NSGA-II) (Deb et al., 2002). The chosen optimal operating point is denoted by the star symbol in Figure 5.5 and the corresponding optimal state trajectories are shown in Figures 5.6 and 5.7.

5.5.2 Training database for JITL modeling

To proceed to the proposed JITL-based C-control strategy, reference database for the JITL method is generated using process data of fifty batches obtained by perturbing the nominal optimal flowrate profile corresponding to the volume profile given in Figure 5.6(a) with a normal distribution of N(0, 1.0) at each sampling instant and varying initial concentrations of monosodium glutamate and sulfuric acid with N(0, 0.02) for each batch. This database is the same as that used for process monitoring discussed in Chapter 4. The resulting concentration data used to construct reference database are shown in Figure 5.8. To evaluate prediction accuracy of the JITL method with local model given in Eq. (5.4), ten additional batches of process data are used for the validation test. As can be seen from Figure 5.9, JITL method gives accurate prediction of solute concentration.

5.5.3 Case studies of process uncertainties

To evaluate the performances of the proposed JITL-based C-control and polymorphic purity control, uncertainties in the kinetics of crystal growth and nucleation of the polymorphic crystallization system, i.e., α- and β-form polymorphs of L-glutamic acid, as well as the disturbances in feeding concentrations are considered. For the purpose of comparison, optimal flowrate control obtained by the multi-objective optimization is used as the benchmark design.

The first case study considers a 20% reduction of the growth rate of α-form crystal. Figure 5.10 shows that the JITL-based C-control gives the best tracking of the nominal optimal concentration vs. volume trajectory, which is denoted by the optimal trajectory in Figure 5.10, compared with the other two control strategies. This demonstrates the capability of the proposed C-control to handle nonlinearity in the nominal optimal trajectory. However, the improvement of three important performance indices for crystallization, i.e., polymorphic purity, mean crystal size and product yield, attained by the proposed C-control is modest as shown by Table 5.1 and Figure 5.11, where the evolution of three performance indices is shown. This

finding is in sharp contrast to batch cooling or antisolvent crystallization processes, where conventional C-control strategy has produced robust performance by only tracking the nominal optimal concentration trajectory. The degraded performance of C-control in this particular pH-shift reactive crystallization process is because the glutamic acid concentration is affected by competing polymorphic crystallizations and the relative rates of these competing processes cannot be observed by measuring only the glutamic acid concentration. For example, the stable β-form polymorph can consume the solute at the expense of the α-form that is less active than normal for a 20% decrease in crystal growth rate. In contrast, applications of conventional C-control to the cooling and antisolvent crystallization processes are operated under condition that either the formation of alternative polymorphic forms is suppressed or only one polymorph can grow and other polymorphs dissolve (Hermanto, 2008; Kee et al., 2009a; 2009b).

On the other hand, the direct design and control by polymorphic purity gives quite promising result as shown in Figure 5.11 and Table 5.1, with the three performance indices trajectory closest to the optimal trajectory, as well as their batch-end values approach the nominal optimal. This is because the polymorphic purity more directly reflects the progress of a polymorphic crystallization than the concentration. The tracking of the nominal optimal local batch time trajectory, with a weight of $w = 1$, based on polymorphic purity is shown in Figure 5.12. Actually, the control actions started only after the polymorphic purity measurements by Raman spectroscopy were steadily available at the batch time of 12 minute, before that the nominal optimal flowrate profile is followed. The corresponding control actions or flowrate profiles of the three controllers are given in Figure 5.13, wherein the extended total batch time are observed for JITL-based C-control and polymorphic purity control.

Next, performance of the three controller designs is compared when 20% reduction of nucleation rate of the α-form crystal is considered. In this case, the JITL-based C-control also gives best tracking of the nominal optimal concentration vs. volume trajectory (Su et al., 2012a), but with only slight improvement over the flowrate control in the three performance indices as indicated by Table 5.1 and Figure 5.14. It

is noted that the polymorphic purity control gives higher polymorphic purity and larger crystals than those obtained by the optimal flowrate control (see Table 5.1 and Figure 5.14).

Lastly, process disturbances in the initial concentration of MSG and the feed concentration of SA are taken into account. It is assumed that the former is decreased to 0.95 mol/L and the latter increased to 1.05 mol/L so that higher supersaturation is generated at the initial phase of the batch but less durable at the later phase of the batch (see Figure 5.15). High supersaturation favors growth of the α-form polymorph, which increases the crystal product yield, as seen in Table 5.1. Also observed is that polymorphic purity control gives the best control performance, though the C-control achieves the best tracking of the optimal concentration trajectory in Figure 5.15.

Table 5.1: Summary of the three case studies.

Case study	Controller	Batch time, min	Polymorphic purity	Mean crystal size, μm	Product yield
Nominal case	Flowrate control	40	0.826	250.615	0.809
-20% of growth rate for the α-form crystals	Flowrate control	40	0.707	210.839	0.804
	JITL-based C-control	44	0.736	219.721	0.816
	Polymorphic purity control	42	0.793	241.432	0.806
-20% of nucleation rate for the α-form crystals	Flowrate control	40	0.793	247.389	0.808
	JITL-based C-control	41	0.799	249.311	0.815
	Polymorphic purity control	40	0.832	265.166	0.810
Excess SA (MSG = 0.95 mol/L, SA = 1.05 mol/L)	Flowrate control	40	0.798	241.818	0.820
	JITL-based C-control	40	0.797	243.240	0.818
	Polymorphic purity control	41	0.806	245.251	0.821

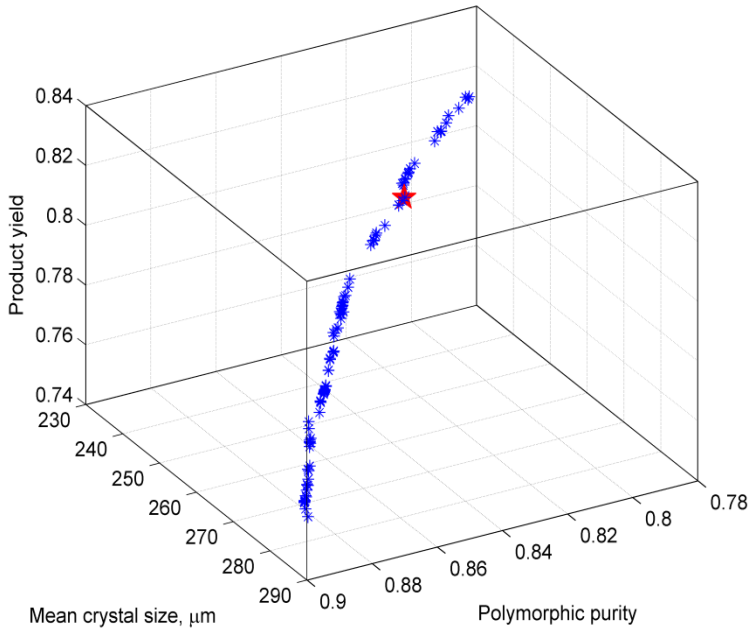

Figure 5.5: Pareto-optimality front obtained for optimal control of a semi-batch pH-shift reactive crystallization.

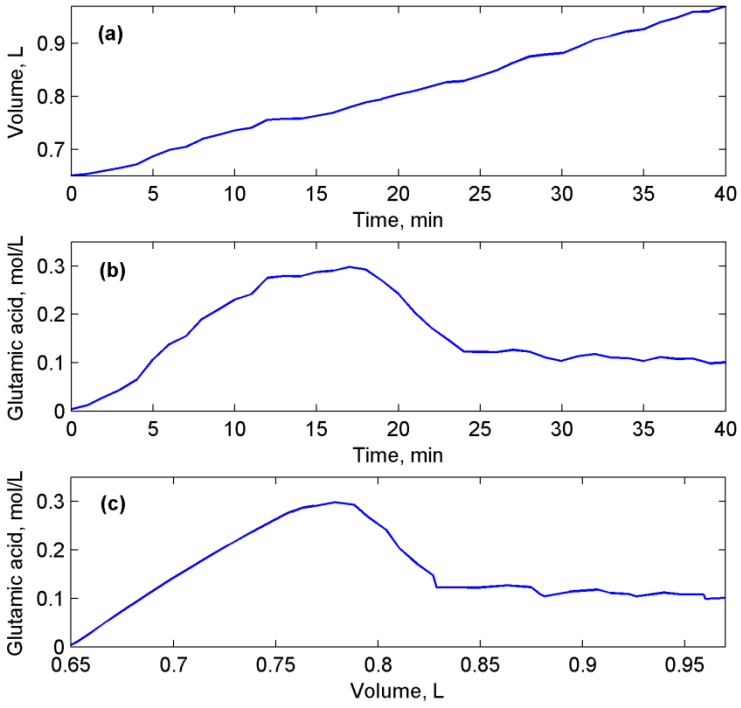

Figure 5.6: Optimal profiles for (a) solution volume, (b) solute concentration, and (c) concentration vs. volume trajectory.

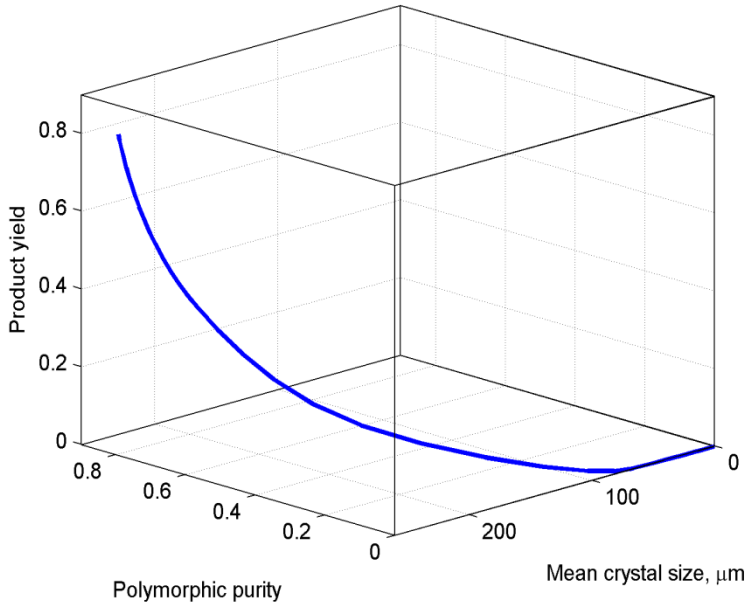

Figure 5.7: Optimal trajectory for the three performance indices.

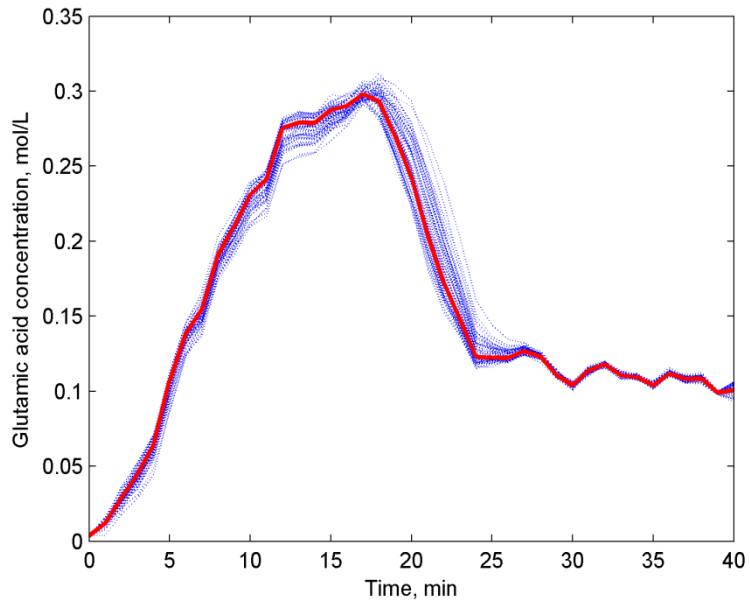

Figure 5.8: Solute concentration data generated to construct reference database for the JITL method.

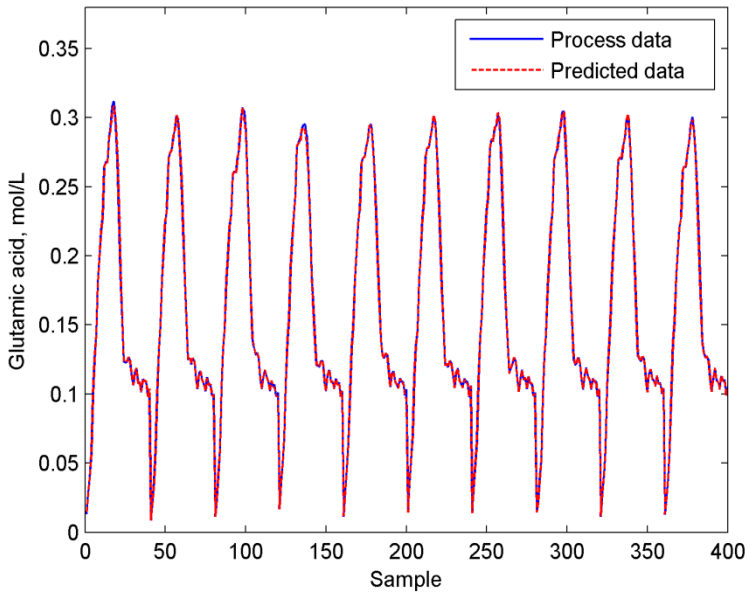

Figure 5.9: Validation result for the JITL method (root mean squared error = 0.0012).

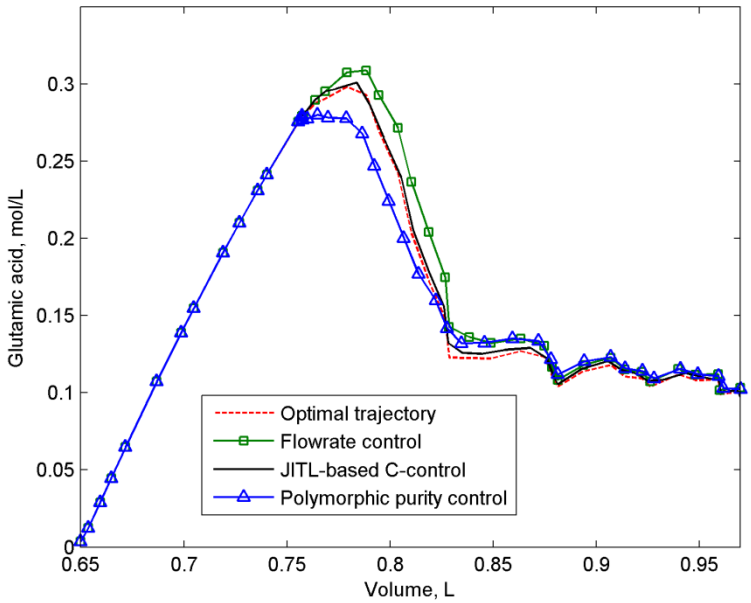

Figure 5.10: Concentration vs. volume trajectories obtained for 20% reduction of growth rate for the α-form crystal.

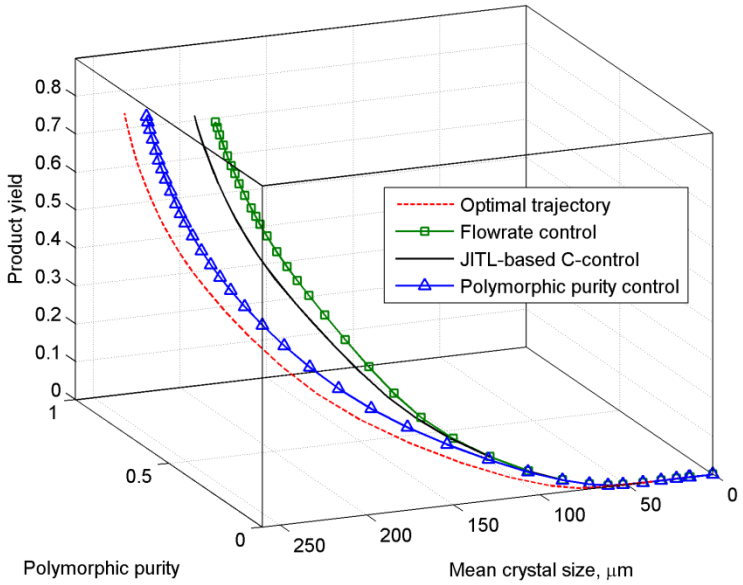

Figure 5.11: Profiles of the three performance indices obtained for 20% reduction of growth rate for the α-form crystal.

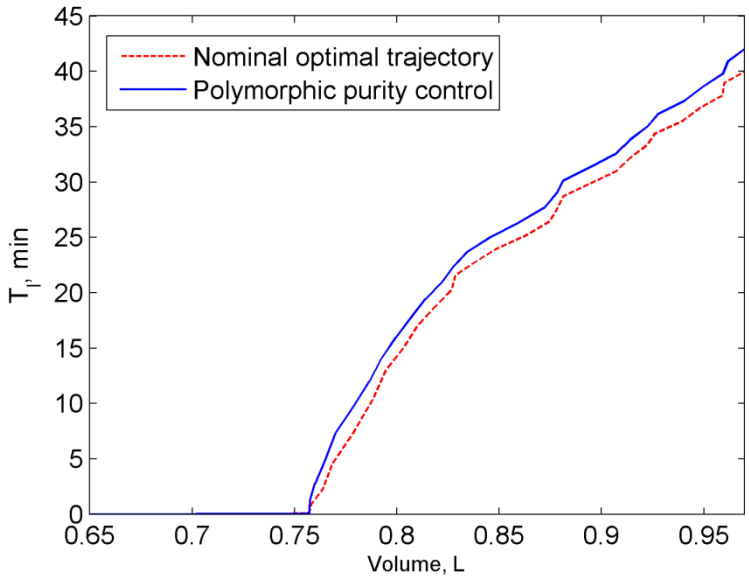

Figure 5.12: Local batch time tracking by polymorphic purity control for 20% reduction of growth rate for the α-form crystal.

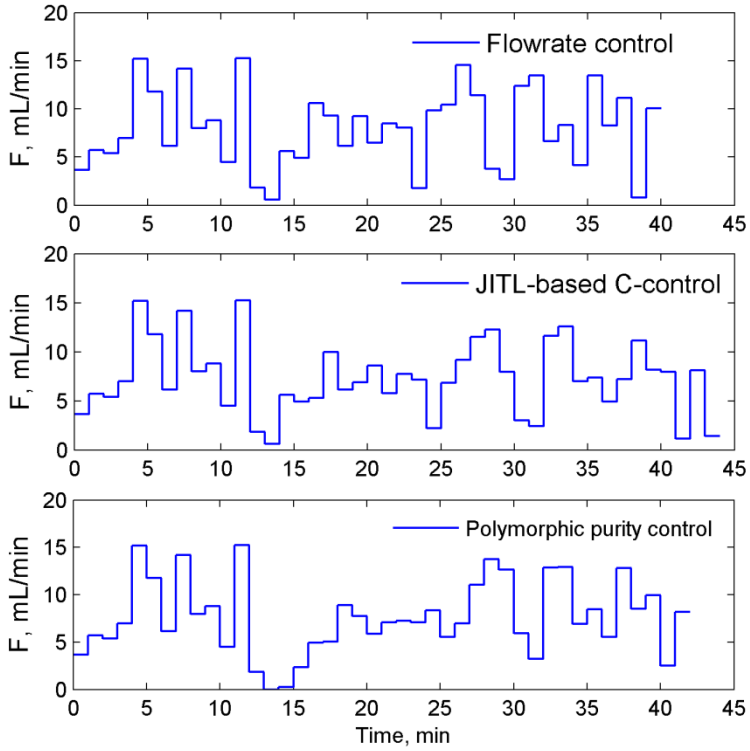

Figure 5.13: Flowrate profiles obtained for 20% reduction of growth rate for the α-form crystal.

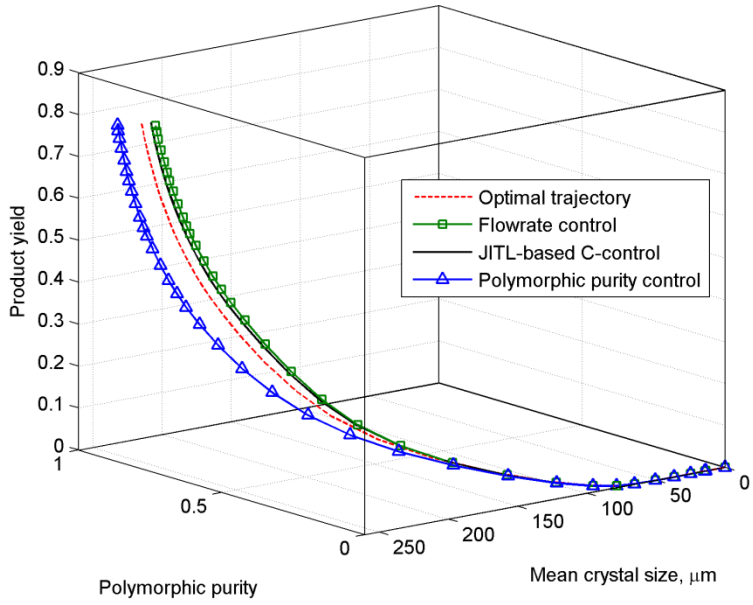

Figure 5.14: Profiles of the three performance indices obtained for 20% reduction of nucleation rate for the α-form crystal.

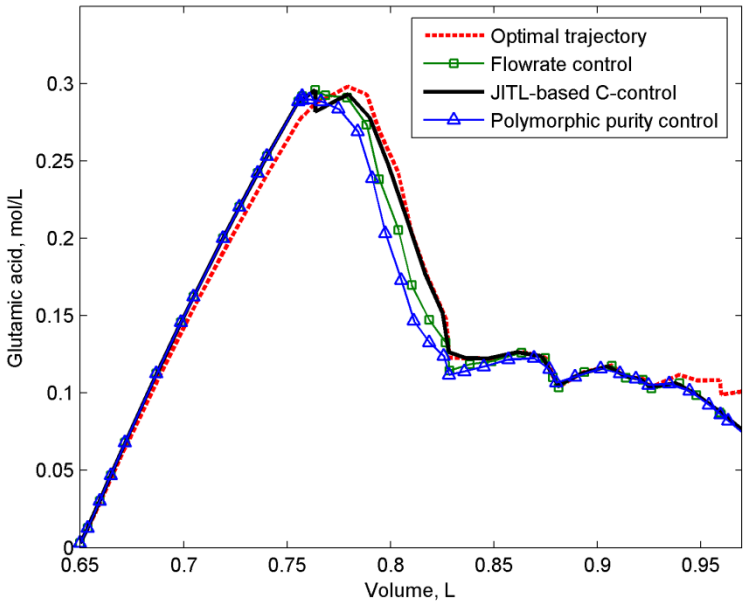

Figure 5.15: Concentration vs. volume trajectories obtained for step disturbances in initial MSG and SA feed concentration.

5.6 Conclusions

This chapter extends the idea of C-control strategy to the studied semi-batch pH-shift reactive crystallization process by incorporating a process model to better cope with the highly nonlinear dynamics inherent in the process. Another direct design and control strategy based on polymorphic purity is also proposed by the definition of local batch time. Although the JITL-based C-control is more robust in tracking the nominal optimal concentration trajectory, the performance improvement gained is either modest or marginal. This may imply that the solute concentration measurement cannot fully reflect the complexity of competitive polymorphic crystallization. Whereas the polymorphic purity control achieves much better performance, as it is closely related to the progress of polymorphic crystallization and is more direct to the product quality than the concentration.

Chapter 6

Nonlinear MPC Control of the pH-shift Reactive Crystallization of L-glutamic Acid

The development of nonlinear model predictive control (NMPC) techniques has been received intensive interests in past decades. However, NMPC techniques that are specifically designed for batch process are rather limited (Morari and Lee, 1999; Qin and Badgwell, 2003; Bonvin et al., 2006). This chapter focuses on the development of an improved extended prediction self-adaptive control (EPSAC) technique and its application to control a semi-batch pH-shift reactive crystallization process.

6.1 Introduction

With the stringent specification on product quality, tighter environmental regulation of effluent stream, and higher competition in the process industry, the development of nonlinear model predictive control (NMPC) is of interest to both the academic and industrial sectors. The major advantage of NMPC lies in its capability of handling nonlinearities and time-varying characteristics inherent in the process dynamics in addition to address constraints and bounds imposed on both state and manipulated variables by performing the real-time dynamic optimization (Manenti, 2011; Darby and Nikolaou, 2012). Toward this end, various NMPC design methods were developed using different techniques to deal with process nonlinearity, including successive linearization (Lee and Ricker, 1994), neural networks (Peng et al., 2007), robust control (Nagy and Braatz, 2003; Nagy and Allgöwer, 2007), multiple models (Özkan et al., 2000; Cervantes et al., 2003; Garcia-Nieto et al., 2008; Kuure-Kinsey and Bequette, 2010), and hybrid models (Hermanto et al., 2011).

Among various NMPC design methods reported in the literature, the extended prediction self-adaptive control (EPSAC) or its variants adopted a unique approach of successive linearization based on the given input trajectory (De Keyser and Cauwenberghe, 1985). In the EPSAC design framework, the model prediction consists of a base and an optimized term. The former is computed from a nominal process model using the current values of input variables obtained from the predefined base input trajectory and the corresponding output variables, while the latter from a finite step or impulse response model obtained along this trajectory. Gálvez-Carrillo et al. (2009) extended the EPSAC algorithm by integration with a dead-time compensator and reported its application to a solar power plant. Hermanto et al. (2009) employed the EPSAC to a polymorphic batch crystallization system with constraints imposed on state variables, better performance was achieved compared to that obtained by quadratic dynamic matrix control (QDMC) based on a set of models obtained by successive linearization at different sampling instants (Garcia and Morshedi, 1986).

However, one potential drawback of the previous EPSAC methods is the incorporation of a convolution model in the formulation of the control algorithms. Since model parameters are obtained by introducing a step change to the current input value specified by the base input trajectory, the predicted outputs by such model for sampling instants further away from the current sampling instant become less accurate due to process nonlinearity, leading to inevitable modeling error that degrades the achievable control performance. This shortcoming may even become worse when the EPSAC is applied in batch process control with operation objective to control the product quality at batch end. As a long prediction horizon is needed at the beginning of the batch run to predict the future process outputs for the remaining batch time, this eventually leads to inaccurate predicted outputs and poor control performance as a result.

Instead of convolution models, state-space model offers an attractive option due to its inherent flexibility to represent nonlinear process and to allow a more

approaches to modeling unmeasured disturbance in the estimator (Darby and Nikolaou, 2012). For example, Lee and Ricker (1994) designed an extended Kalman filter NMPC based on successive linearization, where a series of linear state-space models were constructed for future sampling instants in the prediction horizon. Their linearization started from the current sampling instant and linearized forwardly by calculating Jacobin matrix of the nonlinear model. Cervantes et al. (2003) put forward a nonlinear model predictive control based on Wiener piecewise linear models. The Wiener model consists of two blocks, a linear state-space model cascaded with an invertible continuous piecewise linear functions, to represent the nonlinear dynamic of the system. To explore the special structure of Wiener model, various control schemes were developed with an aim to take advantage of the simple dynamics of linear block in the Wiener model. In this work, a linear MPC algorithm is applied based on the linear block to enjoy the computational simplicity. García-Nieto et al. (2008) reported a NMPC application based on local model networks to a diesel engine. A set of linear local state-space models were identified offline upon selected operating points in the system state space. Basis functions which represent the distance between the current operating point and those selected operating points were used as weights to sum up all the predictions from each local model. Peng et al. (2007) presented a NMPC scheme using local ARX state-space models whose model parameters were estimated using RBF neural network. Motivated by the aforementioned discussion, the aim of this chapter is to formulate the EPSAC algorithm using state-space models for its inherent flexibility to represent stable, integrating, and unstable processes (Garcia et al., 1989; Morari and Lee, 1999; Qin and Badgwell, 2003; Froisy, 2006; Manenti, 2011; Darby and Nikolaou, 2012). Specifically, a new EPSAC algorithm based on the Just-in-Time Learning (JITL) method is developed in this chapter. In the proposed JITL-based EPSAC design, the optimized term is obtained by a set of local state-space models identified by the JITL method along the base trajectories. To evaluate the performance of proposed design for batch process control, simulation results of implementing the JITL-based EPSAC to pH-shift reactive crystallization process are presented and discussed in detail.

This chapter is organized as follows. The conventional EPSAC algorithm is reviewed in section 6.2, followed by the development of proposed JITL-based EPSAC algorithm in section 6.3. Section 6.4 discusses the case studies of the proposed EPSAC algorithm applied to the semi-batch pH-shift reactive crystallization of L-glutamic acid. Finally, concluding remarks are drawn in the last section.

6.2 Conventional EPSAC algorithm

NMPC refers to model based predictive control schemes that are based on nonlinear models and/or consider a non-quadratic cost function and nonlinear constraints (Allgöwer et al., 2004), whose optimal problem to be solved online at every sampling instant is shown below (Hermanto et al., 2009):

$$\min_{\mathbf{u}_k} J\left(\mathbf{x}_k, \mathbf{u}_k\right) \tag{6.1}$$

subject to

$$\mathbf{x}_k = f\left(\mathbf{x}_{k-1}, \mathbf{u}_{k-1}\right) + \mathbf{w}_k \tag{6.2}$$

$$\mathbf{d}_k = \mathbf{d}_{k-1} + \boldsymbol{\xi}_k \tag{6.3}$$

$$\mathbf{y}_k = g\left(\mathbf{x}_k, \mathbf{u}_k\right) + \mathbf{d}_k + \mathbf{v}_k \tag{6.4}$$

$$h\left(\mathbf{x}_k, \mathbf{u}_k\right) \le \mathbf{0} \tag{6.5}$$

where J is the objective function; $\mathbf{x}_k$, $\mathbf{u}_k$, $\mathbf{y}_k$, and $\mathbf{d}_k$ are the vectors of n_x system state variables, n_u inputs, n_y measured variables, and n_y unmeasured disturbances at the kth sampling instant; and $\mathbf{w}_k$, $\boldsymbol{\xi}_k$, and $\mathbf{v}_k$ are the vectors of noise on the state variables, unmeasured disturbances, and the measured variables, respectively. The system dynamics are described by the vector function f, the measurement equations by the vector function g, and the linear and nonlinear constraints for the system are described by the vector function h.

The EPSAC strategy considers that the future response can be expressed as the cumulative result of two effects: (1) a base response that accounts for the effect of past control, a base future control scenario, and the effect of future disturbances; and (2) an optimizing response that accounts for the effect of the optimizing future control actions (Gálvez-Carrillo et al., 2009), as schematically illustrated in Figure 6.1. The future sequences of the input variables $\mathbf{u}_{k+i}$ is considered as the sum of the base input $\mathbf{u}_{b,\,k+i}$ and future incremental control actions $\delta\mathbf{u}_{k+i}$:

$$\mathbf{u}_{k+i} = \mathbf{u}_{b,\,k+i} + \delta\mathbf{u}_{k+i}, \quad i = 0,\, 1,\, \cdots,\, N_u - 1 \tag{6.6}$$

where N_u is the control horizon and $\delta\mathbf{u}_{k+i} = \mathbf{0}$ for $i \geq N_u$. Then the future trajectories of process variables can also be considered as the cumulative result of these two effects:

$$\mathbf{x}_{k+i} = \mathbf{x}_{b,\,k+i} + \mathbf{x}_{l,\,k+i}, \quad i = 1,\, 2,\, \cdots,\, N_p \tag{6.7}$$

where N_p is the prediction horizon and $\mathbf{x}_{b,\,k+i}$ is calculated using the normal model of Eq. (6.2) and the predetermined sequence of $\mathbf{u}_{b,\,k+i}$. On the other hand, $\mathbf{x}_{l,\,k+i}$ is obtained by implementing impulse inputs $\left\{\delta\mathbf{u}_k,\, \delta\mathbf{u}_{k+1},\, \cdots,\, \delta\mathbf{u}_{k+i-1}\right\}$. A similar decomposition into the sum of two parts is also applied to the nonlinear constraints of Eq. (6.5) to arrive at a quadratic program (QP) problem. The soft-constraint approach was used to provide a numerical convergence of QP optimizer (Scokaert and Rawlings, 1999; Hermanto et al., 2009).

The key idea of EPSAC is to predict nonlinear process variables by iterative linearization with respect to future trajectories so that they converge to the same nonlinear optimal solution (Rueda et al., 2005; Hermanto et al., 2009; Gálvez-Carrillo et al., 2009). Generally, the conventional EPSAC algorithms use convolution models to perform linearization around the future trajectories in order to calculate the optimized term $\mathbf{x}_{l,\,k+i}$ in Eq. (6.7) from $\delta\mathbf{u}_{k+i}$ in Eq. (6.6).

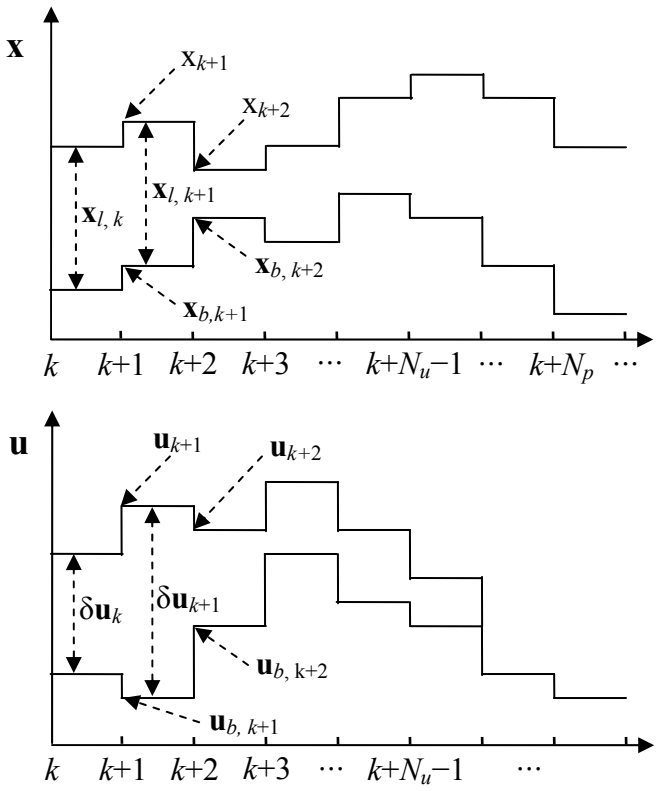

Figure 6.1: The variables decomposition in EPSAC method.

It is worth pointing out that the superposition principle underlying the linearization schemes given in Eqs. (6.6) and (6.7) by previous EPSAC designs becomes invalid for the cases of highly nonlinear and time-varying process characteristics with requirement of long prediction horizon. This is because the process dynamics at the current sampling instant where a convolution model is obtained for model prediction is different from those far away in the prediction horizon, resulting in inaccurate model prediction and consequently has inevitable adverse effect on the control performance achieved by the EPSAC control strategy. To partially address this shortcoming brought about by using the convolution models in the EPSAC design, complicated weights in the objective function were designed and fine-tuned to improve end product quality control of a batch crystallization process (Hermanto et al., 2009). A detailed analysis of the aforementioned results reveals that the resulting fine-tuned EPSAC design with complicated weights attempts to suppress future control moves deep in the control horizon so that the achievable control performance of the EPSAC design is not compromised by the poor prediction of convolution

models. This observation is consistent with our analysis that the predictive performance of convolution models would deteriorate for those future sampling instants in the prediction horizon distant from the current sampling instant. Motivated by this observation and to avoid the tedious design of the weights by trial and error as well as the time-consuming tuning of weights to achieve good control performance, a systematic EPSAC design framework without resorting to the convolution models is developed in the next section.

6.3 The JITL-based EPSAC design

6.3.1 JITL local state-space model

Generally, linear or nonlinear processes operated within a narrow range of an operating point, i.e., $\{\mathbf{x}_0, \mathbf{u}_0\}$, could be described by a state-space model as shown below:

$$\tilde{\mathbf{x}}_{k+i+1} = \mathbf{A}\tilde{\mathbf{x}}_{k+i} + \mathbf{B}\tilde{\mathbf{u}}_{k+i} \tag{6.8}$$

where $\tilde{\mathbf{x}}_{k+i}$ is the deviation between system state vector $\mathbf{x}$ and the chosen operating point $\mathbf{x}_0$, viz., $\tilde{\mathbf{x}}_{k+i} = \mathbf{x}_{k+i} - \mathbf{x}_0$, at kth sampling instant, the deviation variable for process input vector is also defined accordingly, $\tilde{\mathbf{u}}_{k+i} = \mathbf{u}_{k+i} - \mathbf{u}_0$, $\mathbf{A}$ is a $n_x \times n_x$ matrix, and $\mathbf{B}$ is a $n_x \times n_u$ matrix.

Analogically, considering the reference trajectory of $\{\mathbf{x}_{b,\,k+i}, \mathbf{u}_{b,\,k+i}\}$ in Figure 6.1, a series of local state-space models could also be obtained at each sampling instant in the prediction horizon as follows:

$$\mathbf{x}_{l,\,k+i+1} = \mathbf{A}_{k+i}\mathbf{x}_{l,\,k+i} + \mathbf{B}_{k+i}\delta\mathbf{u}_{k+i} \tag{6.9}$$

The implementation of using Eqs. (6.8) and (6.9) in nonlinear modeling is illustrated in Figure 6.2, where Eq. (6.8) employs a single linear model obtained at point $\mathbf{x}_0$ to approximate process nonlinearity, while Eq. (6.9) requires a set of linear

local models constructed for each sampling instant in the reference trajectory $\mathbf{x}_b$ for the same purpose. It is obvious from Figure 6.2 that the latter gives more accurate description of the base trajectory. Thus, Eq. (6.9) is inherently more advantageous than Eq. (6.8) for nonlinear trajectory modeling and therefore is more suitable for the ESPAC design as it can lessen the aforementioned drawbacks due to the use of convolution models in majority of ESPAC design. It also note that the proposed method is in fact a multiple model approach, which has been extensively applied and incorporated into controller design for nonlinear processes (Lee and Ricker, 1994; Foss et al., 1995; Dharaskar and Gupta, 2000; Özkan et al., 2000; Cervantes et al., 2003; Peng et al., 2007; García-Nieto et al., 2008).

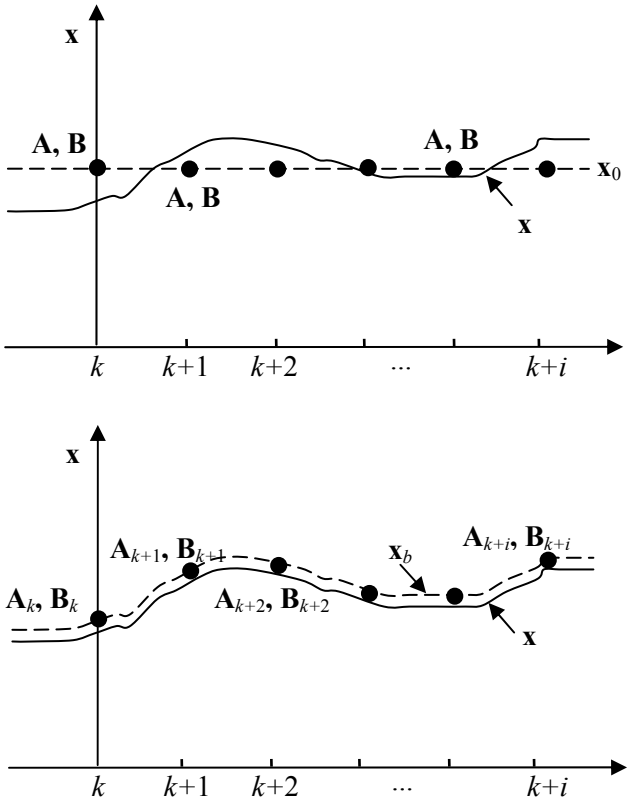

Figure 6.2: Modeling of nonlinear processes using one local state-space model given in Eq. (6.8) (top) and multiple state-space models given in Eq. (6.9) (bottom).

In this work, the JITL method is implemented to obtain a set of models given in Eq. (6.9). The JITL method has received increasing research interest and has been applied to soft sensing, process monitoring, and controller design recently (Cheng and Chiu,

2004; 2005; 2007; 2008; Hlaing et al., 2007; Kalmukale et al., 2007; Kansha and Chiu, 2008; 2010; Nuella et al., 2009; Fujiwara et al., 2009; Ge and Song 2010; Kano et al., 2011; Su et al., 2012b; Yang et al., 2012). The JITL method is a data-based methodology to approximate a nonlinear system by a local model valid in the relevant operating regimes. Its essence lies on the idea of model on demand. When a query data comes, there are generally three steps, viz., relevant data selection from reference database according to some similarity criterion, local model construction based on the relevant data, and model prediction using the local model.

Without the loss of generality, consider the following 2 × 2 state-space model:

$$\begin{bmatrix} x^1_{l,\,k+1} \\ x^2_{l,\,k+1} \end{bmatrix} = \begin{bmatrix} a^{1,1}_k & a^{1,2}_k \\ a^{2,1}_k & a^{2,2}_k \end{bmatrix} \begin{bmatrix} x^1_{l,\,k} \\ x^2_{l,\,k} \end{bmatrix} + \begin{bmatrix} b^{1,1}_k & b^{1,2}_k \\ b^{2,1}_k & b^{2,2}_k \end{bmatrix} \begin{bmatrix} \delta u^1_k \\ \delta u^2_k \end{bmatrix} \tag{6.10}$$

where $x^i_{l,\,k}$ is the ith state variable in the optimized term $\mathbf{x}_{l,\,k}$ and the remaining symbols have obvious definitions.

Then a reference database $\{\mathbf{Y}, \mathbf{\Psi}\}$ designed for the first state variable x^1 could be constructed from process data as follows,

$$\mathbf{Y} = \left[x^1_2,\ x^1_3,\ \cdots,\ x^1_n \right]^T \tag{6.11}$$

$$\mathbf{\Psi} = \begin{bmatrix} x^1_1 & x^2_1 & u^1_1 & u^2_1 \\ x^1_2 & x^2_2 & u^1_2 & u^2_2 \\ \vdots & \vdots & \vdots & \vdots \\ x^1_{n-1} & x^2_{n-1} & u^1_{n-1} & u^2_{n-1} \end{bmatrix} \tag{6.12}$$

where each corresponding row in $\mathbf{Y}$ and $\mathbf{\Psi}$ together represent a sample data and n is the number of sample data collected in the reference database.

During the implementation of the proposed EPSAC design, with a query data $\mathbf{q}_k = \left[x^1_{b,k},\ x^2_{b,k},\ u^1_{b,k},\ u^2_{b,k} \right]$ obtained at the kth sampling instant from the reference trajectories of $\mathbf{x}_b$ and $\mathbf{u}_b$, a relevant dataset $\{\mathbf{Y}_l, \mathbf{\Psi}_l\}$ consisting of l samples is

selected from $\{\mathbf{Y}, \mathbf{\Psi}\}$ according to similarity criterion, for example, distance and angular metrics proposed by Cheng and Chiu (2004). By subtracting $\mathbf{x}_{b,\,k+1}$ and $\mathbf{q}_k$ from each row of $\mathbf{Y}_l$ and $\mathbf{\Psi}_l$, respectively, resulting $\tilde{\mathbf{Y}}_l$ and $\tilde{\mathbf{\Psi}}_l$, all the sample data relevant to the *k*th operating point are in the same form as the optimized term, viz., deviation variables. Therefore, coefficients for the first state variable could be simply obtained, for example, using least squares:

$$\left[a_k^{1,1},\ a_k^{1,2},\ b_k^{1,1},\ b_k^{1,2}\right]^T = \left(\tilde{\mathbf{\Psi}}_l^T \tilde{\mathbf{\Psi}}_l\right)^{-1} \tilde{\mathbf{\Psi}}_l^T \tilde{\mathbf{Y}}_l \tag{6.13}$$

The aforementioned procedure can be similarly applied to the second state variable in Eq. (10) to obtain the corresponding coefficients and hence the matrices $\mathbf{A}_k$ and $\mathbf{B}_k$. The detailed information on the JITL methodology can be referred to the latest JITL algorithm by Su et al., (2012b), which is termed as the JITL with reference to the query point.

It is noted that with the availability of nonlinear process model of Eq. (6.2), a data-rich reference database of (6.11) and (6.12) could be generated off-line for the JITL method to accurately obtain the coefficient matrices $\mathbf{A}_k$ and $\mathbf{B}_k$ on line in a relatively time-saving fashion. Analogous to the finite step/impulse response model that perturbs the nonlinear process model of Eq. (6.2) on line to obtain corresponding coefficients, the proposed method also needs to perturb the process model off-line to a certain extent to obtain a representative database for each state variable of interest. Or equivalently, it can be claimed that JITL remodels the nonlinear process model of Eq. (6.2) in a data-based manner and in a linear form which is only valid around the reference trajectories $\mathbf{x}_b$ and $\mathbf{u}_b$. Note that $\mathbf{x}_b$ and $\mathbf{u}_b$ are not fixed trajectories, they are updated after each iteration within EPSAC algorithm. Additionally, with the development of parallel computing technology, for example the *parfor* command in Matlab environment, each local state-space model coefficient matrices $\mathbf{A}_k$ and $\mathbf{B}_k$ or even each row inside those matrices could be computed independently and in a parallel way to make good use of the multi-core hardware computing environment.

This is because the reference trajectories $\mathbf{x}_b$ and $\mathbf{u}_b$ are already known before identifying each local state-space model, this is different from the successive linearization techniques (Lee and Ricker, 1994), and moreover, they can also be incorporated to update the database on-line (Kansha and Chiu, 2009).

6.3.2 The proposed EPSAC algorithm

After obtaining the local state-space models in the base trajectories, then considering a process with the prediction horizon N_p and control horizon N_u, the sequence of $\mathbf{x}_{l,\,k+i}$ can be calculated as follows:

$$\mathbf{x}_{l,\,k+1} = \mathbf{A}_k \mathbf{x}_{l,\,k} + \mathbf{B}_k \delta\mathbf{u}_k$$

$$\mathbf{x}_{l,k+2} = \mathbf{A}_{k+1}\mathbf{A}_k \mathbf{x}_{l,k} + \mathbf{A}_{k+1}\mathbf{B}_k \delta\mathbf{u}_k + \mathbf{B}_{k+1}\delta\mathbf{u}_{k+1}$$

$$\vdots$$

$$\mathbf{x}_{l,\,k+N_u} = \left(\prod_{i=k}^{k+N_u-1} \mathbf{A}_i\right)\mathbf{x}_{l,\,k} + \left(\prod_{i=k+1}^{k+N_u-1} \mathbf{A}_i\right)\mathbf{B}_k \delta\mathbf{u}_k + \left(\prod_{i=k+2}^{k+N_u-1} \mathbf{A}_i\right)\mathbf{B}_{k+1}\delta\mathbf{u}_{k+1} + \cdots + \mathbf{B}_{k+N_u-1}\delta\mathbf{u}_{k+N_u-1}$$

$$\vdots$$

$$\mathbf{x}_{l,\,k+N_p} = \left(\prod_{i=k}^{k+N_p-1} \mathbf{A}_i\right)\mathbf{x}_{l,\,k} + \left(\prod_{i=k+1}^{k+N_p-1} \mathbf{A}_i\right)\mathbf{B}_k \delta\mathbf{u}_k + \left(\prod_{i=k+2}^{k+N_p-1} \mathbf{A}_i\right)\mathbf{B}_{k+1}\delta\mathbf{u}_{k+1} + \cdots + \left(\prod_{i=k+N_u}^{k+N_p-1} \mathbf{A}_i\right)\mathbf{B}_{k+N_u-1}\delta\mathbf{u}_{k+N_u-1} + \cdots + \mathbf{B}_{k+N_p-1}\delta\mathbf{u}_{k+N_p-1}$$

It is noted that $\mathbf{x}_{l,\,k} = \mathbf{0}$, and $\delta\mathbf{u}_{k+i} = \mathbf{0}$ for $i \geq N_u$ then

$$\mathbf{X}_l = \mathbf{G}_l \delta\mathbf{U} \tag{6.14}$$

where $\mathbf{X}_l = \left[\mathbf{x}_{l,\,k+1}^T,\ \mathbf{x}_{l,\,k+2}^T,\ \cdots,\ \mathbf{x}_{l,\,k+N_p}^T\right]^T$, $\delta\mathbf{U} = \left[\delta\mathbf{u}_k^T,\ \delta\mathbf{u}_{k+1}^T,\ \cdots,\ \delta\mathbf{u}_{k+N_u-1}^T\right]^T$, and

$$\mathbf{G}_l = \begin{bmatrix} \mathbf{B}_k & \mathbf{0} & \cdots & \mathbf{0} \\ \mathbf{A}_{k+1}\mathbf{B}_k & \mathbf{B}_{k+1} & \cdots & \mathbf{0} \\ \mathbf{A}_{k+2}\mathbf{A}_{k+1}\mathbf{B}_k & \mathbf{A}_{k+2}\mathbf{B}_{k+1} & \cdots & \mathbf{0} \\ \vdots & \vdots & \ddots & \vdots \\ \left(\prod_{i=k+1}^{k+N_u-1} A_i\right)B_k & \left(\prod_{i=k+2}^{k+N_u-1} A_i\right)B_{k+1} & \cdots & B_{k+N_u-1} \\ \vdots & \vdots & \ddots & \vdots \\ \left(\prod_{i=k+1}^{k+N_p-1} A_i\right)B_k & \left(\prod_{i=k+2}^{k+N_p-1} A_i\right)B_{k+1} & \cdots & \left(\prod_{i=k+N_u}^{k+N_p-1} A_i\right)B_{k+N_u-1} \end{bmatrix} \tag{6.15}$$

In summary, the future system state variables in the control horizon can be conveniently represented in matrix form as

$$\mathbf{X} = \mathbf{X}_b + \mathbf{G}_l \delta\mathbf{U} \tag{6.16}$$

where $\mathbf{X} = \left[\mathbf{x}_{k+1}^T,\ \mathbf{x}_{k+2}^T,\ \cdots,\ \mathbf{x}_{k+N_p}^T\right]^T$ and $\mathbf{X}_b = \left[\mathbf{x}_{b,\,k+1}^T,\ \mathbf{x}_{b,\,k+2}^T,\ \cdots,\ \mathbf{x}_{b,\,k+N_p}^T\right]^T$, as well as the control trajectory defined as :

$$\mathbf{U} = \mathbf{U}_b + \delta\mathbf{U} \tag{6.17}$$

where $\mathbf{U} = \left[\mathbf{u}_k^T,\ \mathbf{u}_{k+1}^T,\ \cdots,\ \mathbf{u}_{k+N_u-1}^T\right]^T$ and $\mathbf{U}_b = \left[\mathbf{u}_{b,\,k}^T,\ \mathbf{u}_{b,\,k+1}^T,\ \cdots,\ \mathbf{u}_{b,\,k+N_u-1}^T\right]^T$.

With Eqs. (6.16) and (6.17), the conventional routine for a quadratic cost function with nonlinear soft constraints could be straightforwardly implemented to obtain the optimal control moves of $\delta\mathbf{U}$. The detailed derivation and implementation procedure of the proposed control strategy are summarized as follows.

Consider an optimization problem J defined as :

$$J = \min_{\Delta\mathbf{U}} \left[\mathbf{P} - \mathbf{P}_d\right]^T \mathbf{W}_p \left[\mathbf{P} - \mathbf{P}_d\right] + \Delta\mathbf{U}^T \mathbf{W}_u \Delta\mathbf{U} \tag{6.18}$$

where $\mathbf{P}$, $\mathbf{P}_d$, and $\Delta\mathbf{U}$ are the matrices of the interested product quality, desired product quality, and the change in input variables, respectively, given by

$$\mathbf{P} = \left[\mathbf{p}_{k+1}^T,\ \mathbf{p}_{k+2}^T,\ \cdots,\ \mathbf{p}_{k+N_p}^T \right]^T \tag{6.19}$$

$$\mathbf{P}_d = \left[\mathbf{p}_{d,\,k+1}^T,\ \mathbf{p}_{d,\,k+2}^T,\ \cdots,\ \mathbf{p}_{d,\,k+N_p}^T \right]^T \tag{6.20}$$

$$\Delta\mathbf{U} = \left[\mathbf{u}_k^T - \mathbf{u}_{k-1}^T,\ \mathbf{u}_{k+1}^T - \mathbf{u}_k^T,\ \cdots,\ \mathbf{u}_{k+N_u-1}^T - \mathbf{u}_{k+N_u-2}^T \right]^T \tag{6.21}$$

and $\mathbf{W}_p$ and $\mathbf{W}_u$ are the weight matrices for the product quality and the change in input variables, respectively. Then $\mathbf{P}$ and $\Delta\mathbf{U}$ can be decomposed into

$$\mathbf{P} = \mathbf{M}\mathbf{X} = \mathbf{M}\left(\mathbf{X}_b + \mathbf{G}_l \delta\mathbf{U} \right) = \mathbf{M}\mathbf{X}_b + \mathbf{M}\mathbf{G}_l \delta\mathbf{U} \tag{6.22}$$

where $\mathbf{M}$ is designed to extract out the interested combination of product quality variables, defined as:

$$\mathbf{M} = \begin{bmatrix} \mathbf{m}_{k+1} & \mathbf{0} & \cdots & \mathbf{0} \\ \mathbf{0} & \mathbf{m}_{k+2} & \cdots & \mathbf{0} \\ \vdots & \vdots & \ddots & \vdots \\ \mathbf{0} & \mathbf{0} & \cdots & \mathbf{m}_{k+N_p} \end{bmatrix} \tag{6.23}$$

When the first state variable is selected:

$$\mathbf{m}_{k+1} = \mathbf{m}_{k+2} = \cdots = \mathbf{m}_{k+N_p} = \left[1,\ 0,\ 0,\ \cdots,\ 0 \right]_{1\times n_x} \tag{6.24}$$

Equation (6.22) is further simplified as:

$$\mathbf{P} = \mathbf{P}_b + \mathbf{G}_{pl} \delta\mathbf{U} \tag{6.25}$$

where

$$\mathbf{P}_b = \mathbf{M}\mathbf{X}_b \tag{6.26}$$

$$\mathbf{G}_{pl} = \mathbf{M}\mathbf{G}_l \tag{6.27}$$

where $\mathbf{G}_{pl}$ is the state-space model coefficient matrix corresponding to the product quality variable, and $\mathbf{P}_b$ is the predicted product quality calculated using the nonlinear model with predetermined future inputs $\mathbf{U}_b = \left[\mathbf{u}_{b,\,k}^T,\ \mathbf{u}_{b,\,k+1}^T,\ \cdots,\ \mathbf{u}_{b,\,k+N_u-1}^T\right]^T$, and

$$\Delta\mathbf{U}_b = \left[\mathbf{u}_{b,\,k}^T - \mathbf{u}_{b,\,k-1}^T,\ \mathbf{u}_{b,\,k+1}^T - \mathbf{u}_{b,\,k}^T,\ \cdots,\ \mathbf{u}_{b,\,k+N_u-1}^T - \mathbf{u}_{b,\,k+N_u-2}^T\right]^T \tag{6.28}$$

$$\mathbf{C} = \begin{bmatrix} \mathbf{I} & \mathbf{0} & \cdots & \mathbf{0} & \mathbf{0} \\ -\mathbf{I} & \mathbf{I} & \cdots & \mathbf{0} & \mathbf{0} \\ \vdots & \vdots & \ddots & \vdots & \vdots \\ \mathbf{0} & \mathbf{0} & \cdots & -\mathbf{I} & \mathbf{I} \end{bmatrix} \tag{6.29}$$

$$\Delta\mathbf{U} = \Delta\mathbf{U}_b + \mathbf{C}\delta\mathbf{U} \tag{6.30}$$

Hence, the minimization problem becomes:

$$\begin{aligned} J &= \min_{\delta\mathbf{U}} \left(\mathbf{P}_b + \mathbf{G}_{pl}\delta\mathbf{U} - \mathbf{P}_d\right)^T W_p \left(\mathbf{P}_b + \mathbf{G}_{pl}\delta\mathbf{U} - \mathbf{P}_d\right) + \left(\Delta\mathbf{U}_b + \mathbf{C}\delta\mathbf{U}\right)^T W_u \left(\Delta\mathbf{U}_b + \mathbf{C}\delta\mathbf{U}\right) \\ &= \min_{\delta\mathbf{U}} \delta\mathbf{U}^T\mathbf{G}_{pl}^T\mathbf{W}_p\mathbf{G}_{pl}\delta\mathbf{U} + 2(\mathbf{P}_b - \mathbf{P}_d)^T\mathbf{W}_p\mathbf{G}_{pl}\delta\mathbf{U} + \delta\mathbf{U}^T\mathbf{C}^T\mathbf{W}_u\mathbf{C}\delta\mathbf{U} + 2\Delta U_b^T\mathbf{W}_u\mathbf{C}\delta\mathbf{U} \\ &= \min_{\delta\mathbf{U}} \delta\mathbf{U}^T\mathbf{\Gamma}\delta\mathbf{U} + \mathbf{\Phi}^T\delta\mathbf{U} \end{aligned} \tag{6.31}$$

where

$$\mathbf{\Gamma} = \mathbf{G}_{pl}^T\mathbf{W}_p\mathbf{G}_{pl} + \mathbf{C}^T\mathbf{W}_u\mathbf{C}$$

$$\mathbf{\Phi} = 2\left[\left(\mathbf{P}_b - \mathbf{P}_d\right)^T\mathbf{W}_p\mathbf{G}_{pl} + \Delta\mathbf{U}_b^T\mathbf{W}_u\mathbf{C}\right]^T$$

The minimization is subject to the constraints $h\left(\mathbf{x}_j, \mathbf{u}_j\right) \le \mathbf{0},\ \forall j \ge k$, where k is the current sampling instance. For notational convenience, $h\left(\mathbf{x}_j, \mathbf{u}_j\right) \le \mathbf{0}$ is denoted as $\mathbf{h}_j$, which can be decomposed into the base and linear part $\mathbf{h}_j = \mathbf{h}_{b,j} + \mathbf{h}_{l,j}$. Therefore, the matrix form of the constraints in the control horizon is

$$\mathbf{H}_b + \mathbf{G}_{hl}\delta\mathbf{U} \le \mathbf{0} \tag{6.32}$$

where $\mathbf{G}_{hl}$ is the state-space model coefficient matrix corresponding to the constraints function $\mathbf{h}_j$ and $\mathbf{H}_b = \left[\mathbf{h}_{b,k}^T, \cdots, \mathbf{h}_{b,k+N_p}^T\right]^T$.

When the constraints are highly nonlinear, handling (6.32) directly will sometimes cause difficulty for the quadratic programming (QP) used for the optimization to find a feasible solution. Convergence was provided by the soft-constraint approach, which replaces the minimization problem with

$$\min_{\delta\mathbf{U},\boldsymbol{\varepsilon}} J_{sc} \tag{6.33}$$

subject to

$$\mathbf{H}_b + \mathbf{G}_{hl}\delta\mathbf{U} \le \boldsymbol{\varepsilon} \tag{6.34}$$

$$\boldsymbol{\varepsilon} \ge \mathbf{0} \tag{6.35}$$

where $J_{sc} = J + \boldsymbol{\varepsilon}^T\mathbf{W}_\varepsilon\boldsymbol{\varepsilon} + \boldsymbol{\varepsilon}^T\mathbf{w}_\varepsilon$, $\boldsymbol{\varepsilon}$ is a vector of slack variables, $\mathbf{W}_\varepsilon$ is a diagonal matrix of positive weight, and $\mathbf{w}_\varepsilon$ is a vector of positive elements. This modified minimization problem can be written as

$$\begin{aligned} J_{sc}^* &= \min_{\delta\mathbf{U},\boldsymbol{\varepsilon}} \delta\mathbf{U}^T\boldsymbol{\Gamma}\delta\mathbf{U} + \boldsymbol{\Phi}^T\delta\mathbf{U} + \boldsymbol{\varepsilon}^T W_\varepsilon\boldsymbol{\varepsilon} + \boldsymbol{\varepsilon}^T\mathbf{w}_\varepsilon \\ &= \min_{\delta\mathbf{U},\boldsymbol{\varepsilon}} \begin{bmatrix}\delta\mathbf{U}^T & \boldsymbol{\varepsilon}^T\end{bmatrix}\begin{bmatrix}\boldsymbol{\Gamma} & \mathbf{0}\\ \mathbf{0} & \mathbf{W}_\varepsilon\end{bmatrix}\begin{bmatrix}\delta\mathbf{U}\\ \boldsymbol{\varepsilon}\end{bmatrix} + \begin{bmatrix}\boldsymbol{\Phi}^T & w_\varepsilon^T\end{bmatrix}\begin{bmatrix}\delta\mathbf{U}\\ \boldsymbol{\varepsilon}\end{bmatrix} \\ &= \min_{\boldsymbol{\Pi}} \boldsymbol{\Pi}^T\boldsymbol{\Lambda}\boldsymbol{\Pi} + \boldsymbol{\tau}^T\boldsymbol{\Pi} \end{aligned} \tag{6.36}$$

subject to

$$\begin{bmatrix}\mathbf{H}_b\\ \mathbf{0}\end{bmatrix} + \begin{bmatrix}\mathbf{G}_{hl} & -\mathbf{I}\\ \mathbf{0} & -\mathbf{I}\end{bmatrix}\boldsymbol{\Pi} \le \mathbf{0} \tag{6.37}$$

where $\mathbf{\Pi} = \begin{bmatrix} \delta\mathbf{U}^T & \boldsymbol{\varepsilon}^T \end{bmatrix}^T$, $\mathbf{\Lambda} = \begin{bmatrix} \mathbf{\Gamma} & \mathbf{0} \\ \mathbf{0} & \mathbf{W}_{\boldsymbol{\varepsilon}} \end{bmatrix}$, and $\boldsymbol{\tau} = \begin{bmatrix} \mathbf{\Phi}^T & \mathbf{w}_{\varepsilon}^T \end{bmatrix}^T$.

To summarize, the procedure for implementing the EPSAC strategy based on JITL-based local models at each sampling instant *k* is:

(1) Obtain $\mathbf{U}_b$ by the following method:

- If $k = 0$ and $iter = 1$, $\mathbf{U}_b$ is specified to be the control actions implemented in the previous batch;
- If $k > 0$ and $iter = 1$, $\mathbf{U}_b$ is set as the $\mathbf{U}_{optimal}$ obtained at the previous sampling instant of the current batch, where *iter* is the iteration count;
- If $k > 0$ and $iter > 1$, the updated $\mathbf{U}_b$ from the previous iteration is used.

(2) Given the predicted state variables, obtain $\mathbf{P}_b$ and $\mathbf{H}_b$ by using $\mathbf{U}_b$ as the input to the nonlinear process model (6.1) to (6.5).

(3) Obtain the state-space model coefficient matrices $\mathbf{G}_{pl}$ and $\mathbf{G}_{hl}$ by using JITL with reference to the query point.

(4) Obtain $\mathbf{\Pi}^* = \begin{bmatrix} \delta\mathbf{U}^{*T} & \boldsymbol{\varepsilon}^{*T} \end{bmatrix}^T$ from the solution to the minimization problem (6.36) and (6.37), then update the element of U_b using

$$\mathbf{u}_{b,\,k+j} = \mathbf{u}_{b,\,k+j} + \delta\mathbf{u}_{k+j}$$

where $j = 0,\ \cdots,\ N_u - 1$.

(5) Calculate $err = \left\| \begin{bmatrix} \mathbf{G}_{pl} \\ \mathbf{G}_{hl} \end{bmatrix} \delta\mathbf{U}^* \right\|$. If *err* is greater than a specified tolerance, *iter* = *iter* + 1, and go back to Step (1). Otherwise, set $\mathbf{U}_{optimal} = \mathbf{U}_b$ and implemented the first element of $\mathbf{U}_{optimal}$ to the process.

6.4 Results and discussion

6.4.1 Nominal performance

The conventional EPSAC and the proposed JITL-EPSAC techniques were applied to the semi-batch pH-shift reactive crystallization process of L-glutamic acid presented in Chapter 5. As discussed in Chapter 5, the polymorphic purity of metastable α-form, viz., P_α , is an important state variable reflecting the progress of the studied polymorphic crystallization system. Thus, it was chosen as the primary controlled product quality at the end of the batch, while the other two variables of interest are the volume-based mean crystal size (M_s, μm) and crystalline product yield (P_y). The nominal input trajectory was chosen to the optimal input trajectory corresponding to the optimal operation point selected from the Pareto front discussed in Chapter 5, meaning that the batch-end product qualities [P_α, M_s, P_y] is chosen as [0.8255, 250.6, 0.8088]. The constraint for the sulfuric acid addition flowrate (F , mL/min) is between 0 and 16 mL/min, which remains the same as that considered in Chapter 5. The total batch time is 40 minutes with a sampling interval of 1 minute.

To proceed the JITL modeling of the crystallization process, the following local state-space model is considered:

$$\begin{bmatrix} (P_\alpha)_{l,k+1} \\ (M_s)_{l,k+1} \\ (C)_{l,k+1} \\ (V)_{l,k+1} \end{bmatrix} = \mathbf{A}_k \begin{bmatrix} (P_\alpha)_{l,k} \\ (M_s)_{l,k} \\ (C)_{l,k} \\ (V)_{l,k} \end{bmatrix} + \mathbf{B}_k \left[\delta F_k \right] \tag{6.38}$$

where C (mol/L) is the glutamic acid concentration and V is the solution volume in a crystallizer with capacity of 0.97L.

To generate reference database for the JITL identification of local state-space models of Eq. (6.38), one hundred batches process data were obtained by introducing step changes of random magnitude with $N(0, 1)$ to the constant addition flowrate of 8

mL/min as shown in Figure 6.3. To validate the predictive performance of the JITL method, another unseen batch of process data, which was not used in the reference database, was obtained and shown in Figure 6.4. It is clear that the JITL prediction has good agreement with the actual process data.

For comparison purpose, an EPSAC algorithm developed by Hermanto et al. (2009) was introduced in this work. The proposed JITL-EPSAC algorithm differs from the EPSAC by Hermanto et al. (2009) only in the $\mathbf{G}_{pl}$ and $\mathbf{G}_{hl}$, as shown in Eq. (6.15) and (6.32), respectively, where the conventional algorithm uses a finite step response model to develop these two dynamic matrices. Both controllers use a prediction/control horizon starting from current time to the batch end, viz., shrinking horizon mode.

Firstly, both EPSAC controllers were initialized with a reference addition flowrate trajectory set as the nominal constant 8 mL/min. The control actions were activated only after measurements of polymorphic purity by Raman spectroscopy were steadily available, the same as that in polymorphic purity control in chapter 5. The maximum iteration number inside both EPSAC algorithms were limited to one, viz., no iteration was utilized. The effect of increasing maximum iteration number will be discussed later. No-model plant mismatch was considered at this stage and all the state variables in the nonlinear process model were measureable or observable as studied by Mesbah et al., (2011) and Hermanto et al., (2009). Tuning parameters of $\mathbf{W}_p$ and $\mathbf{W}_u$ for product quality and control moves were specifically fine-tuned for conventional EPSAC as $1\times10^{-5}\mathbf{I}$ and unit matrix $\mathbf{I}$, respectively. These two weights were also applied to the proposed JITL-EPSAC algorithm. Thus, the differences in control performance between two EPSAC algorithms were purely resulted from the use of either finite step response model or JITL local state-space model.

The performance of the two EPSAC algorithms are shown by EPSAC-1 and JITL-EPSAC, respectively, in Figure 6.5, where JITL-EPSAC could meet the control target with a smooth addition flowrate trajectory, while EPSAC-1 failed to meet the target

and the input trajectory varied greatly in the later phase of the batch. As discussed in the introduction section, using a finite step response model established at current time to predict the controlled variable deep in the prediction horizon is inappropriate for nonlinear process. In contrast, JITL-EPSAC algorithm specifically designs local state-space models at each sampling instant in prediction horizon, as shown in Figure 6.2. Consequently, process nonlinearity is taken into account, resulting in more accurate prediction of end point of product property.

Toward this end, one remedial approach in conventional EPSAC for batch process control is by the use of an adaptive weight of $\mathbf{W}_u$ which penalizes control moves deep in the control horizon, as reported in Hermanto et al. (2009). Similar weight was also implemented in Lee and Ricker (1994) for successive linearization. However, the tuning of $\mathbf{W}_u$ maybe time consuming and has a risk of obtaining local optimal solution. A fine-tuned $\mathbf{W}_u$ that improves the batch-end property control with smooth control moves is suggested below:

$$\left(\mathbf{W}_u\right)_{i,i} = 1\times 10^{-5}\left[1+60\times\left(i-1\right)\right], \quad i=1,\cdots,N_u \tag{6.39}$$

where $\left(\mathbf{W}_u\right)_{i,i}$ is the diagonal elements of matrix $\mathbf{W}_u$; N_u is the control horizon. The corresponding control performance of EPSAC is shown by EPSAC-2 in Figure 6.5.

It is worth mentioning that the main idea of EPSAC is to iteratively linearize along the reference trajectories, thus the maximum iteration number places an important effect on the control performance of EPSAC. The influence of maximum iteration number on the convergence of the product quality variables is illustrated in Figure 6.6, from which the proposed JITL-EPSAC shows steady convergence to the desired polymorphic purity P_α and mean crystal size M_s with maximum iteration number ranging from 1 to 10, only slight variation is observed for the product yield P_y. It is noted for the EPSAC-2 that there is no much improvement by increasing the maximum iteration number. This is resulted from the use of a conservative weight of $\mathbf{W}_u$ of Eq. (6.39), which penalizes more on the control moves. While the EPSAC-1

seems to be steadily improved by increasing the maximum iteration number larger than 7. Therefore, for conventional EPSAC, if the finite step response model is not accurate for highly nonlinear process, there is no guarantee that maximum iteration number helps to smoothly improve the EPSAC performance. Moreover, the larger the maximum iteration number, the much more heavy of the computational burden for a nonlinear MPC algorithm.

6.4.2 Effects of model-plant mismatch

Generally, model-plant mismatch is, in reality, inevitable for any model-based control approaches. To investigate the influence of parameter uncertainties on the performance of EPSAC algorithms, two case studies of kinetic uncertainties were introduced to the reactive crystallization process. Case 1 considered a 20% decrease of the α-form growth rate, which was the same as that in chapter 5. The case 2 introduced a 20% magnitude of variation to four model kinetic parameters of their Mode value reported in Table 3.2, which were set as $(1+20\%)k_{b,\alpha 1}$, $(1-20\%)k_{g,\alpha 1}$, $(1+20\%)E_{g,\alpha 2}$, $(1-20\%)k_{g,\beta 1}$. Maximum iteration number of 10, 2 and 2 were employed for the EPSAC-1, EPSAC-2 and JITL-EPSAC, respectively. The results are illustrated in Figures 6.7 and 6.8, indicating that the superiority of JITL-EPSAC to EPSAC algorithm is also maintained under the model-plant mismatch, from which the robustness of the JITL-EPSAC algorithm could be confirmed.

Additionally, it should be pointed out that for case 1, though both the polymorphic purity control in chapter 5 and the JITL-EPSAC in this work could alleviate the influence of the model-plant mismatch, deviations of the batch-end product qualities from the desired set point are both encountered, this shows the importance of mitigating the model-plant mismatch in the control practices, which will be further discussed in the following chapter.

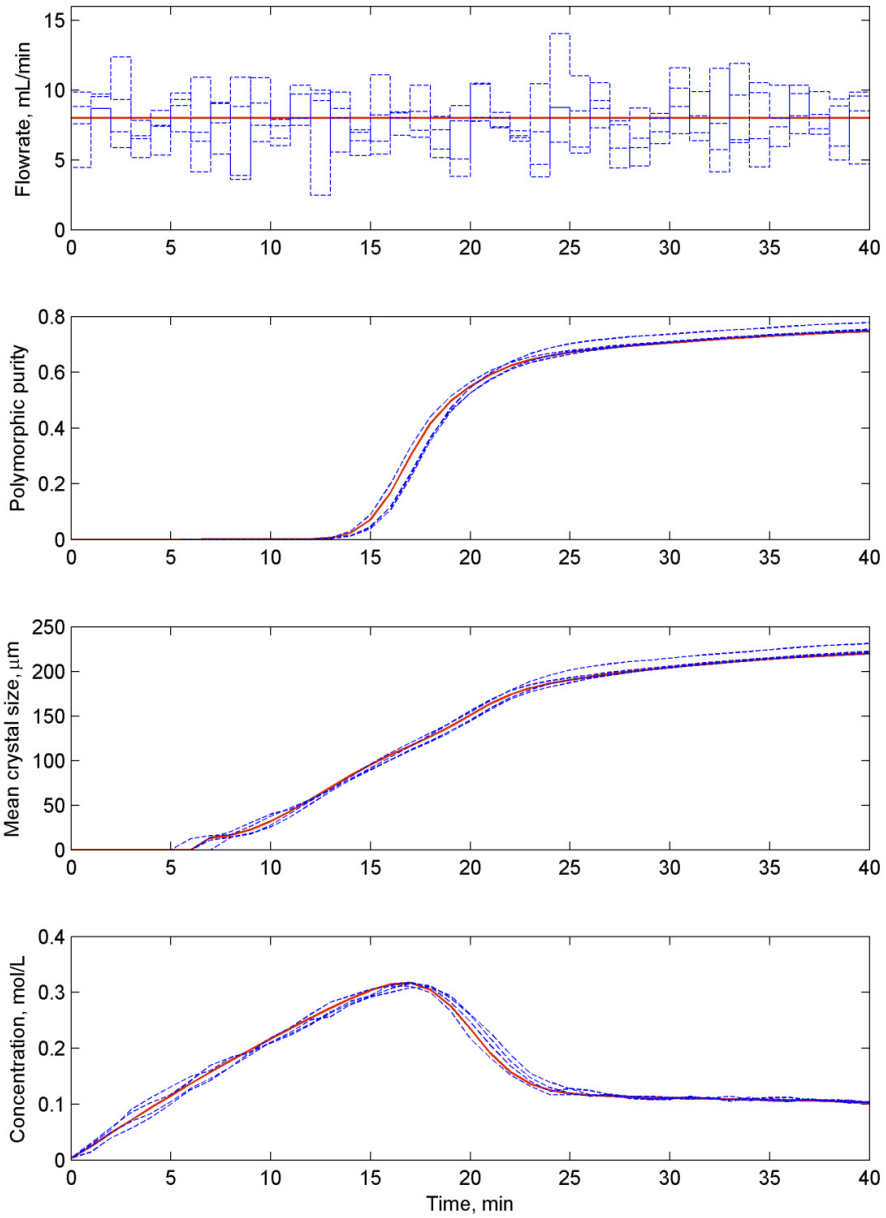

Figure 6.3: Illustration of the four batches process data used for the reference database by the JITL method (solid line: nominal data; dash line: four batches process data).

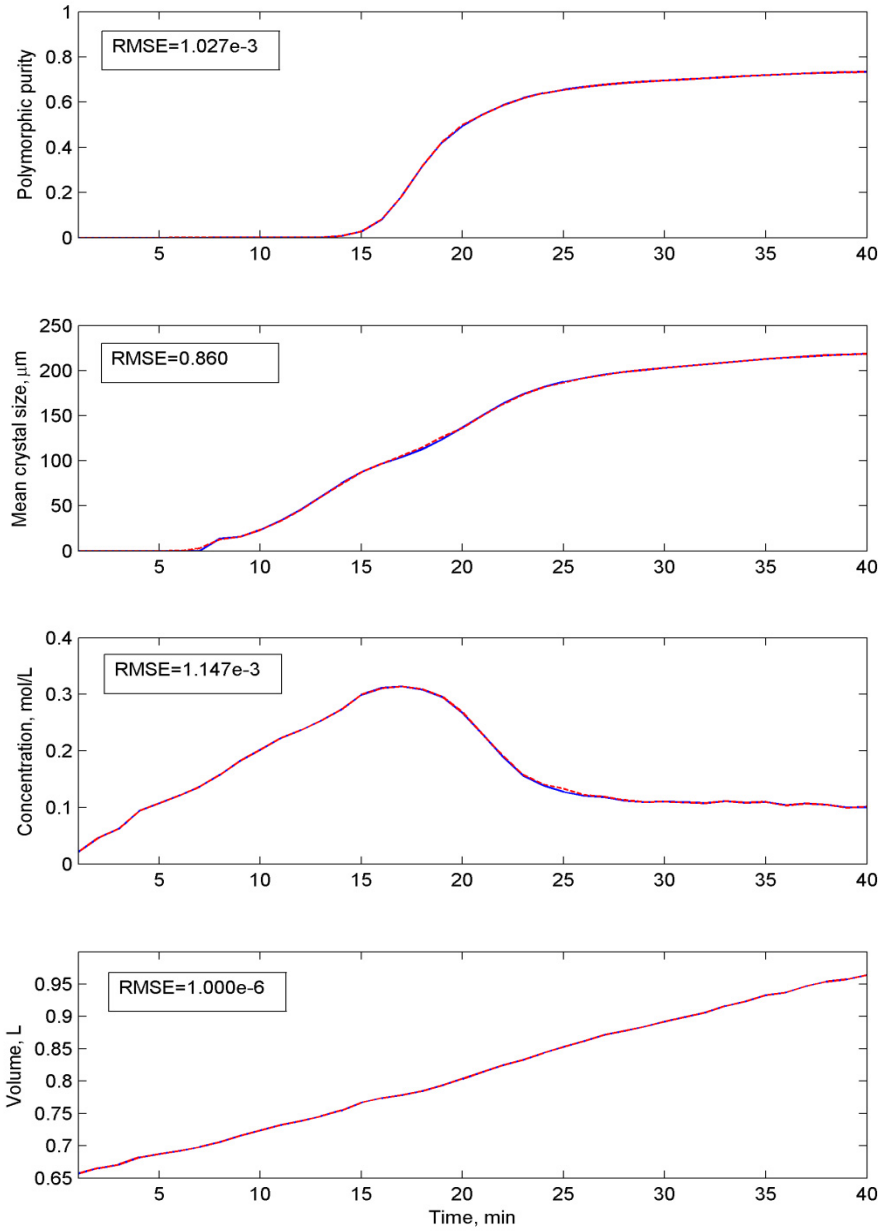

Figure 6.4: Validation results for JITL method (solid line: process data; dash line: JITL prediction; RMSE: root mean square error).

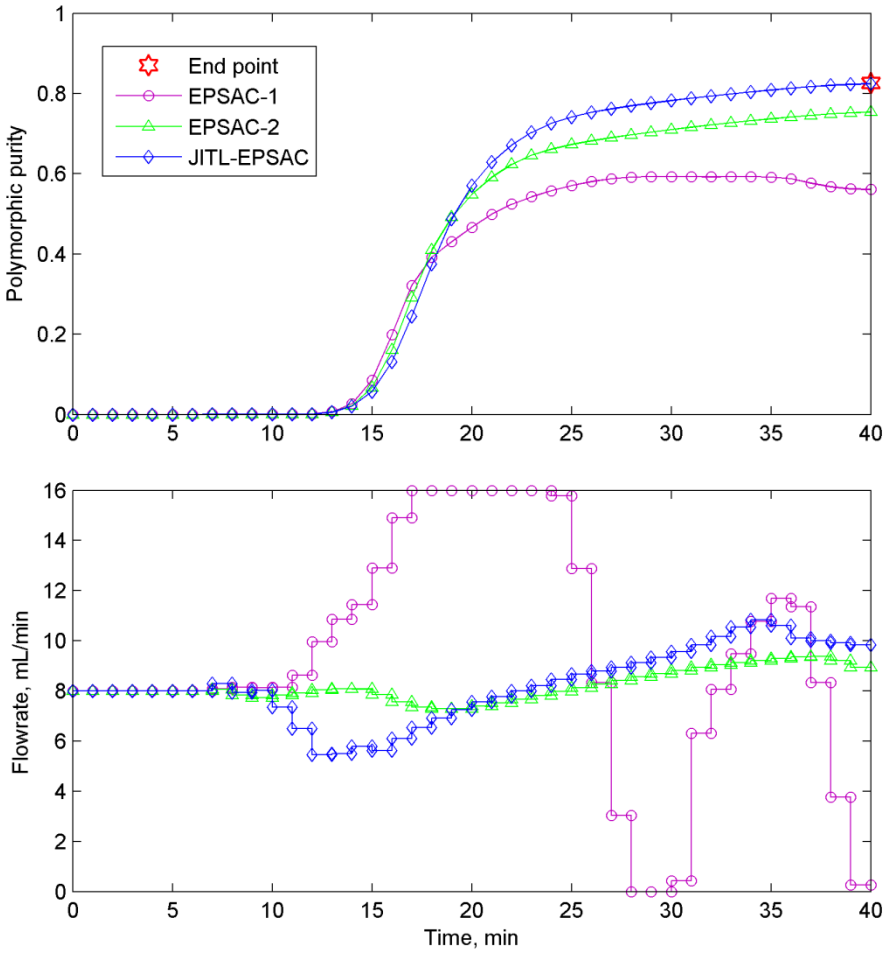

Figure 6.5: Performance comparison between EPSAC and JITL-EPSAC for the reactive crystallization.

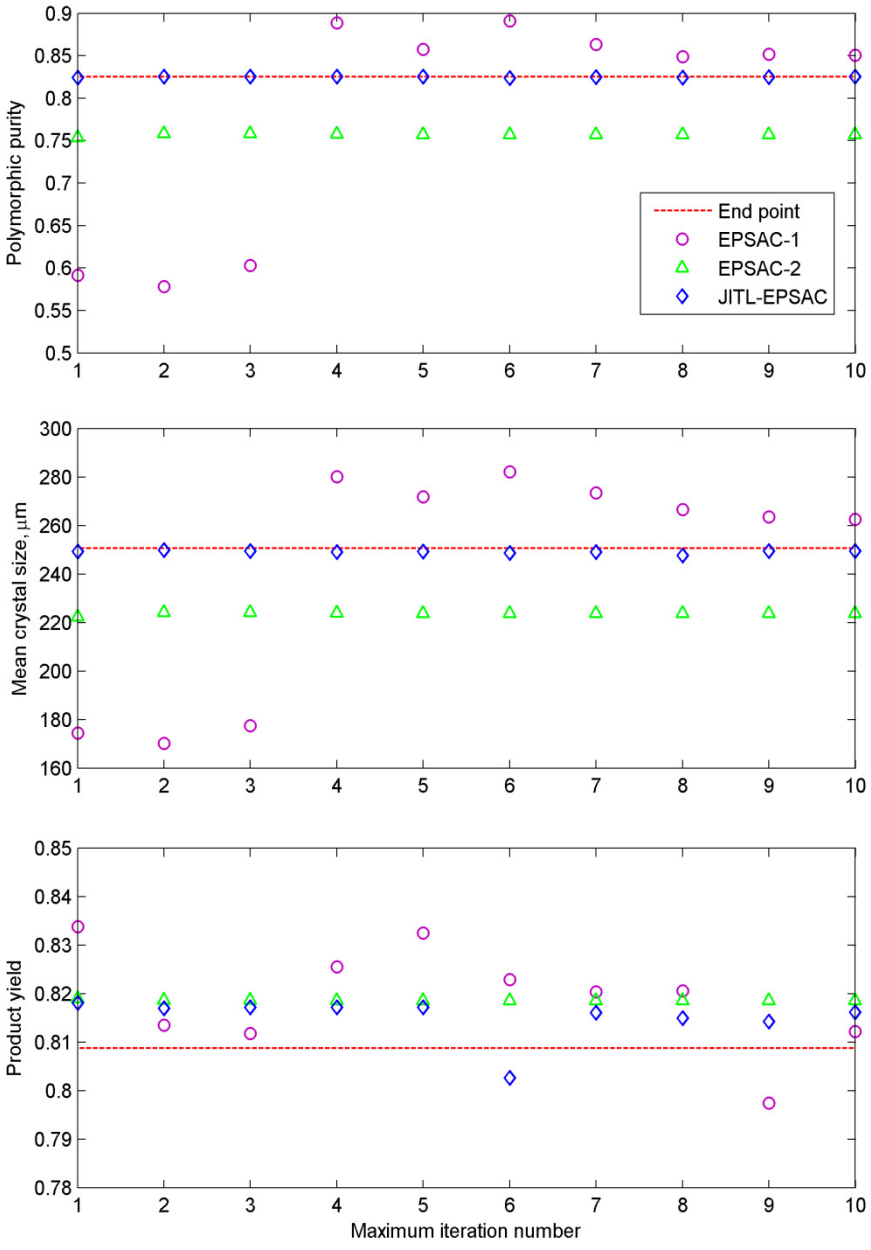

Figure 6.6: Effect of maximum iteration number on EPSAC and JITL-EPSAC control performances.

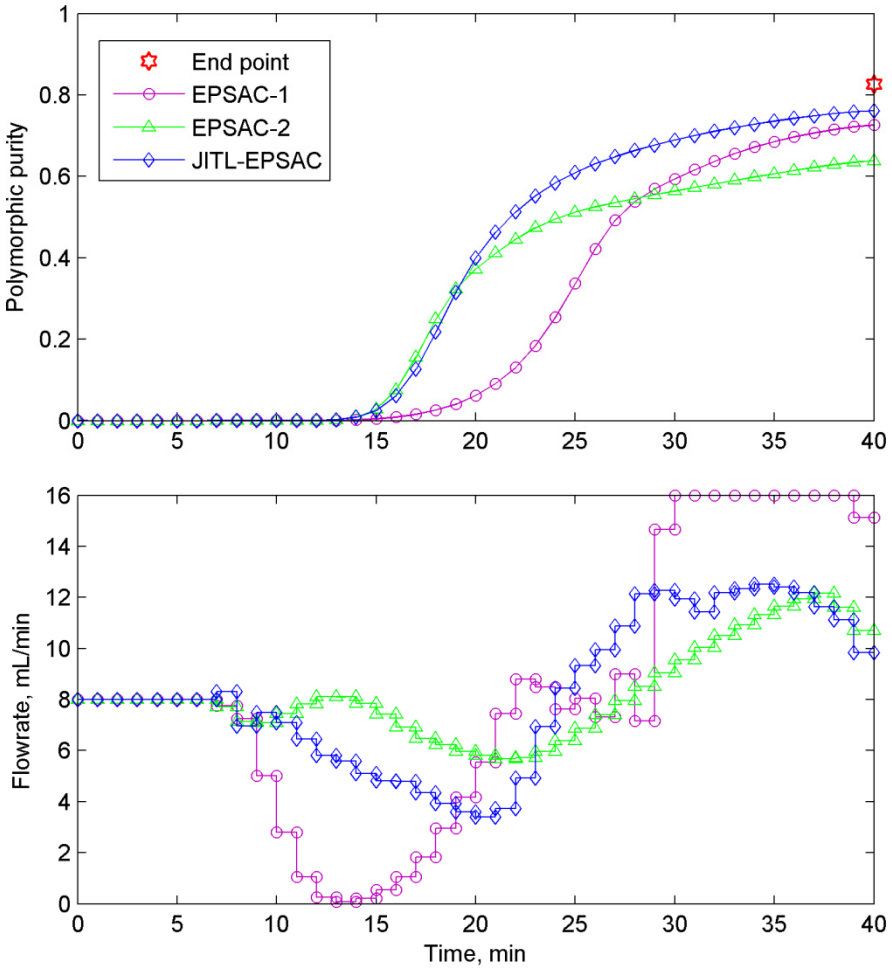

Figure 6.7: Performances of batch-end property control by EPSAC and JITL-EPSAC for the reactive crystallization under model-plant mismatch of case 1.

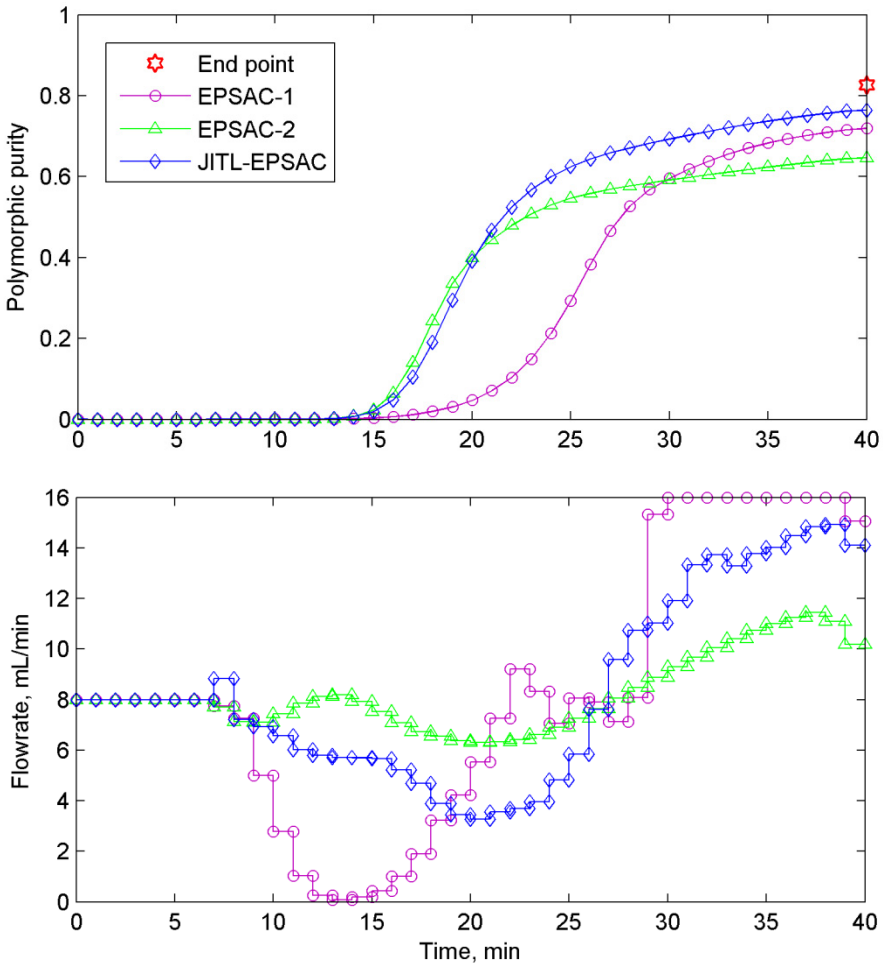

Figure 6.8: Performances of batch-end property control by EPSAC and JITL-EPSAC for the reactive crystallization under model-plant mismatch of case 2.

6.5 Conclusions

The use of finite step/impulse response model for trajectory linearization in EPSAC algorithm is only valid in linear or mildly nonlinear process. In order to enhance the efficiency of linearization along the reference trajectory for EPSAC applications in nonlinear processes, the idea of local state-space models identified by JITL method is proposed in this study. Local state-space models can well represent the high nonlinearity and the time-varying characteristic of chemical processes, particularly in batch/semi-batch processes. Easier weight tuning, smoother control moves, less computational burden and better control performance of the proposed JITL-EPSAC algorithm over conventional EPSAC algorithm for batch-end property control are demonstrated in the semi-batch pH-shift reactive crystallization process.

Chapter 7

Integrated B2B-NMPC Control of the pH-shift Reactive Crystallization of L-glutamic Acid

The disadvantageous open-loop nature of batch-to-batch (B2B) control strategy has brought about the integration of B2B with on-line controller design techniques. A new integrated B2B-NMPC control strategy is proposed in this study to update the model parameters from batch to batch using multiway partial least squares (MPLS) model. The resulting new process model is then incorporated into NMPC design for the next batch to achieve better (closed-loop) control performance than that obtained by the B2B control in an open-loop manner.

7.1 Introduction

In industrial practices, batch process is usually repeatedly proceeded with routine recipes to produce on-spec customized products, the repetitive nature of which in turn helps to boost the learning-type control methods, such as iterative learning control (ILC) and batch-to-batch (B2B) or run-to-run (R2R) controls (Wang et al., 2009). Batch-to-batch control uses information obtained from previous batches to optimize batch operation for next batch with an aim to improve the tracking of final product qualities, which can also address the problems of model-plant mismatches or unmeasured disturbances in batch processes (Xiong et al., 2005).

Batch-to-batch control, which was first proposed in the beginning of 1990s, has been studied extensively in the past decade (Zafiriou et al., 1995; Bonvin, 1998). For example, Clarke-Pringle and MacGregor (1998) introduced the batch-to-batch adjustments to optimize the molecular-weight distribution. Doyle et al. (2003) developed batch-to-batch control based on a hybrid model to realize the particle size distribution control. Zhang (2008) reported a batch-to-batch optimal control of a batch polymerization process based on stacked neural network models. However, B2B control strategies often suffer from its open-loop nature, as the correction is not made until the next batch. On the other hand, with the ability of on-line control strategies, such as model predictive control (MPC), to respond to disturbances occurring during the batch and batch-to-batch control to correct bias left uncorrected, integration of both strategies becomes interesting to researchers (Chin et al., 2000; Lee et al., 2002), which were mostly based on linear time varying (LTV) models. Implementations of the integrated batch-to-batch control for product quality improvement of batch crystallizers are also reported by Paengjuntuek et al. (2008) and Hermanto et al., (2011).

It is worth mentioning that an integrated B2B-NMPC design based on a hybrid model was recently developed for a batch polymorphic crystallization process (Hermanto et al., 2011). The hybrid model, consisting of a nominal first-principles model and a series of correction factors based on batch-to-batch updated PLS models, was used to predict the process variables and final product quality. One major benefit of such hybrid model is the ability to harness the extrapolative capability of the first-principles model while the PLS model provides a means for simple model updating (Hermanto, 2008). Though faster and smoother convergence was observed than that of a conventional B2B control strategy to handle uncertainties in kinetic parameters, the reported method might be restrictive due to a correction factor specifically designed at each sampling instant for each on-line measurement and for each product quality at the batch end. Two scenarios of kinetic uncertainties were considered independently with their respective initial databases. However, the transition between these two scenarios was not investigated, without which the demonstration of the

merits of B2B control strategy that is capable of learning from the batch-to-batch operation is impossible. Thus, from this point of view, the batch-to-batch learning and updating capabilities of the reported method were not adequately demonstrated.

Encouraged by the previous works and the benefits of integrated B2B-NMPC control strategy, a new integrated B2B-NMPC control strategy is proposed in this chapter. First, note that during the batch production, not only the process is repeated from batch to batch, but also the control algorithm undergoes repetition. Previous efforts tend to concentrate on the former, for example, a bias term or a correction factor is measured after the finish of a batch or calculated from a historical operating database, respectively, and is added to the online control algorithm for use in the next batch (Zhang, 2008; Hermanto et al., 2011). Addition of these accessional terms assumes that same deviations will persist during the next batch. Though simple and efficient in some batch process, it may not work properly for a highly nonlinear process, particularly when on-line control is combined with the B2B control as they work at a relatively different time scale. To the contrary, in our new proposal, a historical database of the control algorithm runs is used to update the control algorithm in such a direct manner that a data-based multiway partial least squares (MPLS) model utilizes the initial conditions, measurement trajectories, and end-point product qualities of previous batch operation to re-estimate the kinetic parameters in the first-principles model embedded in the nonlinear model predictive control (NMPC) for implementation in the next batch. Therefore, the NMPC performs the online control to handle the constraints and disturbances while the B2B control refines the model iteratively by inferring from the previous batch operations (Paengjuntuek et al., 2008). The proposed B2B-NMPC algorithm is implemented to the semi-batch pH-shift reactive crystallization process to optimize the addition flowrate profile in order to produce products on specification.

This chapter is organized as follows. The batch-to-batch control strategy considered for comparison purpose is introduced in the next section, which is then followed by the integrated B2B-NMPC control strategy in Section 7.3. Applications of the conventional B2B and integrated B2B-NMPC to the semi-batch pH-shift

reactive crystallization of L-glutamic acid are illustrated and discussed in Section 7.4. Lastly, concluding remarks based on their control performances are given.

7.2 Batch-to-Batch (B2B) control strategy

A batch-to-batch control strategy based on the interaction of a first-principles model and a multiway partial least squares (MPLS) model is introduced in this study, the benefit of which lies in its ability to exploit the extrapolative power of first-principles model while the inevitable model-plant mismatch resulting from the uncertainties in model parameters is addressed through a MPLS model using data from previous operations.

From the perspective of Baye's theory, unknown model parameter shows a probability distribution of certain shape (Gelman et al., 2004), which is distinct from the notion of treating a unknown parameter as a fixed quantity. To update model parameters, rigorous procedures, such as design of experiments (DoE), are generally required (Englezos and Kalogerakis, 2000). Though effective, they are not efficient, particularly for large and complex systems due to the heavy cost in experiment and computation. To this end, an alternative method based on a data-based technique is proposed for the B2B scheme in this research.

Firstly, it is shown in Chapter 3 that probability distributions of unknown model parameters could be conveniently summarized by 95% credible intervals, among which some span considerable wide range. Therefore, it initiates the idea to identify those kinetic parameters provided that enough system dynamic information is obtained, for example, on-line measurement profiles and batch-end product qualities available at the end of each batch. In light of this, the idea of MPLS model, which is previously used in Chapter 4 for process monitoring and batch-end product quality prediction, could serve similar purpose here in that it uses the available initial conditions, measurement trajectories, and batch-end product qualities to form an unfolded dataset $\mathbf{X}$ in order to predict the corresponding kinetic parameters $\mathbf{Y}$.

It is worth mentioning that the initial database for such MPLS model could be simply generated by running the first-principles process model with random combinations of kinetic parameters picked up from their credible intervals and with nominal input profiles subject to some normal disturbances. As this is generated off-line, selections of measurement profiles and product quality variables, as well as the size of the database and number of principle components used, can be well controlled to give predictions of kinetic parameters with good accuracy. Furthermore, the database and MPLS model can also be updated in a batch-to-batch manner during their on-line applications, say, B2B control of a batch process. As the process model is repeatedly updated at the batch end to compute the optimal input profile for the next batch, MPLS model is readily updated from batch to batch by simply running the simulation mention above based on the newly updated first-principles process model.

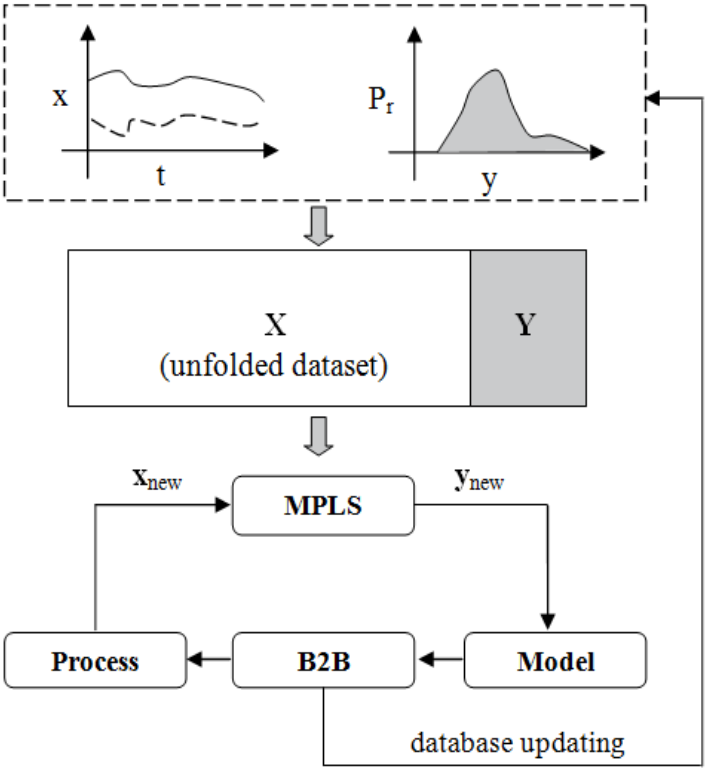

Figure 7.1: The proposed B2B control strategy based on the MPLS model.

When it comes to the prediction of kinetic parameters after each batch, similar procedures of MPLS as that used for process monitoring in Chapter 4 are considered (Geladi and Kowalski, 1986; Nomikos and MacGregor, 1995b). Nevertheless, to avoid abrupt substantial changes in model parameters, averages of parameter predictions obtained from the previous batches are usually adopted as follows.

$$\bar{\mathbf{y}}_j = \frac{1}{m} \sum_{k=j-m+1}^{j} \mathbf{y}_k \tag{7.1}$$

where $\bar{\mathbf{y}}_j$ is an average of parameter predictions for the *j*th batch based on those from the previous *m* batches, which is then incorporated into the first-principles model embedded in the B2B control strategy as illustrated in Figure 7.1.

In the batch-to-batch control strategy, the objective function to be minimized for the *j*th batch is as follows:

$$J_{\text{B2B}} = \min_{\mathbf{U}} \mathbf{W}_p \left(\mathbf{P} - \mathbf{P}_d \right)^2 + \Delta\mathbf{U}^T \mathbf{W}_{\Delta\text{U}} \Delta\mathbf{U} + d\mathbf{U}^T \mathbf{W}_{d\text{U}} d\mathbf{U} \tag{7.2}$$

where

$$\mathbf{U} = \left[\mathbf{u}_{j,0}^T, \mathbf{u}_{j,1}^T, \cdots, \mathbf{u}_{j,N-1}^T \right]^T,$$

$$\Delta\mathbf{U} = \left[\mathbf{u}_{j,1}^T - \mathbf{u}_{j,0}^T, \mathbf{u}_{j,2}^T - \mathbf{u}_{j,1}^T, \cdots, \mathbf{u}_{j,N-1}^T - \mathbf{u}_{j,N-2}^T \right]^T,$$

$$d\mathbf{U} = \left[\mathbf{u}_{j,0}^T - \mathbf{u}_{j-1,0}^T, \mathbf{u}_{j,1}^T - \mathbf{u}_{j-1,1}^T, \cdots, \mathbf{u}_{j,N-1}^T - \mathbf{u}_{j-1,N-1}^T \right]^T,$$

and $\mathbf{P}$ and $\mathbf{P}_d$ are the predicted and desired final product qualities, respectively, $\mathbf{u}_{j,k}$ is the input vector at the *k*th sampling instant of *j*th batch, N is the total number of samples in one batch, $\mathbf{W}_p$ is the weight vector corresponding to the final product quality, $\mathbf{W}_{\Delta U}$ and $\mathbf{W}_{dU}$ are the weight matrices to penalize excessive changes in the input variables for within-batch and inter-batch, respectively.

The above minimization problem is subject to the first-principles process model updated after each batch and inequality constraints $\mathbf{H}(\mathbf{U}) \le 0$. Differential evolution

(DE) (Storn and Price, 1997; Lampinen, 2002; Hermanto et al., 2011) or sequential quadratic programming (SQP) (Nocedal and Wright, 2006) technique can be implemented to solve the above minimization problem. The resulting optimal input **U** obtained is then implemented in an open-loop manner for the next batch.

7.3 Integrated B2B-NMPC control strategy

As aforementioned, the main drawback of a standard batch-to-batch control strategy results from its open-loop nature, where the correction is not made until the next batch. Therefore, the control performance of the current batch depends only on the accuracy of the process model, which is updated based on the information of previous batch. Consequently, its control performance may become sluggish or even diverging when the updated model is still not accurate, which is likely the case in the first few batches (Hermanto, 2008; Hermanto, et al., 2011). In light of this, combinations of the best efforts of B2B and online control strategies receive great interests decades ago. For example, it is possible and beneficial to integrate the nonlinear model predictive control (MMPC) technique proposed in Chapter 6 into the batch-to-batch control strategy to develop a new integrated B2B-NMPC control strategy, wherein both control strategies complement each other in an interactively way such that the online control can be tackled effectively by NMPC whose embedded nonlinear process model is refined through the batch-to-batch control by re-estimating model parameters from the previous batches (Paengjuntuek et al., 2008).

In the proposed integrated control strategy, the updating policy of the first-principles model in B2B as shown in Figure 7.1 remains the same. Whereas, the objective function to be minimized at every sampling time is as follows:

$$J_{\text{B2B-NMPC}} = \min_{\mathbf{U}} \mathbf{W}_p \left(\mathbf{P} - \mathbf{P}_d\right)^2 + \Delta\mathbf{U}^T \mathbf{W}_{\Delta\text{U}} \Delta\mathbf{U} + d\mathbf{U}^T \mathbf{W}_{d\text{U}} d\mathbf{U} \tag{7.3}$$

where

$$\mathbf{U} = \left[\mathbf{u}_{j,k}^T, \mathbf{u}_{j,k+1}^T, \cdots, \mathbf{u}_{j,N-1}^T\right]^T,$$

$$\Delta\mathbf{U} = \left[\mathbf{u}_{j,k}^T - \mathbf{u}_{j,k-1}^T, \mathbf{u}_{j,k+1}^T - \mathbf{u}_{j,k}^T, \cdots, \mathbf{u}_{j,N-1}^T - \mathbf{u}_{j,N-2}^T\right]^T,$$

$$d\mathbf{U} = \left[\mathbf{u}_{j,k}^T - \mathbf{u}_{j-1,k}^T, \mathbf{u}_{j,k+1}^T - \mathbf{u}_{j-1,k+1}^T, \cdots, \mathbf{u}_{j,N-1}^T - \mathbf{u}_{j-1,N-1}^T \right]^T,$$

and $\mathbf{W}_{\Delta U}$ and $\mathbf{W}_{dU}$ are the weight matrices which penalize excessive changes in the input variables which occur within-batch and inter-batch, respectively. The above minimization problem is subject to process model and inequality constraints $\mathbf{H}(\mathbf{U}) \le 0$.

The NMPC strategy considered here is based on the JITL-EPSAC technique (Su et al., 2012c) as described in Chapter 6 to achieve the desired final product qualities in a shrinking horizon way, where similar representations of $\mathbf{P}$, $\Delta\mathbf{U}$, and $d\mathbf{U}$ in Eq. (7.3) can be decomposed into:

$$\mathbf{P} = \mathbf{P}_b + \mathbf{G}_{pl}\delta\mathbf{U} \tag{7.4}$$

$$\Delta\mathbf{U} = \Delta\mathbf{U}_b + \mathbf{C}\delta\mathbf{U} \tag{7.5}$$

$$d\mathbf{U} = \mathbf{U}_b + \delta\mathbf{U} - \mathbf{U}_{prev} \tag{7.6}$$

where $\mathbf{P}_b$ is product quality calculated using the first-principles model with updated model parameters and with predetermined future inputs $\mathbf{U}_b = \left[\mathbf{u}_{b,k}^T, \mathbf{u}_{b,k+1}^T, \cdots, \mathbf{u}_{b,N-1}^T \right]^T$, $\mathbf{G}_{pl}$ is the state-space model coefficients matrix corresponding to the product quality, $\mathbf{U}_{prev} = \left[\mathbf{u}_{j-1,k}^T, \mathbf{u}_{j-1,k+1}^T, \cdots, \mathbf{u}_{j-1,N-1}^T \right]^T$ is the input sequence implemented in the previous batch, $\Delta\mathbf{U}_b = \left[\Delta\mathbf{u}_{b,k}^T, \Delta\mathbf{u}_{b,k+1}^T, \cdots, \Delta\mathbf{u}_{b,N-1}^T \right]^T$ is the change in the predetermined future inputs, and matrix $\mathbf{C}$ is as shown below.

$$\mathbf{C} = \begin{bmatrix} \mathbf{I} & \mathbf{0} & \cdots & \mathbf{0} & \mathbf{0} \\ -\mathbf{I} & \mathbf{I} & \cdots & \mathbf{0} & \mathbf{0} \\ \vdots & \vdots & \ddots & \vdots & \vdots \\ \mathbf{0} & \mathbf{0} & \cdots & -\mathbf{I} & \mathbf{I} \end{bmatrix} \tag{7.7}$$

Therefore, the minimization problem (7.3) becomes:

$$J_{B2B-NMPC} = \min_{\delta \mathbf{U}} \delta \mathbf{U}^T \boldsymbol{\Gamma} \delta \mathbf{U} + \boldsymbol{\Phi}^T \delta \mathbf{U} \tag{7.8}$$

where

$$\boldsymbol{\Gamma} = \mathbf{G}_{pl}^T \mathbf{W}_p \mathbf{G}_{pl} + \mathbf{C}^T \mathbf{W}_{\Delta u} \mathbf{C} + \mathbf{W}_{dU}$$

$$\boldsymbol{\Phi} = 2\left[\left(\mathbf{P}_b - \mathbf{P}_d \right)^T \mathbf{W}_p \mathbf{G}_{pl} + \Delta \mathbf{U}_b^T \mathbf{W}_{\Delta u} \mathbf{C} + \left(\mathbf{U}_b - \mathbf{U}_{prev} \right)^T \mathbf{W}_{dU} \right]^T$$

Analogously, the inequality constraints $\mathbf{H}(\mathbf{U})$ can be decomposed into:

$$\mathbf{H}_b + \mathbf{G}_{hl} \delta \mathbf{U} \le 0 \tag{7.9}$$

where $\mathbf{G}_{hl}$ is the state-space model coefficient matrix corresponding to the constraints and $\mathbf{H}_b$ is the constraints calculated using the updated first-principles model with predetermined future inputs $\mathbf{U}_b$. In this study, the soft-constraints approach (Hermanto et al., 2011) is utilized and the minimization problem is modified as follows:

$$\min_{\delta U, \varepsilon} J_{\text{sc, B2B-NMPC}} \tag{7.10}$$

subject to

$$\mathbf{H}_b + \mathbf{G}_{hl} \delta \mathbf{U} \le \boldsymbol{\varepsilon} \tag{7.11}$$

$$\boldsymbol{\varepsilon} \ge \mathbf{0} \tag{7.12}$$

where $J_{\text{sc, B2B-NMPC}} = J_{\text{B2B-NMPC}} + \boldsymbol{\varepsilon}^T \mathbf{W}_\varepsilon \boldsymbol{\varepsilon} + \boldsymbol{\varepsilon}^T \mathbf{w}_\varepsilon$, $\boldsymbol{\varepsilon}$ is a vector of slack variables, $\mathbf{W}_\varepsilon$ is a diagonal matrix of positive weight, and $\mathbf{w}_\varepsilon$ is a vector of positive elements.

Hence, the solution to the modified minimization problem is as follows:

$$J^*_{\text{sc, B2B-NMPC}} = \min_{\delta \mathbf{U}, \boldsymbol{\varepsilon}} \delta \mathbf{U}^T \boldsymbol{\Gamma} \delta \mathbf{U} + \boldsymbol{\Phi}^T \delta \mathbf{U} + \boldsymbol{\varepsilon}^T W_\varepsilon \boldsymbol{\varepsilon} + \boldsymbol{\varepsilon}^T \mathbf{w}_\varepsilon$$

$$= \min_{\delta\mathbf{U},\boldsymbol{\varepsilon}} \begin{bmatrix} \delta\mathbf{U}^T & \boldsymbol{\varepsilon}^T \end{bmatrix} \begin{bmatrix} \boldsymbol{\Gamma} & \mathbf{0} \\ \mathbf{0} & \mathbf{W}_\varepsilon \end{bmatrix} \begin{bmatrix} \delta\mathbf{U} \\ \boldsymbol{\varepsilon} \end{bmatrix} + \begin{bmatrix} \boldsymbol{\Phi}^T & w_\varepsilon^T \end{bmatrix} \begin{bmatrix} \delta\mathbf{U} \\ \boldsymbol{\varepsilon} \end{bmatrix}$$

$$= \min_{\boldsymbol{\Pi}} \boldsymbol{\Pi}^T \boldsymbol{\Lambda} \boldsymbol{\Pi} + \boldsymbol{\tau}^T \boldsymbol{\Pi} \tag{7.13}$$

subject to

$$\begin{bmatrix} \mathbf{H}_b \\ \mathbf{0} \end{bmatrix} + \begin{bmatrix} \mathbf{G}_{hl} & -\mathbf{I} \\ \mathbf{0} & -\mathbf{I} \end{bmatrix} \boldsymbol{\Pi} \le \mathbf{0} \tag{7.14}$$

where $\boldsymbol{\Pi} = \begin{bmatrix} \delta\mathbf{U}^T & \boldsymbol{\varepsilon}^T \end{bmatrix}^T$, $\boldsymbol{\Lambda} = \begin{bmatrix} \boldsymbol{\Gamma} & \mathbf{0} \\ \mathbf{0} & \mathbf{W}_\varepsilon \end{bmatrix}$, and $\boldsymbol{\tau} = \begin{bmatrix} \boldsymbol{\Phi}^T & \mathbf{w}_\varepsilon^T \end{bmatrix}^T$.

In summary, the procedure of implementing the integrated B2B-NMPC control strategy for each batch *j* and sampling time *k* is as follows:

(1) Prepare the database matrices **X** and **Y** for the MPLS model as follows:

- if $j = 1$, the database matrices **X** and **Y** for the MPLS model can be obtained by offline simulation runs. For example, input sequences around the optimal input trajectory for the nominal first-principles model, as well as a random combinations of model parameters selected from their probability distributions, are implemented to the process model and the resulting state variables profiles are used to construct the database.
- if $j > 1$, update the database matrices by including the previous simulation runs computed by NMPC during the online control into the database. In this study, the moving window approach is adopted, where the dataset from the earliest runs is removed every time a new dataset is included.

(2) Update the process model: collect the initial conditions, measurement trajectories and batch-end product qualities from previous batch to form vector $\mathbf{x}_{new}$ and predict the model parameters $\mathbf{y}_{new}$ through the updated MPLS model. And average the prediction of model parameters by Eq. (7.1)

(3) Obtain $\mathbf{U}_b$ by the following method:

- If $k = 0$ and *iter* = 1, $\mathbf{U}_b$ is chosen from the nominal operating point which was used in the previous batches;
- If $k > 0$ and *iter* = 1, $\mathbf{U}_b$ is set as the $\mathbf{U}_{optimal}$ obtained in the previous sampling instance;
- If *iter* > 1, the updated $\mathbf{U}_b$ from the previous iteration is used; where *iter* is the iteration count.

(4) Obtain $\mathbf{P}_b$ and $\mathbf{H}_b$ by using $\mathbf{U}_b$ as the input to the updated first-principles process model. In this study, it is assumed that the state variables are measured.

(5) Obtain the state space model coefficient matrices $\mathbf{G}_{pl}$ and $\mathbf{G}_{hl}$ by using JITL with reference to the query point.

(6) Obtain $\mathbf{\Pi}^* = \begin{bmatrix} \delta\mathbf{U}^{*T} & \boldsymbol{\varepsilon}^{*T} \end{bmatrix}^T$ from the solution to the minimization problem (7.13) and (7.14), then update the element of $\mathbf{U}_b$ using

$$\mathbf{u}_{b,\,k+j} = \mathbf{u}_{b,\,k+j} + \delta\mathbf{u}_{k+j}$$

where $j = 0,\ \cdots,\ N-1$.

(7) Calculate $err = \left\| \begin{bmatrix} \mathbf{G}_{pl} \\ \mathbf{G}_{hl} \end{bmatrix} \delta\mathbf{U}^* \right\|$. If *err* is greater than a specified tolerance, *iter* = *iter* + 1, and go back to Step (3). Otherwise, set $\mathbf{U}_{optimal} = \mathbf{U}_b$ and implemented the first element of $\mathbf{U}_{optimal}$ to the process.

(8) If the end of the current batch is reached, repeat from step (1) and go to the next batch.

7.4 Results and discussion

To illustrate and compare the control performances of the standard B2B and integrated B2B-NMPC control strategies, simulation studies of their applications to the semi-batch pH-shift reactive crystallization of L-glutamic acid were investigated. Details of the reactive crystallization process for controlling purpose can be found in Chapters 3 and 6 with some of the features specifically defined as follows.

7.4.1 Process and controllers specification

Three scenarios of the crystallization process are summarized in Table 7.1 with four crystallization kinetic parameters of α and β polymorphs, which have relatively high sensitivities to the process, were taken into account, while others remained the same as in Table 3.2. Of the three scenarios, the Case 1 considers a nominal crystallization process, Case 2 has fast nucleation and slow growth rate parameters, while Case 3 has slow nucleation and fast growth rate parameters. The process was first started in Case 1 and then shifted to abnormal Case 2 after the first batch and stayed at this scenario until the 30th batch. From batch 31 to batch 60, the process entered the Case 3, after which it resumed to the nominal Case 1 from the 61th batch till the 90th batch.

The first batch was initialized with a nominal optimal flowrate profile as shown in Figure 7.2, which was obtained under nominal process by JITL-EPSAC in Chapter 6 to achieve a desired α-form polymorphic purity, P_α, of 0.8255. In addition, the initial database for MPLS model was generated by introducing random disturbances of $N(0, 0.5)$ to this nominal optimal flowrate profile at each sampling instant, with some of them depictured in Figure 7.2. Besides, variations of the four studied kinetic parameters within their respective 95% credible intervals were also introduced during the simulation runs for initial database generation. With the recent development in process analytical techniques (PAT), more abundant process data are now available, though correlated to each other. Nevertheless, initial concentrations of monosodium glutamate and sulfuric acid, complete state variable trajectories of pH value, crystallizer volume, solute concentrations by ATR-FTIR, mean crystal size by FBRM

or PVM, the zeroth and first moments of crystal size distribution by FBRM, and polymorphic purity of α-form by Raman spectroscopy, as well as the batch-end product yield, are all collected to construct the unfolded dataset **X**, similar as that in Chapter 4 for process monitoring. While the four kinetic parameters formed the dataset **Y**. Totally 200 batches of simulation runs were used to construct the MPLS model with the number of principle components fine-tuned as 7 by cross-validation. Incidentally, during the online application, here we assumed that all these state variables are measured or observable by observers, such as extended Kalman filter (EKF) or unscented Kalman filter (UKF) (Hermanto et al., 2009; Mesbah et al., 2011; Li et al., 2012). Additional unseen 30 batches were employed for validation test given in Figure 7.3, which shows the MPLS model is capable of inferring the kinetic parameters from the provided system dynamic information.

It should be pointed out that this initial database was used for both B2B and B2B-NMPC control strategies and was then updated by their control techniques individually during on-line implementation for all the 90 batches, from which the merit of the batch-to-batch control can be demonstrated by gradually learning, from the previous batches, the system dynamic information while the process suffered from shifting among scenarios of abnormality.

For the controller implementation, the minimization problem of (7.2) for standard B2B was solved by the DE method (Lampinen, 2002; Hermanto et al., 2011), while the integrated B2B-NMPC was transferred to a soft-constrained problem of (7.10) and therefore a time-saving quadratic programming method was conveniently adopted (Hermanto et al., 2009; 2011). The tuning parameters for the studied two controllers are listed in Table 7.2.

7.4.2 Results comparison and discussion

For the batch-end product quality control of α-form polymorphic purity, performances of the B2B and integrated B2B-NMPC control strategies, when crystallization process underwent from Case 1 to Case 2 during the first 30 batches, are illustrated in Figures

7.4 and 7.5 for addition flowrate profiles of sulfuric acid, respectively. Figure 7.6 shows the final product quality, while Figures 7.7 and 7.8 demonstrate the convergences of the four kinetic parameters.

It is observed that the integrated B2B-NMPC shows smoother and faster convergences in both flowrate profile and final product quality compared to the standard B2B control strategy, though not only the penalty weights for excessive changes inter and within the batches are the same for both control strategies, as shown in Table 7.2, but also the kinetic parameters updated by MPLS model converged at nearly the same rate, as can be seen from Figures 7.7 and 7.8. This well explains the fact that the open-loop nature of B2B results into the unsatisfied control performance when the model-plant mismatch are large. On the other hand, the robustness of the proposed JITL-EPSAC in Chapter 6 is further enhanced since under large model-plant mismatch, the JITL-EPSAC gradually improved the final polymorphic purity with the embedded first-principles model refined by MPLS model from batch to batch.

The second simulation study considered the crystallization process shifted from Case 2 to Case 3 in the 31th batch and continued the Case 3 to the 60th batch. Interestingly, the standard B2B slowly reached the final product quality set point, however, it then diverged as shown in Figure 7.6. To the contrary, the integrated B2B-NMPC more steadily reduced the unexpected high polymorphic purity to the set point to maintain a constancy of the product quality. Worth to note is that the database for MPLS model was not regenerated around the current flowrate profile, but renewed by gradually incorporating the simulation runs computed by B2B or integrated B2B-NMPC techniques, upon which the convergences of the four kinetic parameters by MPLS model can also be found in Figures 7.7 and 7.8, respectively.

Lastly, the crystallization process returned to the nominal Case 1 from abnormal Case 3 after the 61th batch. Consistent results as of the above simulation studies for both control strategies are observed as given in Figures 7.6 and 7.8 for batches from 61 to 90.

Table 7.1: Variations in model kinetic parameters for B2B control study: Case 1 is the nominal model, Case 2 has fast nucleation and slow growth rate parameters, Case 3 has slow nucleation and fast growth rate parameters.

Cases	$k_{b,\alpha 1}$	$k_{g,\alpha 2}$	$E_{g,\alpha 2}$	$k_{g,\beta 1}$
1	1.00×10^{11}	9.84×10^{-7}	0.888	1.07×10^{-7}
2	1.20×10^{11}	7.87×10^{-7}	1.066	0.86×10^{-7}
3	0.80×10^{11}	1.18×10^{-6}	0.710	1.28×10^{-7}

Table 7.2: Tuning parameters for two controllers.

B2B Control	B2B-NMPC Control
$\mathbf{W}_p = 1$	$\mathbf{W}_p = 1$
$\left(\mathbf{W}_{\Delta U}\right)_{i,i} = 1\times10^{-5}$ *	$\left(\mathbf{W}_{\Delta U}\right)_{i,i} = 1\times10^{-5}$
$\left(\mathbf{W}_{dU}\right)_{i,i} = 1\times10^{-4}$	$\left(\mathbf{W}_{dU}\right)_{i,i} = 1\times10^{-4}$
$\mathbf{W}_\varepsilon = \mathbf{I}$	
$\mathbf{w}_\varepsilon = \left[1,1,\cdots 1\right]^T$	

* The diagonal elements of matrices, where i = 1, ..., N.

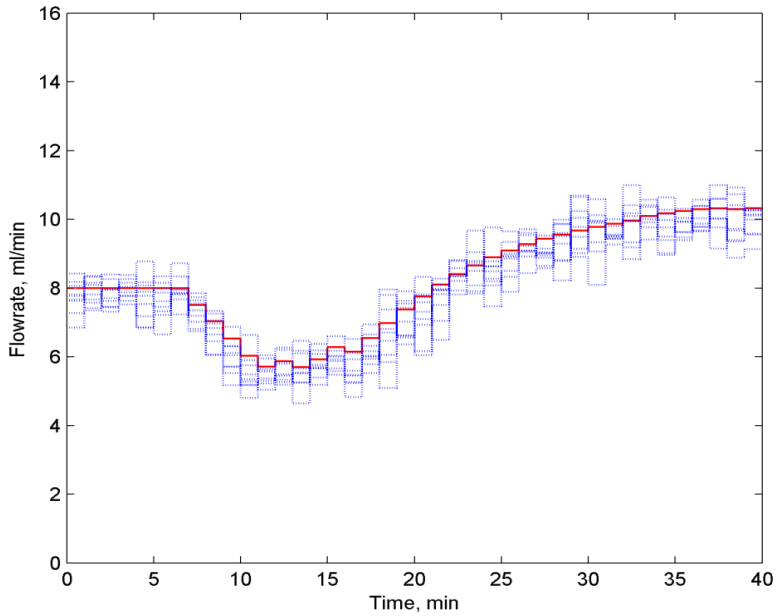

Figure 7.2: Flowrate profiles for initial database generation of MPLS model (solid line: nominal optimal flowrate trajectory; dash line: random flowrate profiles around the nominal one).

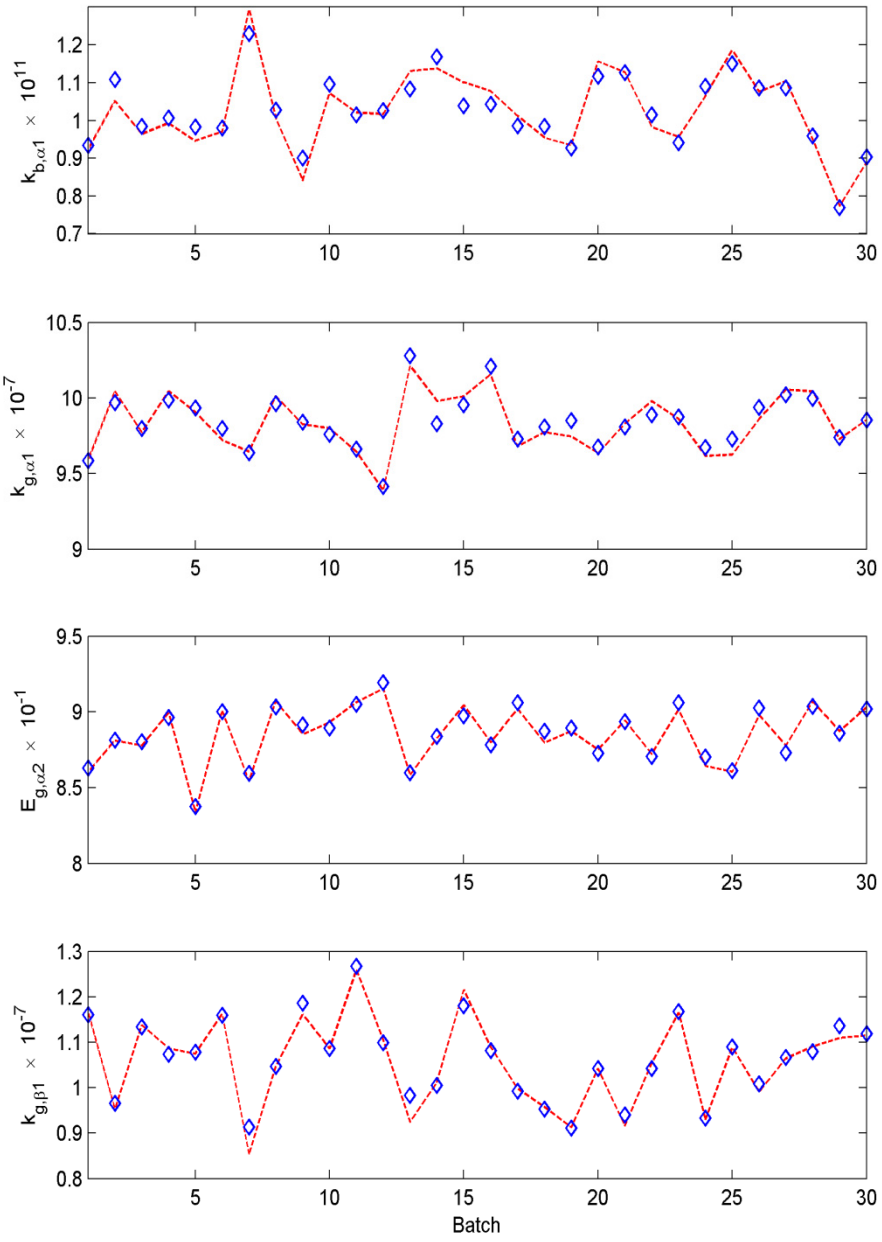

Figure 7.3: Validation result of MPLS model for kinetic parameters estimation (dash line: process value; symbol: predicted data by MPLS).

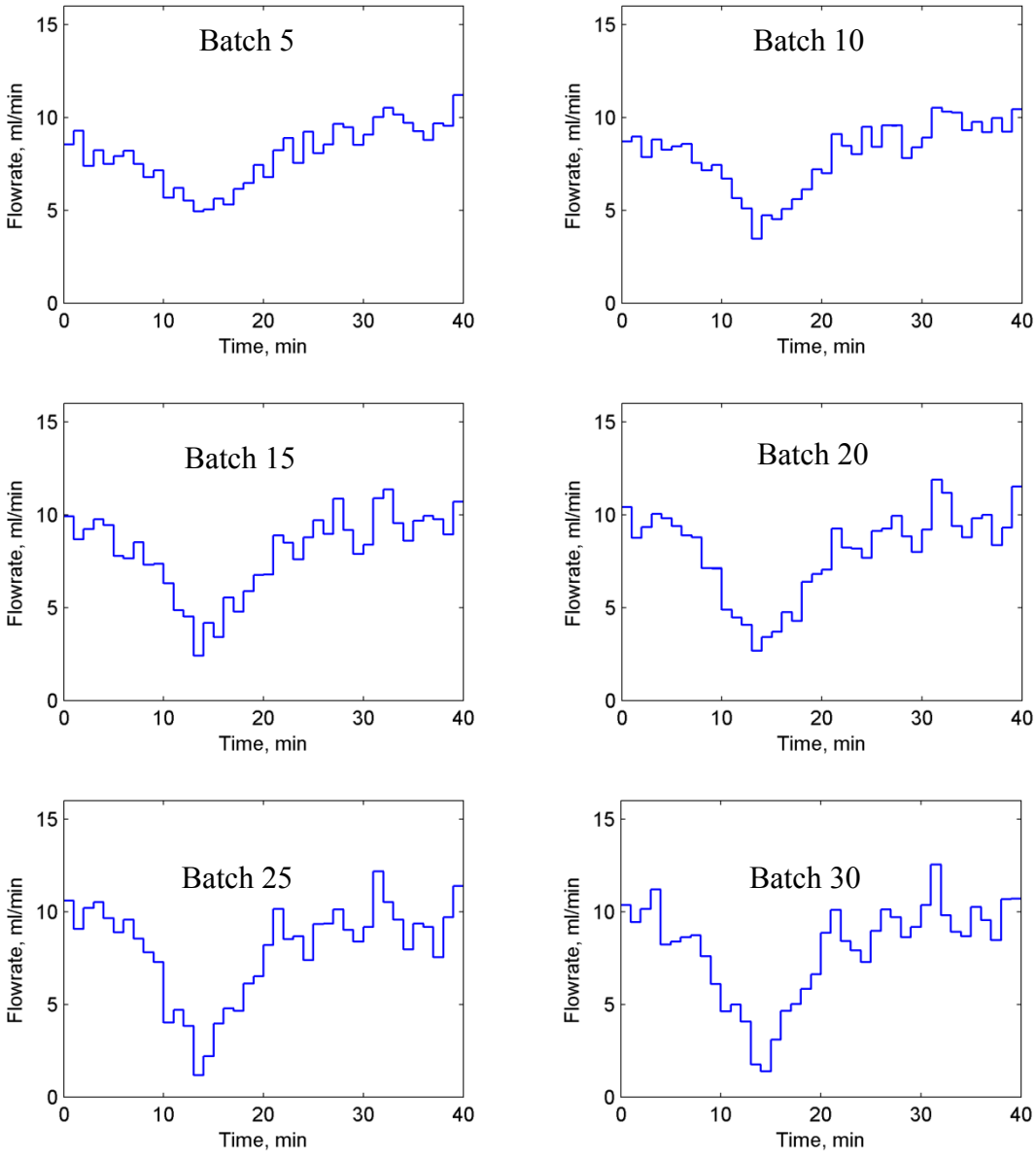

Figure 7.4: Flowrate profiles of B2B control strategy from nominal process of Case 1 to abnormal Case 2.

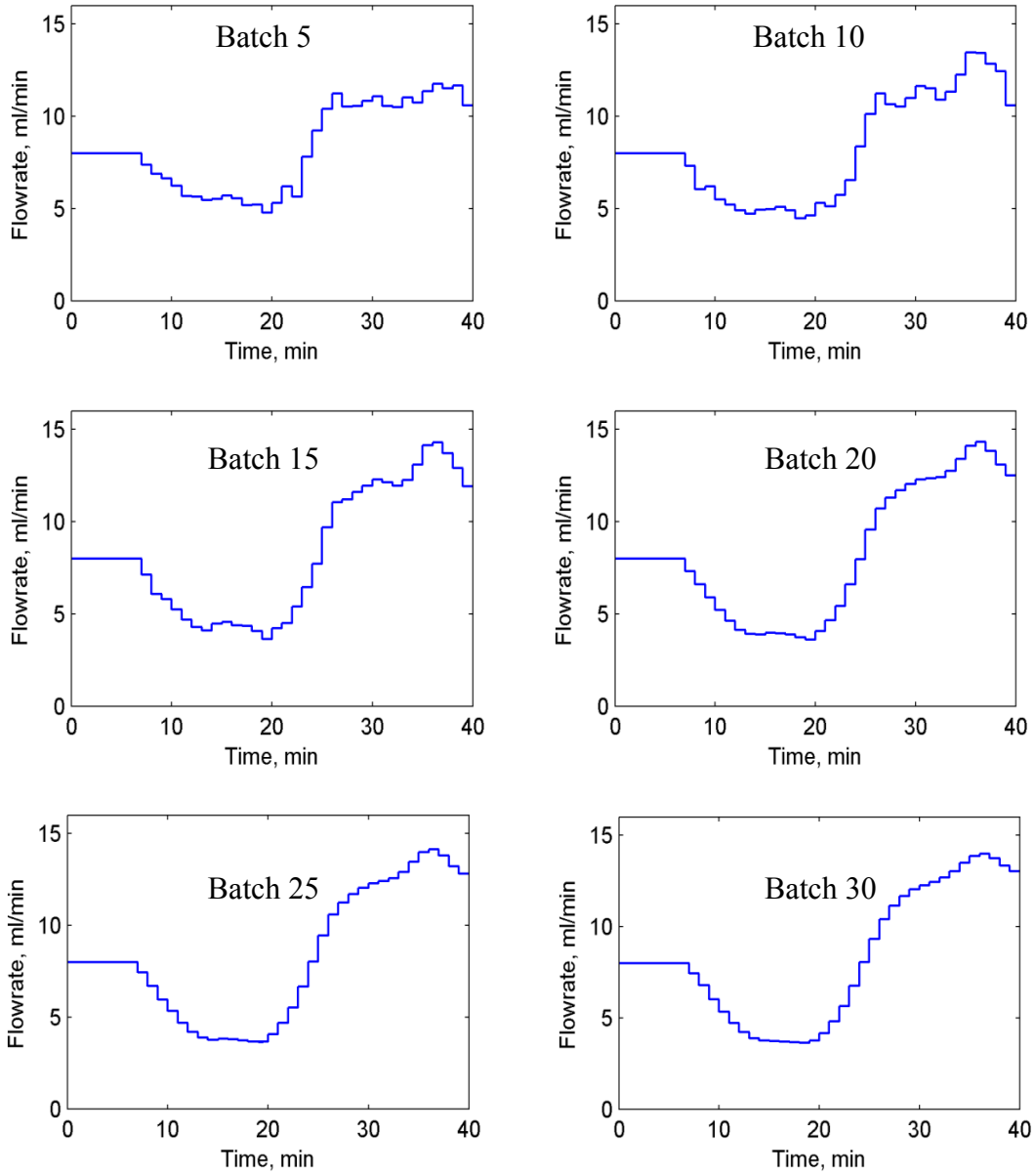

Figure 7.5: Flowrate profiles of B2B-NMPC control strategy from nominal process of Case 1 to abnormal Case 2.

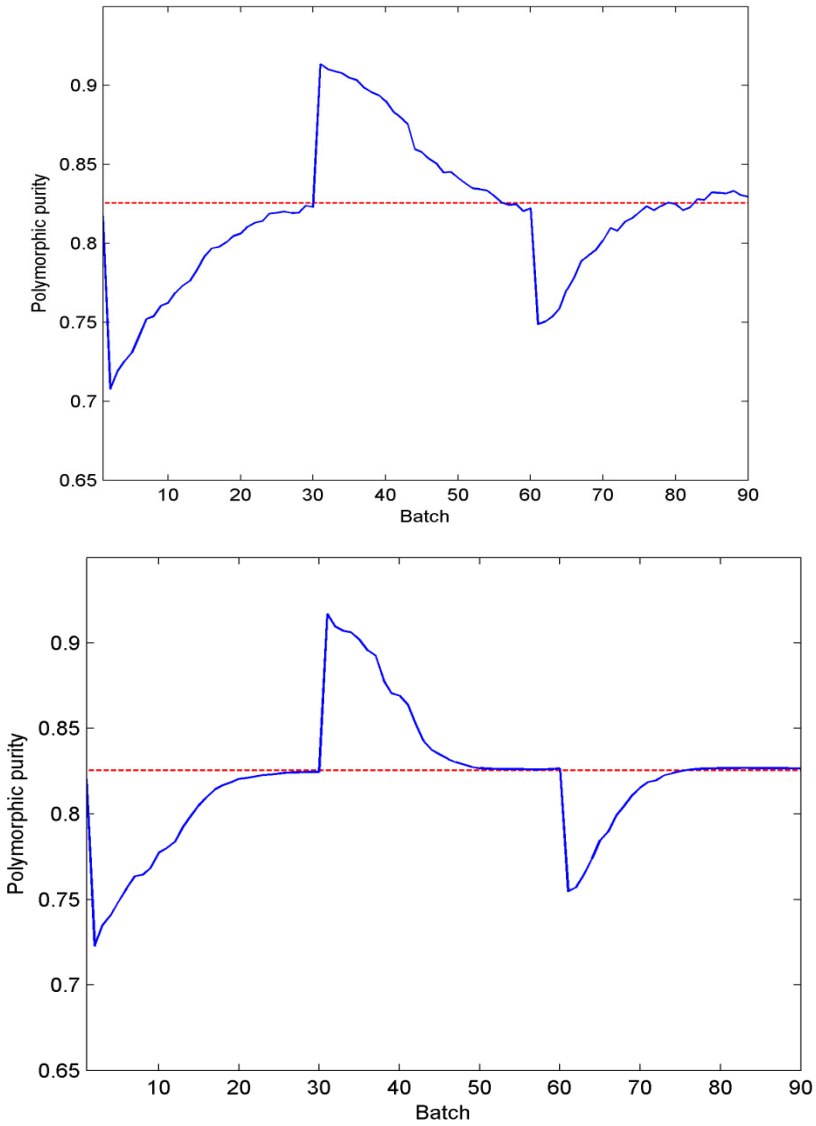

Figure 7.6: Polymorphic purity of B2B (top) and B2B-NMPC (bottom) control strategies for Case 1, Case 2 and Case 3 (dash line: final quality setpoint; solid line: final quality).

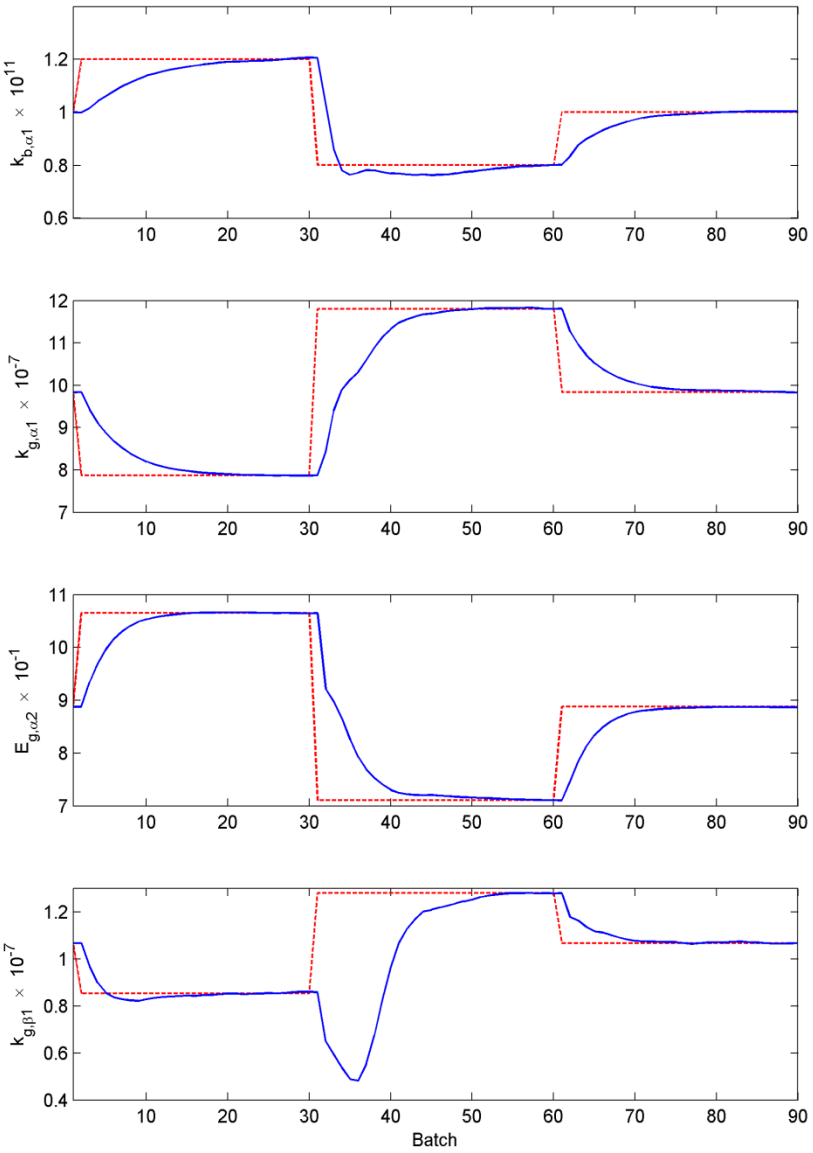

Figure 7.7: Kinetic parameters updating of B2B control strategies for Case 1, Case 2 and Case 3 (dash line: process value; solid line: estimated value).

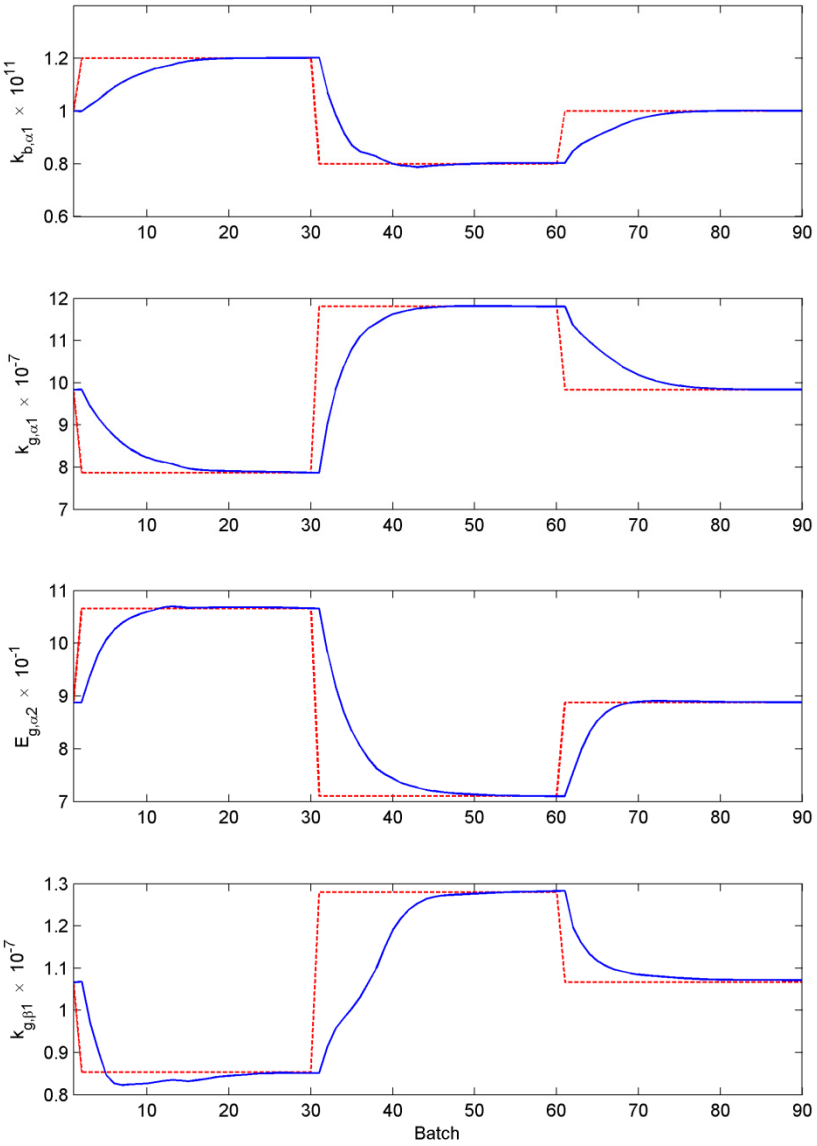

Figure 7.8: Kinetic parameters updating of B2B-NMPC control strategies for Case 1, Case 2 and Case 3 (dash line: process value; solid line: estimated value).

7.5 Conclusions

A new integrated B2B-NMPC control strategy based on a MPLS model and the JITL-EPSAC technique was proposed in this chapter. The MPLS model is capable of inferring the model kinetic parameters from the system dynamic information obtained from previous batches, which updates the first-principles model for the JITL-EPSAC. While the robustness of the JITL-EPSAC helps to improve the batch-end product quality online even under large model-plant mismatch. Moreover, the proposed integrated B2B-NMPC was applied to the studied semi-batch pH-shift reactive crystallization process and also compared to a standard B2B control strategy. The simulation results showed that the proposed integrated control strategy performed a much smoother and faster convergence to the final product quality set point under multiple shifts of abnormal scenarios, showing the capability to maintain consistent production of on-spec product, which has never been demonstrated by direct design control or NMPC control discussed in previous works.

Chapter 8

Conclusions and Future Work

8.1 Conclusions

In the wake of the recent research development prompted by the process analytical techniques (PAT) in batch cooling and antisolvent crystallization processes, the reactive crystallization process has also been receiving increasing interest (Borissova et al. 2005; Alatalo et al., 2008; Qu et al., 2009) due to its importance and wide application in industry. This thesis investigated the modeling, monitoring, and control of a semi-batch pH-shift reactive crystallization process using the polymorphic L-glutamic acid as a model compound.

Chapter 3 presented a first-principles mathematical model for the semi-batch pH-shift reactive crystallization process taking into account the effects of protonation and deprotonation of glutamic acid, crystal size distribution, polymorphic crystallization, and non-ideal solution properties. The kinetic parameters were estimated by Bayesian inference from experimental data available in the open literature (Alatalo et al., 2008; Qu et al., 2009), such as pH value, solute concentration by attenuated total reflectance-Fourier transformed infrared (ATR-FTIR), polymorphic purity by Raman spectroscopy, etc., from which marginal probability distributions of the parameters can be obtained by Markov Chain Monte Carlo (MCMC) simulation. Validation results showed that the model predictions were in good agreement with the experimental observations. To the best of our knowledge, this model is the first one in the literature capable of dealing with high supersaturation level, viz., kinetically controlled polymorphic crystallization,

A moving-window multiway principle component analysis (MPCA) was put forward in Chapter 4 for online monitoring in the reactive crystallization process. Various *in situ* measurements, such as focused beam reflectance measurement (FBRM), could be incorporated to construct a batch-wise unfolded dataset summarizing a reference distribution of normal batches, against which the performance of independent new batches can be compared (Zhao et al., 2011). The moving-window idea of building multiple MPCA models at different time points was successfully introduced to tackle the transitional phase changes due to process nonlinearity and time-varying characteristics inherent in the pH-shift reactive crystallization process. In comparison with the conventional MPCA and multiway partial least squares (MPLS) (Nomikos and MacGregor, 1994; 1995a; 1995b), the proposed method can not only efficiently detect the abnormal batch, but also reflect the contributions of the control actions to revert the process to in-control state. This is a significant advantage in batch process operation to reduce the false alarms when control actions are implemented and working.

In Chapter 5, direct design control strategies based on solute concentration and polymorphic purity were developed to track the predetermined nominal optimal solute and polymorphic purity trajectories, respectively. The first method is the JITL-based C-control strategy capable of coping with highly nonlinear dynamics encountered in pH-shift reactive crystallization process. The second method tracked the polymorphic purity trajectory and achieved better performance than that of the solute concentration trajectory, indicating the deficiency of C-control strategy in dealing with the complicated polymorphic crystallization, whereas the polymorphic purity control gives improved performance because it is closely related to the progress of polymorphic crystallization and hence is more direct to the product quality.

Chapters 6 and 7 focused on the implementation of nonlinear model predictive control (NMPC) strategies in the batch/semi-batch crystallization process, which is rather limited, particularly, in the shrinking horizon mode for batch-end product quality control. Toward this end, the extended prediction self-adaptive control

(EPSAC), which iteratively linearizes the nonlinear process dynamics around the base input and output trajectories using convolution models, was reformulated as the JITL-EPSAC in Chapter 6 using state-space models. Simulation studies showed the proposed EPSAC method outperformed the previous ESPAC method developed by Hermanto et al. (2009) in final product quality control for the pH-shift reactive crystallization process, as well as the ease of tuning of weights and reduction of computational efforts.

In an attempt to correct the bias left uncorrected during online batch-end product quality control in the presence of model-plant mismatch, a new integrated B2B-NMPC control strategy based on a MPLS model and the JITL-EPSAC technique was proposed in Chapter 7 to explore the repetitive nature of batch process to update kinetic parameters in the process model using process information from previous batches (Paengjuntuek et al., 2008). Comparing to the conventional B2B control strategy, the new integrated JITL-EPSAC scheme showed a much smoother and faster convergence to the set point of final product quality under multiple shifts of abnormal scenarios, showing its capability of maintaining consistent production of on-spec product. This has never been demonstrated by direct design control or NMPC control discussed in previous works (Hermanto et al., 2011).

8.2 Suggestions for future work

To improve the current studies in the semi-batch pH-shift reactive crystallization process, further investigations are suggested as follows.

First, it would be of importance to further determine the root causes of the discrepancies between model predictions of crystal size distribution and experimental data in Chapter 3, for example, applying the ultrasound to the slurry samples to assure the disperse of small crystal particles adhered to the larger ones before laser diffraction measurement. Breakage and agglomeration effects could also be taken into account in the population balance model to characterize the possible effects of mixing intensity on secondary nucleation and large particles observed in crystal size

measurement. In respect to the noises of Raman spectroscopy and corresponding correction term for polymorphic purity measurement, further confirmations from experimental observations and more detailed calibration method are motivated.

Besides, the current work in Chapter 4 only took into account the monitoring effort of the multivariate statistical process control (MSPC) (Nomikos and MacGregor,1995a; Kano et al., 2011), which could be followed by the diagnosis step in future to detect the causes of the monitoring alarms, as well to classify the abnormal scenarios into several categories, such as, excessive nucleation, sluggish crystal growth, containments in solvent, or detector fouling, in order to take remedial control actions or emergent procedures accordingly (Kamaraju and Chiu, 2012).

In Chapter 5, instead of using the phase diagram of glutamic acid solubility against the temperature, alternative solubility of glutamic acid considering other ionic species against pH value at constant temperature (Hatakka et al., 2010) could also be considered for the direct design and control to calculate the pH value set point using the same JITL framework developed in this thesis. By including the dynamics of PID controller designed to regulate pH value, a comparative study of different direct design and control strategies, including the proposed polymorphic purity control by local time, is worthwhile investigation

In Chapters 6 and 7, other than the uncertainties in kinetic parameters considered to evaluate the robustness of proposed JITL-EPSAC and integrated B2B-NMPC techniques, other uncertainties due to the model structure and initial conditions of the crystallization process can be investigated in the future case studies. Furthermore, to address the possible slow convergence of the B2B-NMPC, the effect of weight parameters designed for the objective function on the convergence speed of the B2B-NMPC warrants further studies.

Furthermore, the computational cost is always one of the largest barriers for the practical implementation of nonlinear model predictive control (NMPC), in which the state variables estimation by observers, like unscented Kalman filter (UKF) (Hermanto et al., 2009; 2011; Mesbah et al., 2011), and the modeling of crystal size

distribution by population balance model are always computationally demanding, in particular for reactive crystallization systems, where the mass balance equations are highly complex and interactive with population balance model. In this respect, it has been investigated that by tracking the necessary conditions of optimality, assuming it exists, the optimality of product quality is enforced by implementing the fundamental controllers, such as PI- or PID-type controllers (Welz et al., 2008; Srinivasan et al., 2008; Gros et al., 2009; Chachuat et al., 2009). Hence, it would be of both theoretical and practical interests to apply those techniques to the semi-batch pH-shift reactive crystallization process in the future.

Lastly, crystallization is generally only one of the major separation and purification steps in process industries, for example, the reactive crystallization is usually serving as those initial steps to separate the product from raw materials, further unit operations, such as recrystallization, filtration, grinding, etc., are of equivalent importance in determining the end-user product qualities (Randolph and Larson, 1988). Therefore, from a plant-wide point of view, complete flow sheet simulation, monitoring, and control of a pilot- or large-scale crystallization process is alluring and contributing to the industrial practices, which is a good way for the current work in this thesis to be further directed.

References

Aamir E, Nagy ZK, Rielly CD, Kleinert T, Judat B. Combined quadrature method of moments and methods of characteristics approach for efficient solution of population balance models for dynamic modeling and crystal size distribution control of crystallization processes. *Industrial & Engineering Chemistry Research.* 2009;48:8575-8584.

Abbas A, Nobbs D, Romagnoli JA. Investigation of on-line optical particle characterization in reaction, and cooling crystallization systems-Current state of the art. *Measurement Science & Technology.* 2002;13:349-356.

Ahn HS, Chen YQ, Moore KL. Iterative learning control: brief survey and categorization. *IEEE Transaction on Systems, Man and Cybernetics-Part C: Applications and Reviews.* 2007;37:1099-1121.

Alatalo H, Kohonen J, Qu H, Hatakka H, Reinikainen SP, Louhi-Kultanen M, Kallas J. In-line monitoring of reactive crystallization process based on ATR-FTIR and Raman spectroscopy. *Journal of Chemometrics.* 2008;22:644-652.

Alatalo H, Hatakka H, Kohonen J, Reinikainen S, Louhi-Kultanen M. Process control and monitoring of reactive crystallization of L-glutamic acid. *AIChE Journal.* 2010a;56:2063-2076.

Alatalo HM, Hatakka H, Louhi-Kultanen M, Kohonen J, Reinikainen S. Closed-loop control of reactive crystallization. Part I: supersaturation-controlled crystallization of L-glutamic acid. *Chemical Engineering Technology.* 2010b;33:743-750.

Allgöwer F, Findeisen R, Nagy ZK. Nonlinear model predictive control: From theory to application. *Journal of Chinese Institute of Chemical Engineers.* 2004;35:299-315.

Arteaga F, Ferrer A. Dealing with missing data in MSPC: several methods, different interpretations, some examples. *Journal of Chemometrics.* 2002;16:408-418.

Bard Y. *Nonlinear parameter estimation.* New York: Academic Press, 1974.

Bates DM, Watts DG. *Nonlinear regression analysis and its application.* New York: Wiley, 1988.

Beck JV, Arnold KJ. *Parameter estimation in engineering and science.* New York: Wiley, 1977.

Black SN, Davey RJ. Crystallization of amino acids. *Journal of Crystal Growth.* 1988;90:136-144.

Blagden N, Davey R. Polymorphs take place. *Chemistry in Britain.* 1999;35:44-47.

Bois FY, Fahmy T, Block JC, Gatel D. Dynamic modeling of bacteria in a pilot drinking-water distribution system. *Water Research.* 1997;31:3146-3456.

Bonvin D, Srinivasan B, Hunkeller D. Control and optimization of batch processes. *IEEE Control Systems Magazine.* December, 2006.

Bonvin D. Optimal operation of batch reactors-a personal view. *Journal of Process Control.* 1998;8:355-368.

Borissova A, Jammoal Y, Javed KH, Lai X, Mahmud T, Penchev R, Roberts KJ, Wood W. Modeling the precipitation of L-glutamic acid via acidification of monosodium glutamate. *Crystal Growth & Design.* 2005;5:845-854.

Botsaris GD. *Secondary nucleation-a review.* Plenum Press, New York, 1976.

Box GEP, Draper NR. The Bayesian estimation of common parameters from several responses. *Biometrika.* 1965;52:355-365.

Braatz RD. Advanced control of crystallization processes. *Annual Reviews in Control.* 2002;26:87-99.

Bretthorst GL. An introduction to parameter estimation using Bayesian probability theory. *In: Fougere PF. Maximum Entropy and Bayesian Methods.* Dordrecht: Kluwer Academic Publishers, 1990:53-79.

Caillet A, Sheibat-Othman N, Fevotte G. Crystallization of monohydrate citric acid. 2. Modeling through population balance equations. *Crystal Growth & Design.* 2007;7:2088-2095.

Camacho J, Picó J, Ferrer A. Bilinear modelling of batch processes. Part I: theoretical discussion. *Journal of Chemometrics.* 2006;22:299-308.

Camacho J, Picó J, Ferrer A. The best approaches in the on-line monitoring of batch processes based on PCA: Does the modelling structure matter? *Analytica Chimica Acta.* 2009;642:59-68.

Carlin BP, Louis TA. *Bayes and Empirical Bayes Methods for Data Analysis.* Boca Raton: Chapman & Hall/CRC, 2000.

Cervantes AL, Agamennoni OE, Figueroa JL. A nonlinear model predictive control system based on Wiener piecewise linear models. *Journal of Process Control.* 2003;13:655-666.

Chachuat B, Srinivasan B, Bonvin D. Adaptation strategies for real-time optimization. *Computers and Chemical Engineering.* 2009;33:1557-1567.

Chen WS, Bakshi BR, Goel PK, Ungarala S. Bayesian estimation via sequential Monte Carlo sampling: unconstrained nonlinear dynamic systems. *Industry & Engineering Chemistry Research.* 2004;43:4012-4025.

Cheng C, Chiu MS. A new data-based methodology for nonlinear process modeling. *Chemical Engineering Science.* 2004;59:2801-2810.

Cheng C, Chiu MS. Nonlinear process monitoring using JITL-PCA. *Chemometrics and Intelligent Laboratory Systems.* 2005;76:1-13.

Cheng C, Chiu MS. Adaptive IMC Controller Design for Nonlinear Process Control. *Chemical Engineering Research and Design.* 2007;85:234-244.

Cheng C, Chiu MS. Robust PID controller design for nonlinear processes using JITL technique. *Chemical Engineering Science.* 2008;21:5141-5148.

Chin IS, Lee KS, Lee JH. A technique for integrated quality control, profile control, and constraint handling of batch processes. *Industrial & Engineering Chemistry Research.* 2000;39:693-705.

Cisternas LA, Vásquez CM, Swaney RE. On the design of crystallization-based separation processes: Review and extension. *AIChE Journal.* 2006;52:1754-1769.

Clarke-Pringle TL, MacGregor JF. Optimization of molecular-weight distribution using batch-to-batch adjustments. *Industry & Engineering Chemistry Research.* 1998;37:3660-3669.

Clontz NA, McCabe WL. Contact nucleation of magnesium sulfate heptahydrate. *AIChE Symposium Series.* 1971;67:6-17.

Coleman MC, Block DE. Bayesian parameter estimation with formative priors for nonlinear systems. *AIChE Journal.* 2006;52:651-667.

Cornel J, Lindenberg C, Mazzotti M. Experimental characterization and population balance modeling of the polymorph transformation of L-glutamic acid. *Crystal Growth & Design.* 2009;9:243-252.

Costa CBB, Maciel MRW, Filho RM. Considerations on the crystallization modeling: population balance solution. *Computers and Chemical Engineering.* 2007;31:206-218.

Cote A, Zhou G, Stanik M. A novel crystallization methodology to ensure isolation of the most stable crystal form. *Organic Process Research & Development.* 2009;13:1276-1283.

Darby ML, Nikolaou M. MPC: Current practice and challenges, Control Engineering Practice. *Control Engineering Practice.* 2012;20:328-342.

Davey R, Garside J. *From molecules to crystallizers: an introduction to crystallization.* Oxford University Press, 2000.

De Keyser RMC, Cauwenberghe ARV. Extended prediction self-adaptive control. *In: IFAC Symposium on Identification and System Parameter Estimation.* 1985;1255-1260.

De Keyser R, Donald III J. Application of the NEPSAC nonlinear predictive control strategy to a semiconductor reactor. *Lecture Notes in Control and Information Sciences.* 2007;358:407-417.

Deb K, Pratap A, Agarwal S, Meyarivan T. A fast and elitist multiobjective genetic algorithm: NSGA-II. *IEEE Transactions on Evolutionary Computation.* 2002;6:182-197.

Dharaskar KP, Gupta YP. Predictive control of nonlinear processes using interpolated models. *Trans IChemE.* 2000;78:573-580.

Doan XT, Srinivasan R. Online monitoring of multi-phase batch processes using phase-based multivariate statistical process control. *Computers and Chemical Engineering.* 2008;32:230-243.

Doyle III FJ, Harrison CA, Crowley TJ. Hybrid model-based approach to batch-to-batch control of particle size distribution in emulsion polymerization. *Computers and Chemical Engineering.* 2003;27:1153-1163.

Duran MA, White BS. Bayesian estimation applied to effective heat transfer coefficients in a packed bed. *Chemical Engineering Science.* 1995;50:495-510.

Englezos P, Kalogerakis N. *Applied parameter estimation for chemical engineers.* New York: Marcel-Dekker, 2000

Fevotte G, Alexandre C, Nida SO. A population balance model of the solution-mediated phase transition of citric acid. *AIChE Journal.* 2007;53:2578-2589.

Fevotte G. New perspectives for the on-line monitoring of pharmaceutical crystallization processes using in situ infrared spectroscopy. *International Journal of Pharmaceutics.* 2002;241:263-278.

Foss BA, Johansen TA, Sørensen AV. Nonlinear Predictive control using local models-applied to a batch fermentation process. *Control Engineering Practice.* 1995;3:389-396.

Froisy JB. Model predictive control building a bridge between theory and practice. *Computers and Chemical Engineering.* 2006;30:1426-1435.

Fujiwara M, Nagy ZK, Chew JW, Braatz RD. First-principles and direct design approaches for the control of pharmaceutical crystallization. *Journal of Process Control.* 2005;15:493-504.

Fujiwara K, Kano M, Hasebe S, Takinami A. Soft-sensor development using correlation-based Just-in-Time Modeling. *AIChE Journal.* 2009;55:1754-1765.

Gálvez-Carrillo M, De Keyser R, Ionescu C. Nonlinear predictive control with dead-time compensator: Application to a solar power plant. *Solar Energy.* 2009;83:743-752.

Garcia CE, Morshedi AM. Quadratic programming solution of dynamic matrix control (QMDC). *Chemical Engineering Communications.* 1986;46:73-87.

Garcia CE, Prett DM, Morari M. Model predictive control: theory and practice - a survey. *Automatica.* 1989;25;1753-1758.

García-Nieto S, Martínez M, Blasco X, Sanchis J. Nonlinear predictive control based on local model networks for air management in diesel engines. *Control Engineering Practice.* 2008;16:1399-1413.

Garside J, Phillips VR, Shah MB. On size-dependent crystal growth. *Industrial & Engineering Chemistry Fundamentals.* 1976;15:230-233.

Ge Z, Song Z. A comparative study of just-in-time-learning based methods for online soft sensor modeling. *Chemometrics and Intelligent Laboratory Systems.* 2010;104:306-317.

Geladi P, Kowalski B. Partial least squares regression: a tutorial. *Analytica Chimica Acta.* 1986;185:1-17.

Gelman A, Carlin JB, Stern HS, Rubin DB. *Bayesian Data Analysis.* New York: Chapman & Hall/CRC, 2004.

Girolami MW, Rousseau RW. Size-dependent crystal growth-a manifestation of growth rate dispersion in the potassium alum-water system. *AIChE Journal.* 1985;31:1821-1828.

Golshan M, MacGregor JF, Bruwer MJ, Mhaskar P. Latent variable model predictive control (LV-MPC) for trajectory tracking in batch processes. *Journal of Process Control.* 2010;20:538-550.

Grootscholten PAM, De Leer BGM, De Jong EJ, Asselbergs C. Factors affecting secondary nucleation rate of sodium chloride in an evaporative crystallizer. *AIChE Journal.* 1982;28:728-737.

Gros S, Srinivasan B, Bonvin D. Optimizing control based on output feedback. *Computers and Chemical Engineering.* 2009;33:191-198.

Grön H, Borissova A, Roberts KJ. In-Process ATR-FTIR spectroscopy for closed-loop supersaturation control of a batch crystallizer producing monosodium glutamate crystals of defined size. *Industry & Engineering Chemistry Research.* 2003;42:198-206.

Gunawan R, Jung MY, Seebauer EG, Braatz RD. Maximum a posterior estimation of transient enhanced diffusion energetics. *AIChE Journal.* 2003; 49:2114-2122.

Gunawan R, Fusman I, Braatz RD. High resolution algorithms for multidimensional population balance equations. *Journal of American Institute of Chemical Engineers.* 2004;50:2738-2749.

Hatakka H, Alatalo H, Louhi-Kultanen M, Lassila I, Hæggström E. Closed-loop control of reactive crystallization PART II: Polymorphism control of L-glutamic acid by sonocrystallization and seeding. *Chemical Engineering Technology.* 2010;33:751-756.

Hermanto MW, Braatz RD, Chiu MS. Robust optimal control of polymorphic transformation in batch crystallization. *AIChE Journal.* 2007;53:2643-2650.

Hermanto MW, Kee NC, Tan RBH, Chiu MS, Braatz RD. Robust Bayesian estimation of kinetics for the polymorphic transformation of L-glutamic acid crystals. *AIChE Journal.* 2008;54:3248-3259.

Hermanto MW, Chiu MS, Braatz RD. Nonlinear model predictive control for the polymorphic transformation of L-glutamic acid crystals. *AIChE Journal.* 2009;55:2631-2645.

Hermanto MW, Braatz RD, Chiu MS. Integrated batch-to-batch and nonlinear model predictive control for polymorphic transformation in pharmaceutical crystallization. *AIChE Journal.* 2011;57:1008-1019.

Hermanto MW. *Modelling, simulation, and control of polymorphic crystallization.* PhD Thesis. National University of Singapore, 2008.

Hlaing YM, Chiu MS, Samavedham L. Modeling and Control of Multivariable Processes Using Generalized Hammerstein Model. *Chemical Engineering Research and Design.* 2007;85:445-454.

Hojjati H, Sheikhzadeh M, Rohani S. Control of supersaturation in a semibatch antisolvent crystallization process using a fuzzy logic controller. *Industrial & Engineering Chemistry Research.* 2007;46:1232-1240.

Hu Q, Rohani S, Wang DX, Jutan A. Optimal control of a batch cooling seeded crystallizer. *Powder Technology.* 2005;156:170-176.

Hursthouse MB, Huth LS, Threlfall TL. Why do organic compounds crystallise well or badly or ever so slowly? Why is crystallization nevertheless such a good purification technique? *Organic Process Research & Development.* 2009;13:1231-1240.

Ionescu C, De Keyser RMC. EPSAC predictive control of blood glucose level in type I diabetic patients. *In: Proceedings of the 44th Conference on Decision and Control, and the European Control Conference.* 2005;4845-4850.

Jackson JE, Mudholak GS. Control procedures for residuals associated with principal analysis. *Technometrics.* 1979;21;341-349.

Janse AH, De Jong EJ. *The occurrence of growth dispersion and its consequences.* New York: Plenum Press, 1976.

Jazwinski AA. *Stochastic Processes and Filtering Theory.* New York: Academic Press, 1970.

Johnson RT, Rousseau RW, McCabe WL. Factors affecting contact nucleation. *AIChE Symposium Series.* 1972;68:31-41.

Jones HP, Davey RJ, Cox BG. Crystallization of a salt of a weak organic acid and base: solubility relations, supersaturation control and polymorphic behavior. *Journal of Physics Chemistry B.* 2005;109:5273-5278.

Kalmukale AK, Chiu MS, Wang QG. Partitioned Model-Based IMC Design Using JITL Modeling Technique. *Journal of Process Control.* 2007;17:757-769.

Kamaraju VK, Chiu MS. An integrated approach for C-control of antisolvent crystallization processes. *In: Proceedings of the 8th International Symposium on Advanced Control of Chemical Processes.* 2012;762-767.

Kano M, Sakata T, Hasebe S. Just-In-Time statistical process control: adaptive monitoring of vinyl acetate monomer process. *In: The 18th IFAC World Congress.* Milano, 2011.

Kansha Y, Jia L, Chiu MS. Self-Tuning PID Controllers Based on the Lyapunov Approach. *Chemical Engineering Science.* 2008;63:2732-2740.

Kansha Y, Chiu MS. Adaptive generalized predictive control based on JITL technique. *Journal of Process Control.* 2009;19:1067-1072.

Kansha Y, Jia L, Chiu MS. Adaptive IMC Controller Design Using Linear Multiple Models. *Journal of the Taiwan Institute of Chemical Engineers.* 2010;41:446-452.

Kee CSN, Tan BHR, Braatz RD. Selective crystallization of the metastable α-form of L-glutamic acid using concentration feedback control. *Crystal Growth & Design.* 2009a;9:3044-3051.

Kee NCS, Arendt PD, Tan RBH, Braatz RD. Selective crystallization of the metastable anhydrate form in the enantiotropic pseudo-dimorph system of L-phenylalanine using concentration feedback control. *Crystal Growth & Design.* 2009b;9:3052-3061.

Kee NCS, Tan RBH, Braatz RD. Semiautomated identification of the phase diagram for enantiotropic crystallizations using ATR-FTIR spectroscopy and laser backscattering. *Industrial & Engineering Chemistry Research.* 2011;50: 1488-1495.

Kitamura M. Strategy for control of crystallization of polymorphs. *CrystEngComm.* 2009;11:949-964.

Koren B. A robust upwind discretization method of advection, diffusion and source terms. *In: Vreugdenhill CB & Koren B. Numerical methods for advection-diffusion problems.* Braunschweigh: Vieweg Verlag, 1993:117-138.

Kuure-Kinsey M, Bequette BW. A Multiple Model Predictive Control Strategy for Disturbance Rejection. *Industry and Engineering Chemistry Research.* 2010;49:7983-7989.

Lampinen J. A constraint handling approach for the differential evolution algorithm. *In: Proceedings of the 2002 Congress on Evolutionary Computation.* 2002;2:1468-1473.

Lang L, Chen WS, Bakshi BR, Goel PK, Ungarala S. Bayesian estimation via sequential Monte Carlo sampling-constrained dynamic systems. *Automatica.* 2007;43:1615-1622.

Lee JH, Lee KS. Iterative learning control applied to batch processes: an overview. *Control Engineering Practice.* 2007;15:1306-1318.

Lee JH, Ricker NL. Extended kalman filter based nonlinear model predictive control. *Industrial & Engineering Chemistry Research.* 1994;33:1530-1541.

Lee K, Lee JH, Yang DR, Mahoney AW. Integrated run-to-run and on-line model-based control of particle size distribution for a semi-batch precipitation reactor. *Computers and Chemical Engineering.* 2002;26:1117-1131.

Li H, Grover M, Kawajiri Y, Rousseau RW. Development of an empirical framework for monitoring CSD using FBRM in batch crystallization. *AIChE Annual Meeting*, Pittsburg, USA, 2012.

Lindenberg C, Mazzotti M. Effect of temperature on the nucleation kinetics of α L-glutamic acid. *Journal of Crystal Growth.* 2009;311:1178-1184.

Lindenberg C, Schöll J, Vicum L, Mazzotti M, Brozio J. L-glutamic acid precipitation: Agglomeration effects. *Crystal Growth & Design.* 2008;8:224-237.

Liu JS. *Monte Carlo strategies in scientific computing.* New York: Springer, 2001.

Loizeau JL, Arbouille D, Santiago S, Vernet JP. Evaluation of a wide-range laser diffraction grain-size analyzer for use with sediments. *Sedimentology*. 1994;41:353-361.

Lundager Madsen HE. Calculation of the thermodynamic driving force in crystallization from solution. *Journal of Crystal Growth.* 1987;85:377-385.

Ma CY, Wang XZ, Roberts KJ. Multi-dimensional population balance modeling of the growth of rod-like L-glutamic acid crystals using growth rates estimated from in-process imaging. *Advanced Powder Technology.* 2007;18:707-723.

Majumder A, Kariwala V, Ansumali S, Rajendran A. Entropic Lattice Boltzmann Method for crystallization processes. *Chemical Engineering Science.* 2010;65:3928-3936.

Manenti F. Considerations on nonlinear model predictive control techniques. *Computers and Chemical Engineering.* 2011;35:2491-2509.

Mangin D, Puel F, Veesler S. Polymorphism in processes of crystallization in solution: A practical review. *Organic Process Research & Development.* 2009;13:1241-1253.

Mendes P, Kell DB. Non-linear optimization of biochemical pathways: applications to metabolic engineering and parameter estimation. *Bioinformatics.* 1998;14:869-883.

Mesbah A, Kramer HJM, Huesman AEM, Van den Hof PMJ. A control oriented study on the numerical solution of the population balance equation for crystallization processes. *Chemical Engineering Science.* 2009;64:4262-4277.

Mesbah A, Huesman AEM, Kramer HJM, Nagy ZK, Van de Hof PMJ. Real-time control of a semi-industrial fed-batch evaporative crystallizer using different direct optimization strategies. *AIChE Journal.* 2011;57:1557-1569.

Morari M, Lee JH. Model predictive control: past, present and future. *Computers and Chemical Engineering.* 1999;23: 667-682.

Mullin JW. *Crystallization.* London: Butterworth, 1961.

Nagy ZK, Allgöwer F. A nonlinear model predictive control approach for robust end-point property control of a thin-film deposition process. *International Journal of Robust and Nonlinear Control.* 2007;17:1600-1613.

Nagy ZK, Braatz RD. Robust nonlinear model predictive control of batch processes. *AIChE Journal.* 2003;49:1776-1786.

Nagy ZK, Braatz RD. Advances and new directions in crystallization control. Annual Review of Chemical and Biomolecular Engineering. 2012;3:55-75.

Nagy ZK, Chew JW, Fujiwara M, Braatz RD. Comparative performance of concentration and temperature controlled batch crystallizations. *Journal of Process Control.* 2008a;18:399-407.

Nagy ZK, Fujiwara M, Braatz RD. Modelling and control of combined cooling and antisolvent crystallization processes. *Journal of Process Control.* 2008b;18:856-864.

Nagy ZK. Model based robust control approach for batch crystallization product design. *Computers and Chemical Engineering.* 2009;33:1685-1691.

Nelson PPC, Taylor PA, MacGregor JF. Missing data methods in PCA and PLS: score calculations with incomplete observations. *Chemometrics and Intelligent Laboratory Systems.* 1996;35:45-65.

Ng JD, Lorber B, Witz J, Théobald-Dietrich A, Kern D, Giege R. The crystallization of biological macromolecules from precipitates: Evidence for Ostwald ripening. *Journal of Crystal Growth.* 1996;168:50.

Niño J, De Keyser R, Syafiie S, Ionescu C, Struys M. EPSAC-controlled anesthesia with online gain adaptation. *International Journal of Adaptive Control and Signal Processing.* 2009;23:455-471.

Nocedal J, Wright S. *Numerical optimization.* New York: Springer, 2006

Nomikos P, MacGregor JF. Monitoring batch processes using multiway principal component analysis. *AIChE Journal.* 1994;40:1361-1375.

Nomikos P, MacGregor JF. Multivariate SPC charts for monitoring batch processes. *Technometrics.* 1995a;37:41-59.

Nomikos P, MacGregor JF. Multi-way partial least squares in monitoring batch processes. *Chemometrics and Intelligent Laboratory Systems.* 1995;30:97-108.

Nuella I, Cheng C, Chiu MS. Adaptive PID Controller Design for Nonlinear Systems. *Industrial & Engineering Chemistry Research.* 2009;48:4877-4883.

Ono T, Kramer HJM, ter Horst JH, Jansens PJ. Process modeling of the polymorphic transformation of L-glutamic acid. *Crystal Growth & Design.* 2004;4:1161-1167.

Ostwald, W. Studien uber die Bildung und Umwandlung fester Korper. *Zeitschrift für Physikalische Chemie*.1897;22:289.

Özkan L, Kothare MV, Georgakis C. Model predictive control of nonlinear systems using piecewise linear models. *Computer and Chemical Engineering.* 2000;24:793-799.

Paengjuntuek W, Arpornwichanop A, Kittisupakorn P. Product quality improvement of batch crystallizers by batch-to-batch optimization and nonlinear control approach. *Chemical Engineering Journal.* 2008;139:344-350.

Peng H, Nakano K, Shioya H. Nonlinear predictive control using neural nets-based local linearization ARX model-stability and industrial application. *IEEE Transactions on Control Systems Technology.* 2007;15:130-143.

Pouillot R, Albert I, Cornu M, Denis JB. Estimation of uncertainty and variability in bacterial growth using Bayesian inference, Application to listeria monocytogenes. *International Journal of Food Microbiology.* 2003;81:87-104.

Prausnitz JM, Lichtenthaler RN, de Azevedo EG. *Molecular Thermodynamics of Fluid-Phase Equilibria.* New Jersey: Prentice Hall PTR, 1999.

Qamar S, Elsner MP, Angelov IA, Warnecke G, Seidel-Morgenstern A. A comparative study of high resolution schemes for solving population balances in crystallization. *Computers and Chemical Engineering.* 2006;30:1119-1131.

Qin SJ, Badgwell TA. A survey of industrial model predictive control technology. *Control Engineering Practice.* 2003;11: 733-764.

Qu H, Alatalo H, Hatakka H, Kohonen J, Louhi-Kultanen M, Reinikainen SP, Kallas J. Raman and ATR FTIR spectroscopy in reactive crystallization: simultaneous monitoring of solute concentration and polymorphic state of the crystals. *Journal of Crystal Growth.* 2009;311:3466-3475.

Ramesh TS, Davis JF, Schwenzer GM. CATCRACKER: An expert system for process and malfunction diagnosis in fluid catalytic cracking units. *In: AIChE Meeting*, San Francisco, 1989.

Randolph AD, Larson MA. Transient and steady state size distributions in continuous mixed suspension crystallizers. *AIChE Journal.* 1962;5:639-645.

Randolph, AD, Larson MA. *Theory of Particulate Processes: Analysis and Techniques of Continuous Crystallization.* San Diego: Academic Press, 1988.

Randolph AD, White ET. Modeling size dispersion in the prediction of crystal-size distribution. *Chemical Engineering Science.* 1977;32:1067-1076.

Rawlings JB, Miller SM, Witkowski WR. Model identification and control of solution crystallization processes: A review. *Industry Engineering Chemistry & Research.* 1993;32:1275-1296.

Roelands CPM, ter Horst JH, Kramer HJM, Jansens PJ. The unexpected formation of the stable beta phase of L-glutamic acid during pH-shift precipitation. *Journal of Crystal Growth.* 2005;275:1389-1395.

Roelands CPM, ter Horst JH, Kramer HJM, Jansens PJ, Precipitation mechanism of stable and metastable polymorphs of L-glutamic acid. *AIChE Journal.* 2007;53:354-362.

Rueda A, Cristea S, Prada CD, De Keyser RMC. Non-linear predictive control for a distillation column. *In: Proceedings of the 44th IEEE conference on Decision and Control, and the European Control Conference.* 2005;5156-5161.

Schöll J, Vicum L, Müller M, Mazzotti M. Precipitation of L-glutamic acid: Determination of nucleation kinetics. *Chemical Engineering Technology.* 2006a;29:257-264.

Schöll J, Bonalumi D, Vicum L, Mazzotti M. In situ monitoring and modeling of the solvent-mediated polymorphic transformation of L-glutamic acid. *Crystal Growth & Design.* 2006b;6:881-891.

Schöll J, Lindenberg C, Vicum L, Brozio J, Mazzotti M. Precipitation of α L-glutamic acid: determination of growth kinetics. *Faraday Discuss.* 2007;136:247-264.

Scokaert POM, Rawlings JB. Feasibility issues in linear model predictive control. *AIChE Journal.* 1999;45:1649-1659.

Sheng JJ, Kasim NA, Chandrasekharan R, Amidon GL. Solubilization and dissolution of insoluble weak acid, ketoprofen: effects of pH combined with surfactant. European *Journal of Pharmaceutical Science.* 2006;29:306-314.

Srinivasan B, Biegler LT, Bonvin D. Tracking the necessary conditions of optimality with changing set of active constraints using a barrier-penalty function. *Computers and Chemical Engineering.* 2008;32:572-579.

Storn R, Price K. Differential evolution-a simple and efficient heuristic for global optimization over continuous spaces. *Journal of Global Optimization.* 1997;11:341-359.

Strickland-Constable RF. The breeding of crystal nuclei-a review of the subject. *AIChE Symposium Series.* 1972;68:1-7.

Su QL, Braatz RD, Chiu MS. Concentration control for semi-batch pH-shift reactive crystallization of L-Glutamic acid. *In: Proceedings of the 8th International Symposium on Advanced Control of Chemical Processes.* 2012;228-233.

Su QL, Kano M, Chiu MS. A new strategy of locality enhancement for Just-in-Time learning method. *In: Proceedings of the 11th International Symposium on Process System Engineering.* 2012;1662-1666.

Su QL, Hermanto MW, Braatz RD, Chiu MS. A new extended prediction self-adaptive control (EPSAC) strategy for batch process control. *AIChE Annual Meeting*, Pittsburg, USA, 2012.

Sun W, Meng Y, Palazoglu A, Zhao J, Zhang H, Zhang J. A method for multiphase batch process monitoring based on auto phase identification. *Journal of Process Control.* 2011;21:627-638.

Tabora JE. Data-driven modeling and control of batch processes in the pharmaceutical industry. *In: Proceedings of the 8th International Symposium on Advanced Control of Chemical Processes.* 2012;708-714.

Tamas L, Nascu I, De Keyser R. The NEPSAC nonlinear predictive controller in a real life experiment. *In: International Conference on Intelligent Engineering System.* 2007;229-234.

Ter Braak CJ. A Markov Chain Monte Carlo version of the genetic algorithm differential evolution: Easy Bayesian computing for real parameter spaces. *Statistics and Computing.* 2006;16:239-249.

Tierney L. Markov chains for exploring posterior distributions. *Annals of Statistics.* 1994;22:1701-1728.

Togkalidou T, Tung HH, Sun Y, Andrews AT, Braatz RD. Parameter estimation and optimization of a loosely bound aggregating pharmaceutical crystallization using in situ infrared and laser backscattering measurements. *Industrial & Engineering Chemistry Research.* 2004;43:6168-61810.

Torrent-Burgués J. The Gibbs energy and the driving force at the crystallization from solution. *Journal of Crystal Growth.* 1994;140:107-114.

Toschev S. *Crystal Growth: An Introduction.* North Holland/Ames Elsevier Press, Amesterdam, 1973.

Towler CS, Davey RJ, Lancaster RW, Price CJ. Impact of molecular speciation on crystal nucleation in polymorphic systems: the conundrum of γ glycine and molecular 'self poisoning'. *Journal of American Chemistry Society.* 2004;126: 13347-13353.

Walton AG. *Nucleation in liquids and solutions.* New York: Marcel Dekker, 1969.

Wang Y, Gao F, Doyle III FJ. Survey on iterative learning control, repetitive control, and run-to-run control. *Journal of Process Control.* 2009;19:1589-1600.

Ward JD, Yu CC, Doherty MF. A new framework and a simpler method for the development of batch crystallization recipes. *AIChE Journal.* 2011;57:606-617.

Welz C, Srinivasan B, Bonvin D. Measurement-based optimization of batch processes: Meeting terminal constraints on-line via trajectory following. *Journal of Process Control.* 2008;18:375-382.

White ET, Wright PG. Magnitude of size dispersion effects in crystallization. *Chemical Engineering Progress Symposium Series.* 1971;67:81-87.

Wold S, Geladi P, Esbensen K, Ohman J. Multi-way principal components and PLS analysis. *Journal of Chemometrics.* 1987;1:41-56.

Woo XY, Nagy ZK, Tan RBH, Braatz RD. Adaptive concentration control of cooling and antisolvent crystallization with laser backscattering measurement. *Crystal Growth & Design.* 2009;9:182-191.

Xiong Z, Zhang J. Product quality trajectory tracking in batch processes using iterative learning control based on time-varying perturbation models. *Industry & Engineering Chemistry Research.* 2003;42:6802-6814.

Xiong Z, Zhang J, Wang X, Xu Y. Tracking control for batch processes through integrating batch-to-batch iterative learning control and within-batch on-line control. *Industry & Engineering Chemistry Research.* 2005;44:3983-3992.

Yang X, Jia L, Chiu MS. Adaptive Decentralized PID Controllers Design Using JITL Modeling Methodology. *Journal of Process Control.* 2012;22:1531-1542.

Yu LX, Lionberger RA, Raw AS, D'Costa R, Wu HQ, Hussain AS. Applications of process analytical technology to crystallization processes. *Advanced Drug Delivery Reviews.* 2004;56:349-369.

Yu ZQ, Chou PS, Tan RBH, Ang WH. Supersaturation control in cooling polymorphic co-crystallization of caffeine and glutaric acid. *Crystal Growth & Design.* 2011;11:4525-4532.

Zafiriou E, Adomaitis RA, Gattu G. An approach to run-to-run control for rapid thermal processing. *In: Proceedings of the American Control Conference.* 1995;1286-1288.

Zhang J. Batch-to-batch optimal control of a batch polymerisation process based on stacked neural network models. *Chemical Engineering Science.* 2008;63:1273-1281.

Zhao C, Wang F, Jia M. Dissimilarity analysis based batch process monitoring using moving windows. *AIChE Journal.* 2007;53:1267-1277.

Zhao C, Mo S, Gao F, Lu N, Yao Y. Statistical analysis and online monitoring for handling multiphase batch processes with varying durations. *Journal of Process Control.* 2011;21:817-829.

Zhou GX, Fujiwara M, Woo XY, Rusli E, Tung HH, Starbuck C, Davidson O, Ge Z, Braatz RD. Direct design of pharmaceutical antisolvent crystallization through concentration control. *Crystal Growth & Design.* 2006;6:892-898.

Zhu J, Garside J. Controlled batch crystallization by pH variation. *In: Symposium on 1997 Jubilee Research Event.* 1997;1-2:449-452.

Zumstein RC, Rousseau RW. Growth rate dispersion by initial growth rate distributions and growth rate fluctuations. *AIChE Journal.* 1987;33:121-129.

Publications and Presentations

Journal Papers

[1] Su QL, Hermanto MW, Braatz RD, Chiu MS. A new extended prediction self-adaptive control (EPSAC) for pH-shift reactive crystallization of L-glutamic acid. 2014, in preparation.

[2] Su QL, Braatz RD, Chiu MS. Modeling and Bayesian parameter estimation for semi-batch pH-shift reactive crystallization of L-glutamic acid. *AIChE Journal*. 2013; in review.

[3] Su QL, Chiu MS. Monitoring of the pH-shift reactive crystallization of L-glutamic acid. *Journal of Chemical Engineering of Japan*. 2013, in review.

[4] Su QL, Braatz RD, Chiu MS. JITL-based concentration control for semi-batch pH-shift reactive crystallization of L-glutamic acid. *Journal of Process Control*. 2014;2:415-421.

[5] Su QL, Kano M, Chiu MS. A new strategy of locality enhancement for just-in-time learning method. *Computer Aided Chemical Engineering*. 2012;31:1662-1666.

Conference Papers and Presentations

[1] Su QL, Chiu MS. Monitoring of semi-batch pH-shift reactive crystallization process using moving window MPCA. In: *Proceedings of the 6th International Conference on Process Systems Engineering* (*PSE ASIA*). 2013:344-349.

[2] Su QL, Hermanto MW, Braatz RD, Chiu MS. A new extended prediction self-adaptive control (EPSAC) strategy for batch process control. In: *AIChE Annual Meeting*, Pittsburg, USA, 2012.

[3] Su QL, Braatz RD, Chiu MS. Concentration control for semi-batch pH-shift reactive crystallization of L-Glutamic acid. In: *Proceedings of the 8th International Symposium on Advanced Control of Chemical Processes*. 2012;228-233.

[4] Su QL, Kano M, Chiu MS. A new strategy of locality enhancement for Just-in-Time learning method. In: *Proceedings of the 11th International Symposium on Process System Engineering*. 2012;1662-1666.